Optimized Assembly and Covalent Coupling of Single-Molecule DNA Origami Nanoarrays

Ashwin Gopinath & Paul W. K. Rothemund

Contents

DNA origami design, preparation and purification

A variation of the 'sharp triangle' design described previously,[1] was chosen because the sharp triangle is rigid (it rarely folds when deposited on mica), and it has a low tendency to aggregate. The 'sameside sharp triangle' used here (sequences and the caDNAno design occur as `ET_SameSide_StapleOrder.xls` and `Sameside-sharp-triangle-bridged.json`, as part of the zip archive `nn506014s_si_006.zip`) has the same arrangement of scaffold as the original, and the scaffold strand shares the same alignment as in the original structure. The difference between the original and sameside sharp triangles lies in the pattern of nicks along the phosphate backbone of the staple strands: in the original sharp triangle nick positions alternate between the two faces of the triangle, which places the ends of staple strands on both faces of the triangle—this mean that functionalizations can be made to both sides of the original triangle but only ∼100 modifications could be made to each side. The new sameside triangle has all nick positions on the same face of the triangle so that ∼200 modifications can be made to the same side of the triangle.

Staple strands (Integrated DNA Technologies, 100 μM each in water) and the scaffold strand (single-stranded M13mp18, Bayou Biolabs, P-107) were mixed together to target concentrations of 100 nM (each staple) and 40 nM, respectively (a 2.5:1 staple:scaffold ratio) in 10 mM Tris Base, 1 mM EDTA buffer (adjusted to to pH 8.35 with HCl) with 12.5 mM magnesium chloride (TE/Mg^{2+}). 50 μL volumes of staple/scaffold mixture were heated to 90°C for 5 min and annealed from 90°C to 20°C at -0.2°C/min in a PCR machine. Use 0.5 ml DNA LoBind tubes (Eppendorf) to minimize loss of origami to the sides of the tube.

Warning: Do not use acetate in preparation of the formation buffer for DNA origami (*e.g.* using acetic acid to adjust pH). For historical reasons, acetate-containing TAE/Mg^{2+}, a gel electrophoresis buffer has been used for preparing DNA origami. In the context of origami placement, acetate ions cause a high background of small particles to appear, presumably insoluble acetate salts.

Origami were purified away from excess staples using 100 kD molecular weight cut-off filters spin filters. A high concentration of excess staples will prevent origami placement. We began using Millipore YM-100 filters (discontinued) but later used "Amicon Ultra-0.5 Centrifugal Filter Units with Ultracel-100 membranes". By the protocol below, recovery is generally 40–50% and staples are no longer visible by agarose gel:

1. Wet the filter by adding 500 μL TE/Mg^{2+}.
2. Spin filter at 2000 rcf for 6 min at 4°C down to 50 μL. Discard the filtrate.
3. Add 50 μL of unpurified origami and 400 μL TE/Mg^{2+}. Spin at 2000 rcf for 6 min at 4°C .
4. Discard the filtrate. Add 450 μL TE/Mg^{2+} and spin at 2000 rcf for 6 min at 4°C .
5. Repeat step (4) three more times.
6. Invert the filter onto a clean tube and spin at 2000 rcf for 6 min at °C to collect purified origami ($\sim 50\mu$L).

Total time for this purification is roughly 40 minutes. Post-purification, origami are quantified using a NanoDrop spectrophotometer (Thermo Scientific), estimating the molar extinction coefficient of the DNA origami as that of a fully double-stranded m13mp18 molecule (ϵ =123,735,380/M/cm; we do not correct for a small single-stranded loop present on one edge of the origami). We typically work with stock solutions of 15–20 nM DNA origami (2–2.5 OD). The typical working concentration for origami during placement is 110 pM, which is too small to be measured with the NanoDrop, so serial dilutions must be performed. For all of the experiments performed in this paper using the basic, non-amine-functionalized origami, a single 300 μL stock of 16 nM origami was used as the starting point for dilutions.

Note: All of the work reported in this paper was performed with spin-column purified origami. A much easier protocol using PEG precipitation is now available,[2] although we have not verified that it gives quantitatively similar results for placement.

Warning: After purification and quantification, it is especially important to use DNA LoBind tubes (Eppendorf) for storage and dilution of low concentration DNA origami solutions. Low dilutions, *e.g.* 110 pM, must be made fresh from more concentrated solutions and used immediately—even overnight storage can result in total loss of origami to the sides of the tube. Addition of significant amounts of carrier DNA to prevent origami loss may prevent origami placement, just as excess staples do. We have not yet determined whether other blocking agents such as BSA might both prevent origami loss and preserve placement.

Preparation of amine-functionalized origami. Synthesis of amine-functionalized origami is very similar to that for non-functionalized origami. A mixture 40 nM of the scaffold and with 100 nM of each staple strand *except* those staples intended to be labeled on the inner edge of the origami (Supplementary Fig. S67) was prepared. To this strand mixture we added:

1. 500 nM of each of 15 different modified staples with 18-base poly-T linkers concatenated to their 5′ end.
2. 5 μM of a 21-base poly-A strand with an amine modification on its 3′ end.

Note: 500 nM was chosen for modified staples to give a slightly higher staple excess for these strands (a 12.5:1 modified staple:scaffold ratio), in principle to guarantee that origami could not possibly be missing these strands if staple stock concentrations were overestimated. However, too few aminated strands were added: the 5 μM concentration of aminated strand only guarantees that an average of 10 out of 15 of the modified staples will be hybridized to aminated strands. The origami were still well-immobilized by the amine-functionalized strands but we recommend that a different protocol be used, in particular we recommend that 200 nM modified staples be used, and that the same 5 μM aminated strand be used, so that a high excess of modified staples is maintained (a 5:1 modified staple:scaffold ratio) but there is a further excess of aminated strands over linker strands (a 5:3 aminated:linker ratio) so that all 15 sites on the origami are modified.

In addition, a slightly modified version of the spin filtration protocol was used for amine-labled origami to remove staples, linker-modified staples, and the aminated strand. Centrifuge parameters were longer, slower, and warmer: 7 minutes/spin, 1500 rcf at room temperature. We report this difference but do not believe that it made a difference in the origami's performance.

A single stock of amine-functionalized origami was used for all covalent immobilization experiments. Placement was not reoptimized for this stock but typical site occupancy was typically $\sim$90%. Reoptimization might change results because, for example, the aminated strand/linkers may change the stickiness of origami for binding sites.

Placement substrate nanofabrication

Fabrication begins with a thermally grown SiO_2 layer (on Si wafer) or single crystal quartz substrate which is cleaned and silanized with a trimethyl silyl passivation layer by vapor deposition of HMDS (hexamethyldisilazane). A thin (170–180 nm) layer of PMMA is spin-coated on the substrate to be used as resist for lithography. Binding sites in the shape of a DNA origami are defined in the resist either with e-beam lithography (Figs. S1 and S2) or nanoimprint lithography. After the binding sites are defined the trimethyl silyl passivation layer is selectively removed at the binding sites using an anisotriopic O_2-plasma etch, in a process termed 'activation'. Finally, the residual PMMA resist is removed to reveal a substrate that is composed of two chemically distinct regions: (i) triangular features covered with ionizable surface silanols (-OH) and (ii) a neutrally-charged background covered with trimethyl silyl groups. Except for nanoimprint lithography, all steps were carried out in Caltech's Kavli Nanoscience Institute.

Thermal SiO_2 growth

Silicon wafers (100 mm diameter, n-type, phosphorus-doped, <100>orientation, 1–10 ohm-cm resistivity, 500 μm thick, single-side polished, Prime grade) were purchased from University Wafers. Wafers were cleaned using the RCA procedure:

1. Immerse in R1 solution [5:1:1 H_2O:30% H_2O_2(aqueous): NH_4OH] for 20 min.
2. Wash with high purity 18 MΩ-cm resistivity deionized water (DI).
3. Immerse in R2 solution [5:1:1 H_2O:30% H_2O_2(aqueous): HCl] for 20 min at 70°C .
4. Wash with DI.

After RCA cleaning, wafers were subjected to the following procedure:

1. Immerse in 20 wt% HF (aqueous) for 30 s.
2. Immerse in in 40 wt% NH_4F (aqueous) for 60 s.
3. Wash in DI.
4. Bake in an O_2-rich environment (dry oxidation conditions using a Tystar Tytan furnace) at 1000°C for 3.25 hours, to grow a 100 nm layer of SiO_2.
5. Analyze with a Filmetrics F40 thin-film analyzer, to confirm 100 nm thickness of the oxide layer.

Warning: Failing to include HF and NH_4F treatments creates a surface that requires significantly more Mg^{2+} for placement. While RCA cleaning is a standard process used in the semiconductor industry, the subsequent HF immersion and NH_4F immersions are non-standard treatments aimed at decreasing surface roughness.[3] Thermal oxide grown on wafers which received no cleaning procedure had a roughness of 9-10 Å (by AFM). We have not measured roughness of thermal oxide given only an RCA cleaning, but is known to increase surface roughness, and so we assume that oxide deriving from RCA-only cleaned surfaces had a similar or greater roughness. Thermal oxide on wafers which had received RCA/HF had a roughness of 5 Å and thermal oxide on wafers which received RCA/HF/NH_4F had a roughness of 3 Å. (For comparison freshly-cleaved mica substrates have 1 Å roughness.) The amount of Mg^{2+} required for placement of origami seems to correlate with surface roughness: for RCA only 90 mM Mg^{2+} was required (Fig. S30e–g), for RCA/HF 55 mM Mg^{2+} was required (Fig. S30a–d), and for RCA/HF/NH_4F, 35 mM Mg^{2+} was required (Fig. 2k and Figs. S29). We have not yet ruled out that changes to surface chemistry from the cleaning steps are playing a role in the amount of Mg^{2+} required.

Surface passivation with trimethyl silyl groups

After growth of SiO_2, wafers were subjected to the following silanization procedure:

1. Wash with isopropanol (IPA) and dry in a stream of N_2, to remove particulate contaminants.
2. Clean with O_2 plasma in a Plasmatherm Dual Chamber 720/720 RIE, at a flow rate of 50 sccm, pressure of 50 mTorr and a power setting of 80 W (110 W/cm), for 5 minutes to generate surface silanols.
3. Heat on a hot plate at 150°C for 5 min, to dehydrate the surface.
4. Incubate in a 4 liter chamber saturated with HMDS vapor (a 20 cm $\times$ 20 cm $\times$ 10 cm tupperware with a 90 mm petri dish in the corner holding 10 ml HMDS) for 20 min, to add trimethy silyl groups.
5. Heat on a hot plate at 150°C for 30 min, to stabilize the silanized surface.

Warning: It is important to dehydrate the substrate both **before** and **after** HMDS vapor-priming to ensure high quality surface silanization and increase the robustness of the monolayer to hydrolysis. Failure to perform either of these steps leads to high background binding of origami.

E-beam lithography

E-beam lithography was performed on freshly prepared and silanized substrates as follows:

1. Spin on the resist. A thin layer 170–180 nm-thick poly(methyl methacrylate) (MicroChem Corp., 950 PMMA, A3) layer was spin-coated (2500 rpm for 90 s).
2. Bake the resist at 180°C for 30 s.
3. Define binding sites in the resist using EBPG with a 100 keV beam; deliver a dose of 900 μC/cm^2 at 700 pA current.
4. Develop the resist for 70 s in a 1:3 solution of methyl iso butyl ketone (MIBK) and isopropanol (IPA).

Dosage was optimized by imaging control substrates after development (Supplementary Fig. S1) to achieve sites that were as triangular as possible. However, due to the proximity effect (wherein scattered and secondary electrons expose resist in an undesired manner and coarsen a feature), the best sites we achieved were still slightly rounded: corners of the equilateral triangle had a radius of curvature of $\sim$ 20 nm. Corrections for the proximity effect are possible, and, with effort, binding sites could be made to better approximate triangles. The use of a filled triangular binding site, rather than one with a central 'non-sticky' patch (to match the triangular hole in the center of the origami) does increase the number of multiple binding events but such features are very difficult to create.

Before the e-beam write which defined the triangular binding sites, another very similar write/development process was used to define fiducial markers for finding the binding sites on the chip (Supplementary Fig. S2). Fiducial markers were typically 80 nm chromium patches, constructed by lift-off, by depositing metal into resist features, except when the fiducial markers were used for microcontact printing, in which case resist features were etched to create 100 nm depressions.

Note: Substrates that have been exposed to e-beam can be stored undeveloped for up to a year without the loss of function.

Warning: Triangular binding sites (as features in the resist) were sized so that the edges of the binding site coincided with the with the edges of a 127 nm triangle, and the tips of the triangle project beyond the rounded corners. This sizing was chosen with the idea that alignment would be the best possible—otherwise, if binding site size were chosen to contain the entire triangle, it would be able to fit in the site with a range of orientations. So that developed binding sites would be 127 nm in size, we specified 120 nm triangles during the e-beam write.

Warning: Do not bake the PMMA-coated layer for more than 45 s at 180°C . While we recommend 30 s, slightly longer bake times are acceptable. However, over-baking leads to a high background of particulates during placement, as visualized by AFM. Control experiments with overbaked PMMA (2 minute bake time) on an unpatterned background (without the addition of origami) verify that these particulates derive from the resist. When particulates do occur they do not cause spurious binding of origami.

Nanoimprint on nonconductive substrates

Origami nanoarrays are potentially useful for optical experiments on individual biomolecules, wherein each origami in the nanoarray could carry a copy of a particular single-molecule experiment. Typically, single-molecule optical experiments are conducted using total internal relection microscopy for which transparent substrates like glass or quartz are essential. However, e-beam lithography is particularly difficult on such substrates, since they are nonconductive. Thus we explored nanoimprint lithography, which not only allows patterning of nonconductive substrates, it can provide faster patterning since the mold can be reused.

Single crystal quartz substrates (100 mm, X,Y,Z,ST-Cut, 350 microns, double-side polished) on which nanoimprint lithography was performed, were purchased from University Wafers. They were cleaned using an IPA rinse, blown dry with N_2, passivated using HMDS-derived trimethyl silyl groups, and finally coated with 170–180 nm of PMMA following protocols described earlier. In parallel, an SiO_2 mold (whose fabrication is described below), was cleaned with IPA and O_2 plasma (with the same protocol as Step 2 of the surface passivation protocol).

A deadhesion coating of tridecafluoro-1,1,2,2-tetrahydrooctyl)trichorosilane (TFOCS, Gelest, SIT8174.0-50GM) was deposited on the mold to facilitate mold release after the nanoimprint. A few drops of TFOCS, were applied to the mold (just enough to wet it) and allowed to sit for 3 minutes, before being blown off with dry nitrogen.

Finally, thermal nanoimprint lithography was performed using a Nanonex BX-200 system, at 100°C and 500 psi for 30 min (at the UCSB Nanofabrication Facility). After nanoimprint the binding sites were activated and the substrate was stripped identically to e-beam patterned substrates (see below). An example of placement on quartz occurs in Supplementary Fig. S48.

Fabrication of SiO_2 mold for nanoimprint

SiO_2 mold fabrication began by growing a 500 nm layer of SiO_2, using a Tystar Tytan furnace under wet oxidation conditions (in contrast to the dry oxidation conditions used to generate the 100 nm SiO_2 for placement substrates). Freshly-cleaned silicon wafers were annealed in a wet environment at 1000°C for 1 hour and 30 min. E-beam lithography was used to pattern a standard array of triangles. The size of the triangles in the e-beam write for the mold was $\sim$ 15 nm smaller (*i.e.* 110 nm) than the desired binding site size (127 nm), because final nanoimprinted features end up being slightly larger than features in the mold from which they derive.

After development, a 30 nm thick layer of Cr was deposited by e-beam evaporation and excess metal was lifted off using hot NMP during the resist strip. The Cr layer then served as an etch mask to create 400 nm tall pillars in the shape of the DNA origami: a mixed CF_4 and O_2 plasma was applied using a Plasmatherm Dual Chamber 720/720 RIE, at 20 sccm CF_4 flow, 10 sccm O_2 flow, 100 W RF power, and 40 mTorr chamber pressure for 14 minutes.

Binding site activation and resist strip

After e-beam or nanoimprint lithography:

1. Cut wafers into 1 cm$\times$1 cm chips. This process generates some Si or SiO_2 dust.
2. Clean dust off chips by sonicating them in IPA at room temparature for 60 s.
3. Activate binding sites with a short anisotropic O_2 etch (Plasmatherm Dual Chamber 720/720 RIE) at 50 sccm, 50 mTorr, and 80 W power for 15 s.
4. Remove resist by sonicating the chips in bath of n-methyl pyrrolidone (NMP) at 50°C for 10 mins.

Note: The resist strip can also be performed without sonication and heat, using with NMP or acetone, however the substrates need to incubated overnight. If acetone is used, **do not use heat**, and further, because of the acetone's evaporation rate, use a sealed container.

Warning: Tune the O_2 activation time to the particular anisotropic RIE etcher being used to account for the turn-on time. While we report a 15 second etch, the turn-on time of the particular tool is 10–12 seconds. This means that the effective etch time is 3–5 seconds. PMMA etches at high rate under an O_2 plasma, and a full 15 second etch would likely completely remove the resist everywhere and destroy the difference between features and background. It extraordinarily easy to over-etch the features and widen binding sites; in general start with the shortest possible etch time.

Warning: Do not use a regular O_2 plasma cleaner to perform activation, at least with the protocol presented. The features will coarsen, getting larger and rounding out so that multiple bindings are common. The fabrication protocol might be optimized (*e.g.* using a resist that is more resistant to O_2 plasma like ZEP) to allow the use of a non-anisotropic plasma, but we have not achieved this.

Warning: For best results, use activated substrates for placement of origami within 24 hours of activation. All of the data collected in this paper were made on substrates used within 24 hours of activation. While good placement can often be oberved on activated substrates up to 5 days post-activation, the aging of substrates is not very reproducible and typically, after 7 days post activation, no binding is observed at all. One hypothesis is that surface silanols rearrange to make surface siloxanes.

Placement using Mg^{2+} (Method 1)

The origami placement protocol proceeds in four steps (Supplementary Fig. S3):

1. **Binding.** A 50 mm petri dish is prepared with a moistened kimwipe to limit evaporation. Solution with a desired origami concentration is prepared in **placement buffer** (with a desired Mg^{2+} concentration) and a 20 μL drop is deposited in the middle of a 1 cm $\times$ 1 cm chip. (The recipe for our optimized placement buffer is given below.) The chip is placed in the closed, humid petri dish and the origami solution is allowed to incubate on the chip for the desired incubation time (Fig. S3a).

2. **Initial wash.** After incubation, excess origami is washed away with at least 8 buffer washes by pipetting 60 μL of fresh **placement buffer** onto the chip, and pipetting 60 μL off of the chip (Fig. S3b). Each of the 8 washes consists of pipetting the 60 μL volume up and down 2–3 times to **mix** the fresh buffer with existing buffer on the chip. This initial wash takes about 2 minutes.

3. **Tween wash.** Next, in order to remove origami that are non-specifically bound to the passivated background (Fig. S5), the chip is buffer-washed 5 times using a washing buffer with 0.1% Tween 20 (v/v in placement buffer). This takes about 1 minute. Because of the low surface tension of the **Tween washing buffer**, these washes are somewhat tricky: they involve adding 20–40 μL of wash buffer, just enough to cover most of the chip, but not enough to spill over the chip and wet the back side of the chip (this may introduce dust contamination from the petri dish). After the 5th wash, the chip is left to incubate for 30 minutes (Fig. S3c).

4. **Final wash.** Lastly, the chip is buffer-washed 8 times back into a higher pH **imaging buffer** (Fig. S3d) so that origami bind strongly and AFM imaging is more stable. This takes about 2 minutes. These washes are high volume (60 μL) and are intended to completely remove the Tween 20. The amount of Tween 20 left is monitored by the surface tension of the drop (roughly, by eye). When a 20μL drop covers roughly the same area as the initially deposited drop, it is assumed that the Tween 20 has been sufficiently removed. In the last wash the chip is left with roughly 20 μL of imaging buffer, and is ready for imaging.

Our optimized protocol uses the following buffers and parameters:

- **Placement buffer:** 5 mM Tris, pH 8.35, 35 mM Mg^{2+}.
- **Tween washing buffer:** 5 mM Tris, pH 8.35, 35 mM Mg^{2+}, 0.1% Tween 20 (10 μL Tween 20 mixed with 990 μL placement buffer).
- **Imaging buffer:** 5 mM Tris, pH 8.9, 30 mM Mg^{2+}.
- **Incubation time:** 60 min.
- **Origami concentration:** 110 pM.

As reported in Fig. 2 of the main text, changes to the experimental parameters all exhibit the same basic trends. Increasing origami concentration, Mg^{2+}, incubation time, or pH leads to an increase in single origami binding (below some threshhold), followed by an increase in multiple binding and a degradation in the fidelity of orientation. Thus these parameters are subject to some trade-offs. During the binding step, incubation time may be reduced if origami concentration is increased. For example, during the final wash step, a lower pH (8.35) may be used if a higher Mg^{2+} concentration (60 mM) is used (although the elevated pH is helpful if the sample is to be dried, as explained in the section on drying, below). Placement on quartz substrates fabricated using nanoimprint lithography works will with the standard optimized protocol (Fig. S48).

An important question is, how repeatable is placement under optimal conditions? Each of our four optimization experiments involved repeating placement under optimal conditions three times. Our period variation experiment involved another three replications. In addition to these 15 replications, we made another 75 replications, all using the same single preparation of origami, over the course of 16 months. Chips derived from 4 different independently-processed wafers, involving four distinct cleaning, e-beam writes, *etc.* Averaging over these 90 replications we found single-origami binding at 94$\pm$4% of sites, with 90% of these origami having an orientation within $\pm 10^\circ$ of the correct orientation.

The nonlinear dependence of placement quality on origami concentration, Mg^{2+}, incubation time, and pH mean that inconsistency in these parameters (as well as buffer washes) probably causes the greatest variation between experiments. Outright failures of placement can often be traced to one of these variables. Poor quality e-beam writing (*e.g.* overexposure) on the other hand usually results in an increase in multiple bindings, as does over-activation of binding sites—it is easy to make larger-than-desired binding sites with these processes.

Note: This protocol has not been optimized, and it may be possible to skip the initial washes (which remove excess origami) and go straight to the Tween washes (using perhaps more of them). For consistency over all our experiments, we have not yet tried this variation.

Warning: Do not use acetate in preparation of the placement, Tween washing, or imaging buffer. For historical reasons, TAE/Mg^{2+}, a gel electrophoresis buffer has been used for preparing DNA origami. In the context of origami placement, acetate ions cause a high background of small particles to appear, presumably insoluble acetate salts.

Warning: Do not use EDTA in placement, Tween washing, or imaging buffers. It is unnecessary and will change the effective Mg^{2+} concentration for placement slightly.

Warning: Make fresh buffer solutions every week. Here and elsewhere in this work, we use buffers at low strength (typically 10 mM) to minimize background and to make complete washing into different buffers easier. This means the buffers have low buffering capacity and the pH will will decrease (and placement may cease to work, depending on conditions). Weak buffers made to read pH 8.35 can lose 0.05 pH units and read pH 8.3 after week.

Warning: Do not allow the patterned region with binding sites to dry at any point during the binding step or subsequent buffer washes. Inadvertent dewetting of the binding sites leads to distortion of the origami (causing them to ball up) as well as the formation of salt crystals on top of them (Fig. S4). We have not figured out how to salvage origami nanoarrays once the surface has spontaneously dewetted. Sonication removes putative salt crystals but it leads to the removal of origami as well.

Warning: Use Tween 20, rather than other surfactants. Tween 80 and SDS, which are two other common surfactants, lead to very different results. Tween 80 leads to the total removal of placed origami from the substrate. SDS does not remove excess origami from the trimethyl silyl background.

Warning: Make sure that chips are not exposed to Tween 20 until **after** the origami have been deposited. Tween 20 applied before binding completely inactivates the binding sites.

Warning: Before imaging, make sure that all Tween 20 is removed. Tween 20 present during AFM imaging can prevent stable AFM imaging of the sample, and cause false engages. Monitor the removal of Tween 20 from the substrate by observing the surface tension during buffer washes. The size of a 20 μL droplet after Tween 20 removal should have the same size as the initially applied 20 μL droplet.

Drying of origami nanoarrays

For many applications, it may be useful to dry origami nanoarrays, either for analysis or storage. We have dried arrays of origami with extra probe strands attached, rehydrated them after a year, and still observed hybridization of complementary DNA to the probes.

Origami arrays have previously[4] been dried using a short immersion in 50% ethanol/water, followed by an hour long immersion in 90% ethanol water. We have found that a much shorter protocol gives equally good results. Chips are dipped quickly, for just 10 seconds, in each of a series of ethanol water solutions: 25%, 50%, 70%, 80%, and 90%. After the final immersion, chips are dried in air.

Interestingly, base-catalyzed hydrolysis of the trimethyl silyl background greatly changes the quality of the dried arrays which result. For example, an origami array dried from lower pH 8.35 buffer is shown in Fig. S6a. Numerous aggregates of origami are observed, and they are 'balled-up' so that individual origami cannot be perceived. Further, the corners of origami triangles often have additional height contrast indicating that they may be folding back onto the origami. Our interpretation is that, for an intact trimethyl silyl background, multiply bound origami or the tips of origami overlap the passivated background, and thus are weakly held in place. During drying, the binding sites and origami probably hold water better than the surrounding background, and thus the last water on the surface probably exists as small droplets at the binding sites. As these droplets shrink, capillary forces may pull weakly bound origami or corners of origami away from the background and into the binding site. Thus aggregation and distortion are indicators of a high quality, intact passivation layer.

In contrast (Fig. S6b), if origami arrays are allowed to sit for two hours in higher pH buffer (ph $\sim$ 9) before drying then the trimethyl silyl background presumably hydrolyzes, and it becomes stickier for origami and more hydrophilic. If origami arrays are dried after treatment at elevated pH, then multiple origami and the corners of individual origami lie flat on the mica after drying, and few aggregates are observed (instead multiply-bound origami are clearly observed). Imaging buffer (above) has a pH of 8.9, and so post AFM drying from imaging buffer yields few aggregates. We comment that if such an elevated pH treatment is used, then the background may be potentially sticky for other components (*e.g.* DNA strands) which might be added later, either before drying or after rehydration.

Warning: To avoid aggregation of multiply bound origami and deformation of single origami, treat the chip with elevated pH buffer ($\sim$ 9) for two hours **before** drying.

Warning: If nanoarrays are subjected ethanol solutions with less than 80% ethanol for an extended period of time, origami begin to detach from the surface.

Warning: After the 90% ethanol immersion, let the samples air dry rather than using N_2 or compressed air, since streaking or other drying artifacts are observed.

AFM imaging and analysis

Unless otherwise specified, all AFM images were taken in solution tapping mode with a Dimension Icon AFM/Nanoscope V Scanner (Bruker) using the short, fat cantilever from an SNL probe ("sharp nitride lever", 2 nm tip radius, Bruker) resonating at 16–19 kHz. Additionally, all samples were imaged using phase imaging rather than height imaging in order to reduce the tip-sample interaction,[5,6] which can detach origami from the surface. In practice this meant engaging normally and then increasing the amplitude set point until origami were no longer visible in the height image, but were visible with high contrast in the phase image. Images for data were taken during the second scan of a region (the first scan was used for imaging parameter optimization). When installing samples into the microscope, 20 μL of imaging buffer was placed on the sample, and 40 μL of buffer was placed on the tip for a total working volume of 60 μL. Care was taken to prevent the sample from dewetting (*e.g.* keeping chips close to level) since the hydrophobic TMS surface makes it easy for the buffer drop to fall off of the chip. Before imaging each origami nanoarray, an unpatterned O_2 plasma-activated SiO_2 chip with a sample from the same batch of origami was imaged to verify the quality of both the tip and origami. We note that AFM is generally harder on patterned substrates with a large fraction of TMS-passivated background (when compared to unpatterned activated silicon dioxide or mica); it seems harder for the microscope to track the surface. Also, at lower pH values (below 8), higher drive amplitudes or lower amplitude set points were required to track the surface. Typically we used pH 8.9 imaging buffer which made imaging more stable, and fixed origami more strongly to the surface. We note that high pH eventually hydrolyzes the TMS surface—if there is no reason to maintain the TMS background it may be helpful (with respect to dewetting and AFM) to hydrolyze it immediately after placement (*e.g.* 2 hours at pH 9).

Each AFM image was processed using Gwyddion (`http://gwyddion.net/`). We measured binding site occupancy (percentage of sites with one or more origami), number of origami at a site (0, 1, 2, or > 3), as well as origami orientation by hand-annotating images. For global parameter optimizations, 800–1000 sites were analyzed for each of $N = 3$ independent replications. For binding site size variation, 100 sites of each size were analyzed for each of $N = 3$ independent replications. For the binding site spacing experiment ($N = 3$), the number of sites analyzed per replicate depended on the period—more than 2000 sites were analyzed for 200 nm spacing but only $\sim$100 sites were analyzed for 2000 nm spacing. For each of the optimization experiments, we have included a full data set for one of the independent replicates, so that the full range of AFM artifacts and variable quality of the AFM data can be appreciated (origami concentration, Fig. S7 to S16; Mg^{2+} concentration, Fig. S18 to S27; pH, Fig. S31 to S37; Fig. S39 to S46). For some images, origami at edges or corners are impossible to score, or an AFM artifact causes an origami in the middle to impossible to score. In these cases auxillary AFM images are used annotate a site—the 'retrace' image, adjacent and overlapping AFM fields, and occasionally height images were all used.

Here we used AFM because it provides the ability to unambiguously determine the presence (or absence) of single molecules, and to determine the orientation of those molecules. We note that optical imaging could more quickly determine site occupancy, and potentially multiple binding. Origami orientation would require more complex super-resolution optical techniques.

Supplementary Movies 1–4 were taken with a Bruker Dimension Fastcan AFM, by Senli Guo, at 3 frames/second. These movies show a placement substrate after all the sites have already been occupied and so they do not capture placement at early times. Conditions were non-optimized and multiple binding is already very common. Dissociation in these movies is likely induced by the AFM tip. Red triangles indicating binding sites are oversized for clarity.

Movie 1 Shows two origami bound to a site. One origami falls off and the second reorients to correctly bind to the site.

Movie 2 An origami bound to a site reorients. A second origami binds and falls off.

Movie 3 An origami bound in a correct orientation remains bound. Second origami bind and fall off.

Movie 4 A 6×6 array of origami showing some reorientation and tip-induced dissociation of origami. It highlights the variable appearance of origami from one frame to the next under AFM imaging.

Effects and optimization of global parameters

Each experiment testing global parameters was conducted on a chip with 1,960,000 binding sites (1400 × 1400) on a square grid. The center-to-center distance between sites was 400 nm. Each experiment (from activation through binding and washing) was repeated three times using three different chips from the same wafer. To limit experimental variation to the activation / binding / wash process, a single origami stock solution was used for all experiments. Except for the experimental parameter being tested, conditions were fixed at an origami concentration of 110 pM, a Mg^{2+} concentration of 35 mM, a pH of 8.35, and an incubation time of 60 minutes in a 5 mM Tris buffer.

1. **Origami concentration, 55–440 pM (Figs. S7–S17).** We report all concentrations as 'nominal' since solutions are obtained by serial dilution to a concentration at which they can no longer be measured by UV spectrophotometry. We suggest that, in practice, for a new batch of origami, quality of placement should be measured for a higher nominal concentration (*e.g.* 175 pM) and the dilution factor for optimal behavior should be determined based on the binding site occupancy and multiple bindings observed. Alternatively, testing placement for three concentrations around 110 pM (*e.g.* 110±25 pM) should allow quick optimization of placement behavior.

2. **Mg^{2+} concentration, 25–80 mM (Figs. S18–S28).** We observed a large change in placement behavior between 25 mM and 35 mM Mg^{2+} on substrates patterned with binding sites, and wondered whether such a sharp transition could be observed on unpatterned substrates (*i.e.* under a less stringent binding condition wherein origami do not have to encounter and orient to a binding site). Fig. S29 shows that the same sharp transition in binding holds for unpatterned substrates (albeit for a shorter 20 minute incubation at an elevated origami concentration of 500 pM). Thus the sharp transition is not an artifact of nanofabrication, nor of the additional constraints imposed when origami stick to binding sites.

3. **pH, 7.1–9.2 (Figs. S31–S38).** At pH values lower than 8, the quality of AFM imaging decreased markedly. This might be attributed to poor adhesion between orgami and the substrate, or reduced interaction between the tip and the surface. We do not believe that the small amounts of Na^{+} from NaOH used to elevate pH significantly affected binding site occupancy because experiments measuring origami binding to unpatterned SiO_2 showed that origami do not bind the surface below 3 M NaCl, and at 3 M NaCl, only a few origami were observed to bind. We note that we chose to include an image taken at ph 9.1 to represent an example of total hydrolysis of the TMS background for Fig. 3h because this image was of higher quality than our highest pH data taken at pH 9.2

4. **Incubation time, 5–480 minutes (Figs. S39–S47).** The moment of the first buffer wash is taken as the final time point of the incubation.

Effects and optimization of spatial parameters

1. **Binding site size variation (Figs. S49–S55)** Arrays of binding sites of varying size, from 15% to 200% of an origami edge length (127 nm), were constructed and binding of origami to these arrays at Mg^{2+} concentrations from 25 mM to 60 mM were examined. To maintain placement conditions as close to those used for global parameter optimization, we spaced binding sites 400 nm apart, and constrained the total binding area (1.37 x 10^{10} nm^2) to match that equivalent to 1,960,000 sites of standard (100%) size. Conditions were otherwise standard (110 pM origami, 5 mM Tris, ph 8.35, 60 min incubation).

   Note: Because single origami binding (Supplementary Fig. 55) events are maximized (90%) for binding sites that are slightly undersized (85–90% of a full origami edge length), it may be helpful to use such slightly undersized sites if multiple bindings cannot be tolerated. This benefit may come at some degradation to alignment quality, we have not yet studied such an effect.

2. **Binding site spacing variation (Figs. S56–S61).** Square arrays of binding sites with various periods (200 nm, 400 nm, 800 nm, and 2000 nm) were constructed, as well as large square patches of activated area (117 microns on a side, here referred to as 0 nm period arrays). Again, to maintain placement conditions as close to those used for global parameter optimization, we constrained the total binding area to match that equivalent to 1,960,000 standard sites (1.37 x 10^{10} nm^2). Conditions were otherwise standard (110 pM origami, 35 mM Mg^{2+}, 5 mM Tris, ph 8.35, 60 min incubation).

   Warning: In light of our results showing greatly decreased site occupancy from 400 nm to 200 nm, it is important to note that it may be difficult or impossible to optimize placement conditions on a single chip if it contains arrays of different period, especially for closely-spaced arrays.

Comparison of Placement and Langmuir adsorption kinetics

Our initial model for the process of placement was very similar to Langmuir adsorption, and thus we sought to compare their kinetics. Langmuir adsorption is a simple model in which "adsorbate" molecules, O, (*e.g.*, gas or solute molecules) bind to "adsorbent" binding sites $\mathrm{B_{surface}}$ in dynamic equilibrium:

$$\mathrm{O} + \mathrm{B_{surface}} \underset{\mathrm{k_d}}{\overset{\mathrm{k_a}}{\rightleftharpoons}} \mathrm{OB_{surface}} \tag{1}$$

.

Here $\mathrm{k_a}$ is the adsorption rate constant, and $\mathrm{k_d}$ the desorption rate constant. The Langmuir adsorption model makes the following assumptions:

1. Molecules are adsorbed in a monolayer at discrete binding sites, with one molecule per binding site.
2. All binding sites are equivalent (*e.g.* same binding strength).
3. Binding sites are distributed uniformly across a flat surface.
4. Adsorbed molecules are immobile on the surface.
5. There are no interactions between adsorbed molecules.

The existence of multiple origami binding is incompatible with the first assumption but under standard placement conditions, for times less than an hour, few multiple bindings are observed. Kinetics are measured with respect to surface coverage (θ) defined as the fraction of total binding sites which are occupied by adsorbed molecules. Because we do not observe significant desorption of origami, the rate of change of surface coverage is a function of adsorption only:

$$[d\theta/dt]_{\mathrm{a}} = \mathrm{k_a}[\mathrm{O}](1-\theta) \tag{2}$$

When solved this yields simple exponential growth for surface coverage:

$$\theta = 1 - e^{-\mathrm{k_a}[\mathrm{O}]t} \tag{3}$$

Fitting this equation to experimental data from origami nanoarrays (Fig. S64), we find that there is a reasonable fit ($\mathrm{R}^2 = 0.95$ and $\mathrm{RMSE} = 5.9\%$, using least squares, where the largest s.e.m. error bars span $\sim 15\%$), and that the kinetics of binding for placement could be considered to be consistent with Langmuir adsorption. However, our experiments on the effect of binding site spacing (Fig. 3c,d) and on large open binding sites (Fig. 3g,h) demonstrate that origami adsorption on binding sites is a much more complex process than simple Langmuir adsorption—origami are not immobile on the surface and thus the spacing of binding sites and nonuniform arrangement of binding sites greatly affects surface coverage. The lesson here is that systems which break fundamental assumptions of the Langmuir model can be hard to distinguish from Langmuir adsorption if only the kinetics of binding are considered.

Simulations of nanoarray formation

Code for both 3D and 2D simulations is given in the zip archive `nn506014s_si_006.zip`. In our code, the term "filling fraction" is used to mean the number of sites with single origami bound. Multiple binding is not modeled so this quantity is also equivalent to binding site occupancy. When unzipped and untarred:

1. The script for Fig. 62b is in `Solutiondiffusion/ScriptFillingFractionPlot.m`.
2. The script for Fig. 62c is in `Solutiondiffusion/ScriptImgAverage.m`.
3. The script for Fig. 62e is in `SurfaceDiffusion/ScriptFillingFractionPlot.m`.
4. The script for Fig. 62f is in `SurfaceDiffusion/ScriptImgAverage.m`.

Each script includes two sets of parameters. First, a set of parameters used to generate the actual figure in question. These are commented out because the scripts take a long time to run with these parameters. Second, a set of "demo" parameters are given, which are used if the scripts are run without modification. These allow the qualitative behavior of the simulations to be viewed much more quickly.

3D diffusion in solution

Our 3D simulations model placement under the assumption that diffusion occurs only in 3D, that collisions with the background are nonadsorptive, and that collisions with binding sites result in almost irreversible adsorption (Supplementary Fig. 62a). Repeated simulations (10 times) of this model for different spacings of binding sites, from close-packed (period 0) up to nine lattice sites between binding sites (period 9) show that the kinetics of binding is not affected by the spacing of binding sites (Supplementary Fig. 62b). The spatial distribution of bound origami on close-packed sites (period 0), shown as a probability map averaged over 25 repetitions of the simulation, is spatially homogeneous (Fig. 62c). We summarize various features of the 3D simulation:

1. The size of an $M \times M$ array of binding sites is user-defined ($M =$`NumberOfBS`).
2. A single period, or a series of periods, defining the set of different spacings to be simulated is user-defined (`PeriodOfBindingSites`). Periods are defined in terms of the difference in index between adjacent binding sites in an array, rather than the number of lattice sites between binding sites (as above). Thus a "period 0" array described above has a period of 1 in our simulation code. The maximum period to be simulated is P.
3. An $N \times N \times N$ lattice of positions is initialized with $N = C \times M \times P$ where $M \times P$ is the width of the region of lattice sites dedicated to the binding array, for the largest period being examined. C is a multiplier that defines the width of the simulation relative to the width of the binding array, and it is used to define how much background area outside of the binding array there is. The width of the simulation dedicated to background is $(C-1) \times M \times P$. We have used $C = 2.5$ for large M (*e.g.* 20), and $C = 3$ for smaller M (*e.g.* 10).
4. The number of origami (`nOriSolution`) is taken to be $F \times N^3$ where F is a user-defined fraction of the number of simulation sites. We have used $F = 0.01$ for Supplementary Fig. 62b, and $F = 0.02$ for the faster demo simulation.
5. The number of time steps T for the simulation is user-defined (`TimeSteps`).
6. The number of repeats of the simulation is user-defined (`Repeats`).
7. Whether or not video of the simulation is to be output is toggled with a flag (`Video`) taking the value 0 (off) or 1 (on).

8. For each of T simulated timesteps, the simulation cycles through each origami. If the origami is not on a binding site, it is moved in a random direction for a random distance (in each of X, Y, and Z directions, the origami is moved a normally distributed distance with mean 0 and standard deviation `diffusionStep3D`). Periodic boundary conditions are enforced in X and Y dimensions, while absorptive or reflective boundary conditions are enforced in the Z dimensions as appropriate. If the move calculated for an origami would put it in an already occupied lattice position, the origami does not move. If an origami is on a binding site, then it is moved off the binding site (randomly, as above) with a probabilty of $1/O$ =1/100,000 as defined by the parameter $O =$ `OFF_Rate`.

2D diffusion on a surface

Our 2D simulations model placement under the assumption that the background exhibits irreversible binding for origami, and that all origami immediately bind the surface at either background or binding sites when solution is applied to a chip. Our 2D simulations further assume that origami diffuse freely background lattice sites, but that collisions with binding sites are irreversible, or "nearly irreversible" (Fig. 62d). Repeated simulations (10 times) of this model for different spacings of binding sites, from close-packed (period 0) up to nine lattice sites between binding sites (period 9) show that the kinetics of binding are profoundly slowed as the spacing between binding sites decreases (irreversible binding to sites, Supplementary Fig. 62e). The spatial distribution of bound origami on close-packed (period 0) sites, shown as a probability map averaged over 25 repetitions of the simulation, is spatially inhomogeneous with an enhanced probability of origami binding near edges and corners of the binding site array (nearly irreversibly binding to sites, Fig. 62f). For the latter simulation, completely irreversible binding resulted in arrays with the property that: (1) origami-bound interior sites all derived from random placement of origami on the surface during initialization and (2) all other occupied sites occurred in the first layer of binding sites at the very edge of the array. Thus we repeated the experiment with the rate constant for origami leaving a binding site set to a value 200 times lower than the rate constant for origami leaving background sites. This allowed slow diffusion of origami within close-packed arrays, and allowed origami to move beyond the first layer at the very edge of the array, towards the interior. This is reflected in the probability map (Fig. 62f) by a more diffuse band around the edge of the array. Our 2D simulation is essentially similar to the 3D simulation except:

1. Origami move on an $N \times N$ lattice.
2. The number of origami in the simulation is $F \times N^2$.
3. Origami move more simply, taking random steps a single unit distance in strictly the X dimension, or strictly the Y dimension.
4. Each timestep, origami on binding sites in the simulation for Supplementary Fig. 62e are moved with probability 0. Origami on binding sites in the simulation for Supplementary Fig. 62f are moved off with probability 1/200.

Evidence for 2D diffusion: binding to large activated squares

Based on the prediction of 2D diffusion simulations, we examined the binding of origami to large activated squares (Supplementary Fig. S63) with edge lengths of 500 nm, 1 μm, 2 μm, and 5 μm, to see if we could observe spatially heterogeneous binding to the squares. Chips with activated squares were incubated for 30 minutes, with conditions that were otherwise optimized for placement on arrays of triangular sites (5 mM Tris, 35 mM Mg^{2+}, pH 8.35, 110 pM origami).

Spatial heterogeneity was strongest in the case of the largest square (5 μm, Supplementary Fig. S63d). Thus we repeated the 5 μm experiment 25 times. For each image (7.5 μm$\times$ 7.5 μm, 2560 $\times$ 2560 pixels) we measured the position of every origami (thus localizing each origami to a 2.9 nm $\times$ 2.9 nm region) using ImageJ to generate a map like that in Supplementary Fig. S63e. 25 of these maps were averaged to give a coarse probability map (Supplementary Fig. S63f) which was then smoothed with a 1 μm moving window to yield the probability map in Supplementary Fig. S63g (main text Fig. 3h), which gives the probability of finding an origami in each 2.9 nm $\times$ 2.9 nm region. The smoothing of Supplementary Fig. S63f creates a nonzero probability of finding an origami just outside of the 5 μm square, rounds corners, and creates other artifacts but the localization of origami towards the edges and corners of the square is much more easily observed in Supplementary Fig. S63g than in Supplementary Fig. S63f.

Optical imaging (Supplementary Fig. S63h) provides another way to visualize the spatial heterogeneity of origami binding to large square sites, in this case 20 μm across. Averaging of 12 such images yields a probability map (Supplementary Fig. S63i) similar to that generated by AFM in (Supplementary Fig. S63g). Optical imaging is much faster than AFM and the diffraction limited optics provide smoothing, but because we have not correlated intensity with an actual number of origami on the surface, the probability map can only capture relative, rather than absolute probabilites of observing origami at a given site.

A few observations relevant to 2D *vs.* 3D diffusion. First, we observe that there is a large excess of origami, relative to the activated binding area on the chip. Our optimized placement protocol involves applying 20 μL of 110 pM DNA solution to a chip. This means that $\sim$1.3 billion origami are applied to $\sim$ 2 million binding sites, so that there are 675 origami for each binding site. (Also, chips with binding sites of different sizes or large squares have been constructed to have the same activated area as chips with standard arrays.) Thus if diffusion to/from sites occurs exclusively from solution, origami concentration should, in principle, be minimally changed by addition to a placement chip.

Second, we observe that the area of weakly-sticky passivated TMS background is large relative to the total amount of origami. The footprint of a 20 μL drop on a chip is a circle 5 mm in diameter, which is 1400$\times$ the area of the binding sites—more than twice the total area of the origami in solution. Thus the TMS background could easily bind *all* of the origami, confining them to 2D and preventing any 3D diffusion.

Third, we observe that a significant fraction of the origami applied to a chip *are* bound to the TMS background after an hour of incubation. We studied the adsorption of origami to TMS-silanized chips without binding sites. Fig. 3e, shows an unpatterned, TMS-silanized chip after a 60 minute incubation with 1 nM origami (10$\times$ the usual concentration of origami)—no origami are visible. However, after ten buffer washes to remove all origami from solution above the chip, the TMS was hydrolyzed and a high density of origami was observed by AFM (Fig. 3f): 90 origami were present over an area equal to that of 456 origami, a coverage of 20%. Our conclusion is that AFM-invisible origami were weakly bound to the TMS, that they withstood ten buffer washes, and that they were immobilized by TMS hydrolysis. If *all* the origami present in a standard experiment bound, then the coverage would be 675/1400 or 48% of the area exposed to solution. Thus 20%/48% or 42% of total number of origami usually applied (4.2% of the total applied in this particular experiment) were bound weakly to the TMS surface. In this case, we do not think that the amount of origami bound to the surface is proportional to the concentration—*i.e.* that a standard concentration of origami would have yielded 10-fold fewer origami. This is because when the standard concentration of origami was incubated at high pH, a similar coverage of the surface (21%, Fig. 2h, pH 9.1) was observed. (Because TMS hydrolyzes quickly at this pH, during the origami binding, the experiment in Fig. 2h does not have bearing on whether origami bind to a TMS surface.) The fact that 100% coverage is not observed in Fig. 3f (when enough origami were applied to cover the surface 5$\times$), and 48% coverage is not observed in Fig. 2h at pH 9.1 could be due to the vigorous washing that the chip undergoes to get rid of origami in solution—many weakly-bound origami may be removed by washing.

AFM, combined with washing and TMS hydrolysis, is a tedious and indirect way to measure TMS-bound origami. Further, this method may still fail to observe the most weakly-bound origami since they may fall off during washes. To quantitatively understand TMS background binding and subsequent 2D diffusion in our system, different techniques which can directly measure the kinetics of origami binding to the TMS background will have to be used. Optical imaging of fluorescent origami in TIRF seems like the best candidate.

Placement on amine-functionalized binding sites (Method 2)

As one alternative to using Mg^{2+} in conjunction with negatively-charged binding sites, we created placement substrates having positively-charged, amine-functionalized binding sites. Standard chips (with 1,960,000 binding sites) were fabricated and activated with O_2 plasma as usual, but were next amine-functionalized with aminopropyl silatrane [7] (APS): chips were incubated for 2 minutes in a 0.1% solution of APS in phosphate buffer (10 mM phosphate, ph 8.5, used because otherwise 0.1% APS solution is so basic that the trimethyl silyl background can be hydrolyzed). Origami were bound to positively charged arrays from phosphate buffered saline (PBS, 10 mM phosphate, 150 mM, Na^+, pH 8.35, 110 pM origami, 60 minute incubation). Most binding sites are occupied with aggregates of multiple origami, and individual origami are only rarely resolved (Fig. S65). Thus the amine-functionalized sites are too sticky for origami.

One approach would be to perform placement at higher pH: at a pH of 10.5–11, amines on binding sites should begin to become protonated, and the binding sites should become less sticky and in principle might bind single origami with good alignment. However, DNA itself begins to denature [8] around pH 11.5, and the passivated background hydrolyzes quickly above pH 9. A high pH-stable passivation method would be necessary for this approach.

Two other approaches to better placement on positive binding sites include the tuning of binding strength *via* mixed positive/neutral silane layers (to decrease binding site charge), or the addition of solution anions (to partially screen binding site charge). Both deserve to be further explored.

Microcontact printing onto aminated substrates (Method 3)

To realize the benefits of both Mg^{2+}-based placement and amine-functionalized surfaces, we combined the methods using microcontact printing. Origami nanoarrays were placed on standard chips under conditions with slightly higher Mg^{2+} (42.5 mM Mg^{2+}, pH 8.35, 110 pM origami, 5 mM tris, 60 minutes incubation). This 'master' substrate was imaged to verify the quality of the nanoarray, and then dried using the ethanol drying procedure described above.

In parallel, a second unpatterned SiO_2 substrate (the 'copy') was activated with O_2 plasma, incubated with 0.1% APS (in water, no buffer was needed since no passivated background was present) for 20 minutes and sonicated in DI water. Master and copy chips were pressed together, face to face, and clamped together with a 1.25 inch-wide binder clip. The chips were then immersed in (1) 10 mM phosphate buffer, pH 7.2 for 5 minutes and (2) DI water for 30 minutes. At the end of the 30 minute water incubation, the chips were separated while still under water. The copy chip was then imaged under $1\times$ PBS buffer (Fig. S66).

Note: The website `http://home.fuse.net/clymer/buffers/phos.html` is a useful tool for calculating the components of phosphate buffer as a function of desired pH and buffer strength.

Post-placement covalent immobilization with CDAP (Method 4)

To couple origami triangles covalently to placement sites, we functionalized them with an average of 10 amines at 15 sites along their inner edges (Fig. 67, page 3). After placement, we treated these amine-functionalized origami with an agent that would crosslink them to surface silanols. In our first protocol, we made use of 1-cyano-(4-dimethylamino)pyridinium tetrafluoro borate (CDAP, Sigma-Aldrich) which cyanylates surface silanols. The resulting cyano groups are subject to immediate attack from the amines on the origami, which form covalent isourea bonds. After performing our optimized placement protocol:

1. Buffer wash the chip (8×, 60 μL each wash) into MOPS-Mg^{2+} buffer (5 mM MOPS buffer, 250 mM $MgCl_2$, pH 7.0.)
2. Put the petri dish containing the chip on ice in an ice bucket, and let the chip cool for 10 minutes.
3. Make CDAP solution. In a 2 ml eppendorf tube, add 250 mg of CDAP to 1.5 ml of MOPS-Mg^{2+} buffer. Dissolve fully and use fresh or a precipitate will form.
4. Make coupling solution (50% acetonitrile, 50% CDAP solution v/v): mix equal volumes of CDAP solution and acetonitrile.
5. Pipette 60 μL of coupling solution onto the 20 μL of buffer already on the chip. (Mg^{2+} will be $\sim$150 mM.)
6. Incubate for 10 minutes on ice.

After this procedure, the chip is ready to be washed into any solution (*e.g.* pure water) that is compatible with the isourea bond (no amine containing buffers such as Tris), or the coupling buffer (PBS forms a precipitate when mixed with Mg^{2+}-containing buffer). To move chips into a Mg^{2+}-incompatible buffer such as PBS, simply wash away the Mg^{2+} first in plain MOPS buffer:

1. Buffer wash (8 ×, 60 μL each wash) into 10 mM MOPS.
2. Buffer wash (8 ×, 60 μL each wash) into 10 mM phosphate buffer, pH 8.3, 150 mM Na^+.

Note: Literature CDAP protocols typically recommend a pH of 7.0 for coupling. The CDAP-coupled arrays shown here were coupled using MOPS-Mg^{2+} with 5 mM MOPS, 250 mM Mg^{2+} ($\sim$150 mM during coupling), at pH 7.0. However, we have achieved similar results using 10 mM MOPS, 125 mM Mg^{2+} ($\sim$80 mM during coupling), at pH 7.4, and 10 mM MOPS, 35 mM Mg^{2+} ($\sim$22 mM during coupling), at pH 8.35. To reduce buffer washes, we recommend one of these higher pH/lower Mg^{2+} protocols, or trying a previously untested buffer, depending on the final buffer pH and other conditions desired.

Note: Literature CDAP protocols report the use of triethylamine during coupling for the purpose of deprotonating alcohols (pK_a of $\sim$16) to make them appropriately nucleophilic. Here the use of triethylamine appears unnecessary for coupling to much lower pK_a silanols.

Warning: The initial washes in MOPS-Mg^{2+} are vital to remove all traces of Tris which would poison the coupling reaction. A single buffer for placement, coupling, and downstream application would be desirable, however, we have not yet optimized placement of origami in a buffer that does not contain Tris. Placement in MOPS gives 50% site occupancy under standard optimized conditions and it might serve as such a universal buffer. PBS forms a precipitate with Mg^{2+}.

Post-placement covalent immobilization with CTES/EDC (Method 4)

To couple origami triangles covalently to placement sites, we functionalized them with an average of 10 amines at 15 sites along their inner edges (Fig. 67, page 3). After placement, we treated these amine-functionalized origami with an agent that would crosslink them to surface silanols. In our second protocol, origami binding sites are silanized with carboxyethylsilanetriol (Gelest, disodium salt, 25% w/v in water Catalog # SIC2263.0) to yield carboxylic acid groups. Amines on the origami are coupled with these carboxylic acid groups to form highly stable amide bonds using EDC [1-Ethyl-3-(3-dimethylaminopropyl)carbodiimide] catalysis. After performing our optimized placement protocol:

1. Prepare 1% CTES stock solution in water. This solution is stable for months.
2. Buffer wash (8×, 60 μL each wash) into fresh CTES silanization buffer: 0.01% CTES in 10 mM Tris, 35 mM Mg^{2+}, pH 8.3 (*e.g.* mix 10 μL 1% CTES stock solution into 990 μL buffer). Incubate for 2 minutes.
3. Buffer wash (8×, 60 μL each wash) into 10 mM MOPS buffer with 125 mM Mg^{2+}, pH 8.1. (This removes all CTES.)
4. Buffer wash (8×, 60 μL each wash) into coupling buffer: 50 mM EDC, 25 mM sulfo-NHS, in 10 mM MOPS, pH 8.1, 125 mM Mg^{2+}. Incubate for 10 min.

After this procedure, the chip is ready to be washed into any solution (*e.g.* pure water) that is compatible with the coupling buffer (PBS forms a precipitate when mixed with Mg^{2+}-containing buffer). To move chips into a Mg^{2+}-incompatible buffer such as PBS, simply wash away the Mg^{2+} first in plain MOPS buffer:

1. Buffer wash (8×, 60 μL each wash) into 10 mM MOPS, pH 8.1, 150 mM Na^{+}.
2. Buffer wash (8×, 60 μL each wash) into 10 mM phosphate buffer, pH 8.3, 150 mM Na^{+}.

Note: This protocol has not been optimized but we expect that it will be robust to a wide range of buffer conditions, and variations of the protocol. For example, CTES/EDC coupling also works well with a lower Mg^{2+} coupling buffer (35 mM Mg2+, 5 mM MOPS, pH 8.3, 30 mM EDC, 15 mM sulfo-NHS). Because EDC/sulfo-NHS activation is reported to work best at lower pH (4.5–7.2) and the further coupling of NHS-activated carboxyl groups is reported to work best between pH 7 and 8, these steps are sometimes performed separately. Here, the use of a single elevated pH of 8.1 for both reactions *in situ* on the placement substrate does not seem to adversely affect coupling. Here we have used ∼10 amines along the inner edge of the triangle, a position which should make them available for surface coupling whether or not the triangles land rightside-up or upside-down. We have not tested whether the position of these amines affects covalent immobilization or subsequent stability to AFM, nor do we yet know how many amines are required for immobilization.

Warning: Too high a CTES concentration (0.1%), or too long a CTES incubation results in removal of origami from the surface. While silanization by CTES in the central triangular hole of the origami provides carboxylic acid groups for the covalent coupling of amines on the origami to the surface, carboxylation of the surface under the origami (at high CTES concentrations or long incubation times) may disrupt the silanol-Mg^{2+}-origami bonds which hold them to the surface.

CTES-mediated placement. For all CTES/EDC-immobilized origami presented here, the above protocol was used to carboxylate the surface *after* placement. However, it is possible to carboxylate the surface *before* placement, similar to the amine functionalization presented on page 17. Starting from an O_2-plasma activated and resist-stripped chip:

1. Clean the chip with IPA.
2. Incubate the chip in 0.1% w/v CTES solution in 10 mM Tris, pH 8.0 for 10 min. (Higher CTES concentration yields better silanization. Here it is applied *before* origami placement and no Mg^{2+} is present in solution to cause preciptitation.)
3. Sonicate in DI water for 1 minute.
4. Blow dry with N_2 (or compressed air) and bake at 120°C for 10 minutes.
5. Place origami (with lower 12.5 mM Mg^{2+}, if desired) and proceed to step 3 of coupling procedure above.

CTES-carboxylated chips allow placement of origami at low Mg^{2+} (12.5 mM Mg^{2+}, 5 mM Tris, pH 8.3) and, presumably because carboxyl groups have $pK_a<5$, at low pH (7.2 with 12.5 mM Mg^{2+} in 5 mM Tris; 7.0 with 35 mM Mg^{2+} in 10 mM MOPS). We have not yet optimized CTES-mediated placement, but it is our preferred method for covalent coupling because it significantly decreases post-placement processing which can decrease quality of placement (in particular the CTES silanization.)

Troubleshooting

Problem	Likely cause	Solution
Site occupancy below 90%.	• Old chip with inactive sites. • Low origami concentration. • Short incubation time. • Low Mg^{2+} or pH, esp. if site occupancy $<$30%.	• Chips work best $\leq$24 hours after activation. • Use $\sim$100 pM origami. Prepare dilution fresh. Use Lo-Bind tubes. • Incubate origami for an hour. • Use $\geq$35 mM Mg^{2+}. • Use pH 8.3–8.5.
High multiple binding.	Primarily: • High origami concentration. • Long incubation time. • Oversized features. Secondarily: • High pH. • High Mg^{2+}.	First try: • Use $\sim$100 pM origami. • Keep incubation between 30 and 90 min. • Look at features in resist by SEM and adjust e-beam write (feature size, dose) and/or minimize O_2 activation time. Second try: • Keep pH in the range 8.3–8.5. • Use 35 mM Mg^{2+}.
Poor alignment of origami with few multiple bindings.	• High pH. • High Mg^{2+}.	• Keep pH in the range 8.3–8.5. • Use 35 mM Mg^{2+}.
High background binding. • Whole or partial origami on background in AFM. • Unstable AFM, *e.g.* whole scanlines of identical value ("scars"). • For fluorescent origami, high background under optical imaging.	• Poor initial TMS quality. • TMS hydrolyzed by high pH. • TMS hydrolyzed by long incubation. • Failure to wash weakly bound origami from TMS.	• Dehydrate the wafer by baking before *and* after TMS formation. • Keep pH$<$9 preferably in the range 8.3–8.5. • Keep incubation between 30 and 90 minutes. • Remove weakly bound origami with 8$\times$ Tween 20 washes.
Large particulates on sites but few or no origami.	• Sample dewetted or dried. Salts and origami aggregates occupy the site.	• Do not let chip dewet during origami deposition or subsequent buffer washes.
Small particles on background.	• Overbaked PMMA. • Acetate causes fine precipitate.	• Bake PMMA for 30 s at 180°C . • Use non-acetate salts/acids when preparing buffers, *e.g.* use $MgCl_2$, and HCl to adjust.
Placement requires more than 35 mM Mg^{2+}.	• Surface is too rough or improperly cleaned.	• Include HF and NH_4F cleaning steps.
AFM unstable; false engages.	• Tween 20 still present.	• Increase buffer washes until surface tension is restored.
Origami fall off during ethanol drying.	• Too much time spent in dilute ethanol $<$80%.	• Move quickly from low to high % ethanol.
Origami ball up into site during ethanol drying and corners are double height.	• Origami project onto non-sticky TMS surface.	• Hydrolyze TMS surface before drying by incubating in pH 9 buffer.

Continues on next page...

Problem	Likely cause	Solution
Origami fail to couple by CDAP method, and fall off in low Mg^{2+} buffer.	• Incomplete removal of Tris buffer before coupling. • Poor amine-labelling of origami. • Coupling time too short or coupling buffer may be old.	• Wash substrate more thoroughly before coupling. Do not subject surface to Tris or other primary amines after coupling. • Check stoichimetry, concentration, and quality of amine-labelled strands. • Make fresh coupling buffer and incubate for full 10 minutes.
Origami fail to couple by CTES/EDC method, and fall off in low Mg^{2+} buffer.	• Incomplete removal of Tris buffer before coupling. • Poor amine-labelling of origami. • Coupling time too short or coupling buffer may be old. • High concentration of CTES or CTES incubation too long.	• Wash substrate more thoroughly before coupling. It is OK to subject surface to Tris or other primary amines *after* coupling. • Check stoichimetry, concentration, and quality of amine-labelled strands. • Make fresh coupling buffer and incubate for full 10 minutes. • Check to see if origami fall off right after CTES silanization step. If so, make sure that CTES concentration is no more than 0.01% w/v and incubate for 2 minutes. Or, try CTES-mediated placement, then perform EDC coupling.
After covalent coupling, moving chip into phospate buffer causes particulates to appear.	• Incomplete removal of Mg^{2+} from coupling buffer.	• Increase number of washes in non-phosphate buffer before adding phosphate buffer.
After CTES/EDC covalent coupling (post-placement) high background binding of additional components occurs.	• High pH of CTES solution has hydrolyzed TMS (after placement).	• Use 0.01% CTES in a buffer adjusted to a pH of $\leq$8.5.
CTES-mediated placement yields binding of origami everywhere.	• High pH of CTES solution has hydrolyzed TMS (before placement).	• Use 0.1% CTES in a buffer adjusted to a pH of $\leq$8.5.
APS-mediated placement yields binding of origami everywhere.	• High pH of APS solution has hydrolyzed TMS (before placement).	• Use 0.1% APS in a buffer adjusted to a pH of $\leq$8.5.

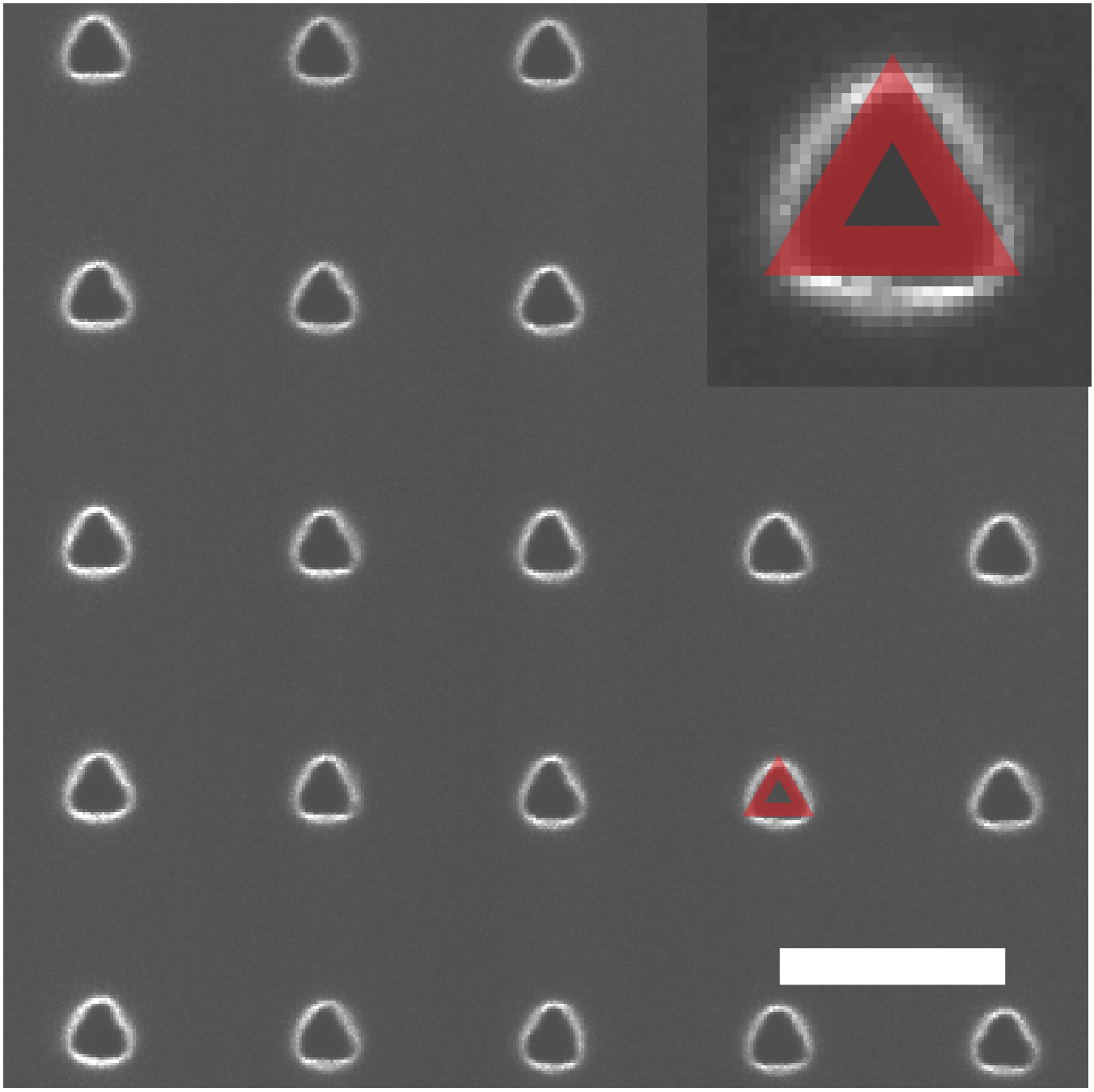

Figure S1. Verification of e-beam write quality. SEM image of a lithographically-defined pattern in PMMA resist after the resist has been developed (scale bar, 400 nm). Superimposed model of an origami (red) highlights that the proximity effect causes the corners of the equilateral triangles to be rounded with a radius of curvature of ~ 20 nm. Triangular binding sites (as features in the resist) were sized so that the edges of the binding site coincided with the with the edges of a 127 nm triangle, and the tips of the triangle project beyond the rounded corners. This sizing was chosen with the idea that alignment would be the best possible—otherwise, if binding site size were chosen to contain the entire triangle, it would be able to fit in the site with a range of orientations. To achieve 127 nm sites in the resist, 120 nm sites were written.

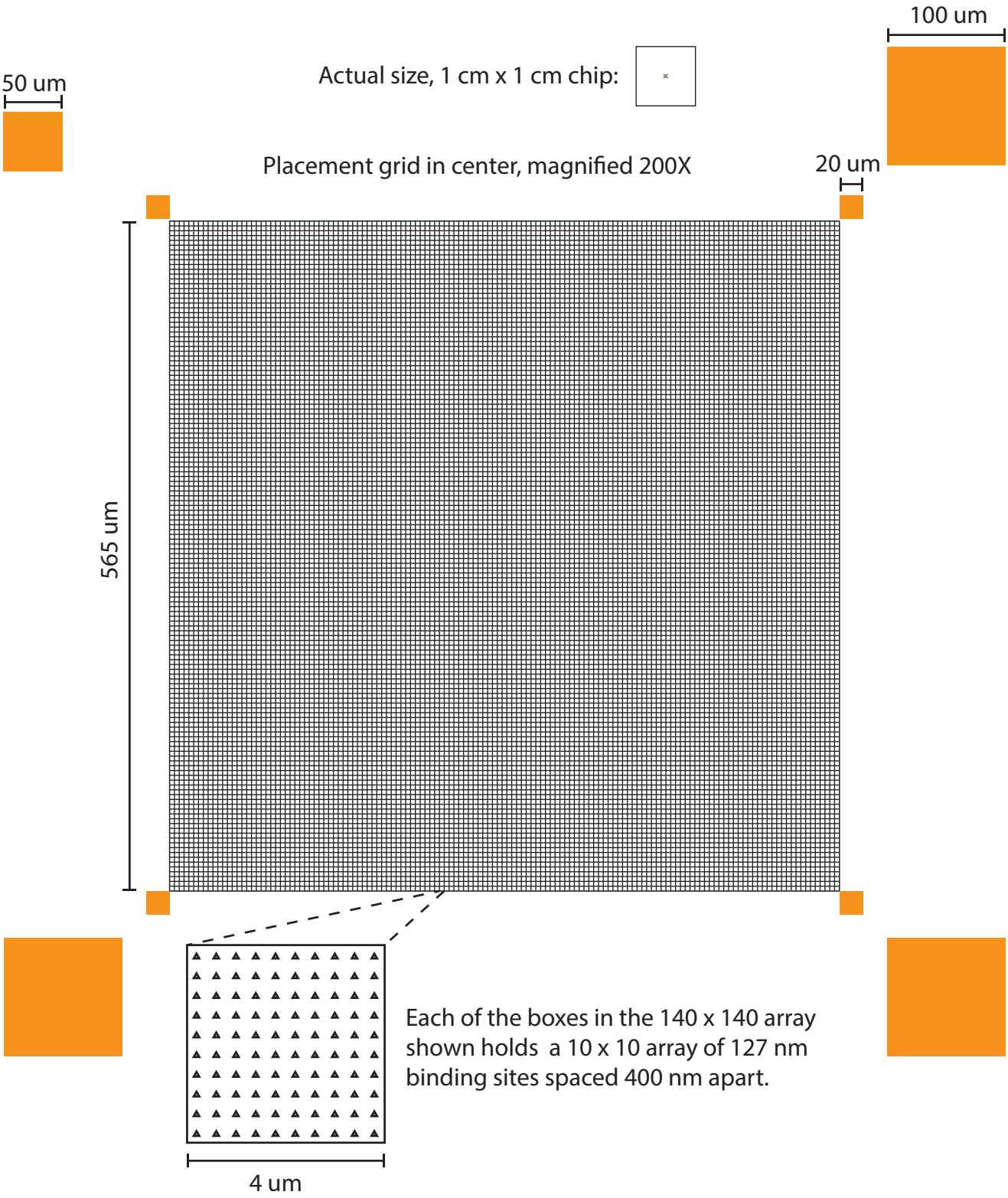

Figure S2. Schematic of a placement chip. 1,960,000 binding sites are fabricated on each chip. Fiducial markers (orange) are typically 80 nm chromium, constructed by lift-off, except when used for microcontact printing in which case they are etched depressions, 100 nm deep.

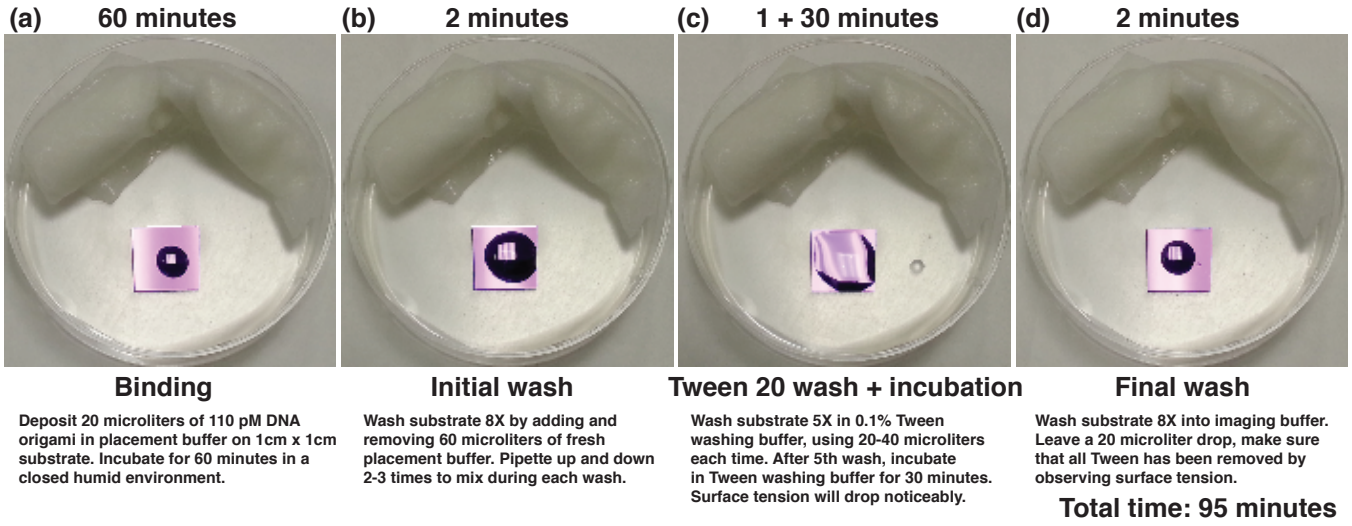

Figure S3. Protocol for origami placement. (a)–(d) provide examples of what the chip looks like at each step.

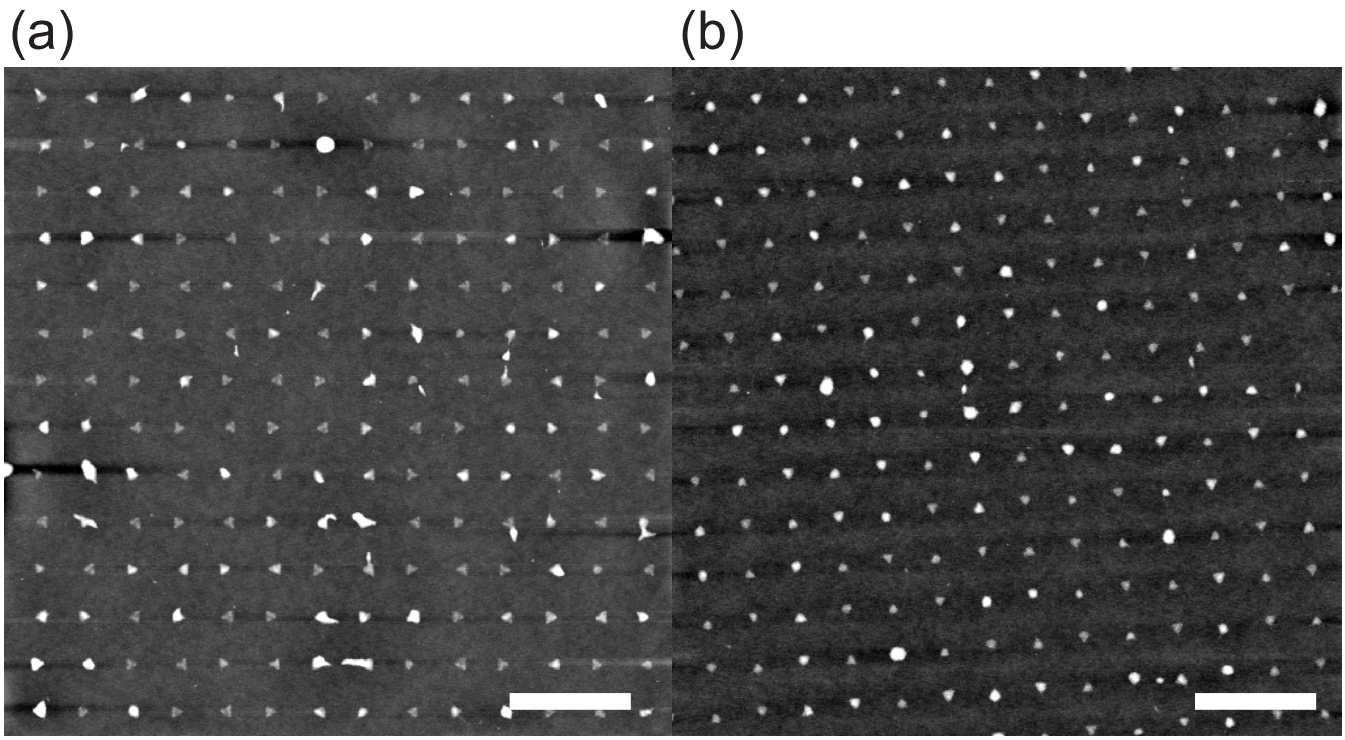

Figure S4. Dewetting artifacts. (a),(b) AFM images of two different chips that have momentarily dewetted during the buffer wash, which leads to what we believe are salt crystals (or potentially aggregates of origami and salt) on the hydrophilic origami binding sites. Scale bars, 1μm.

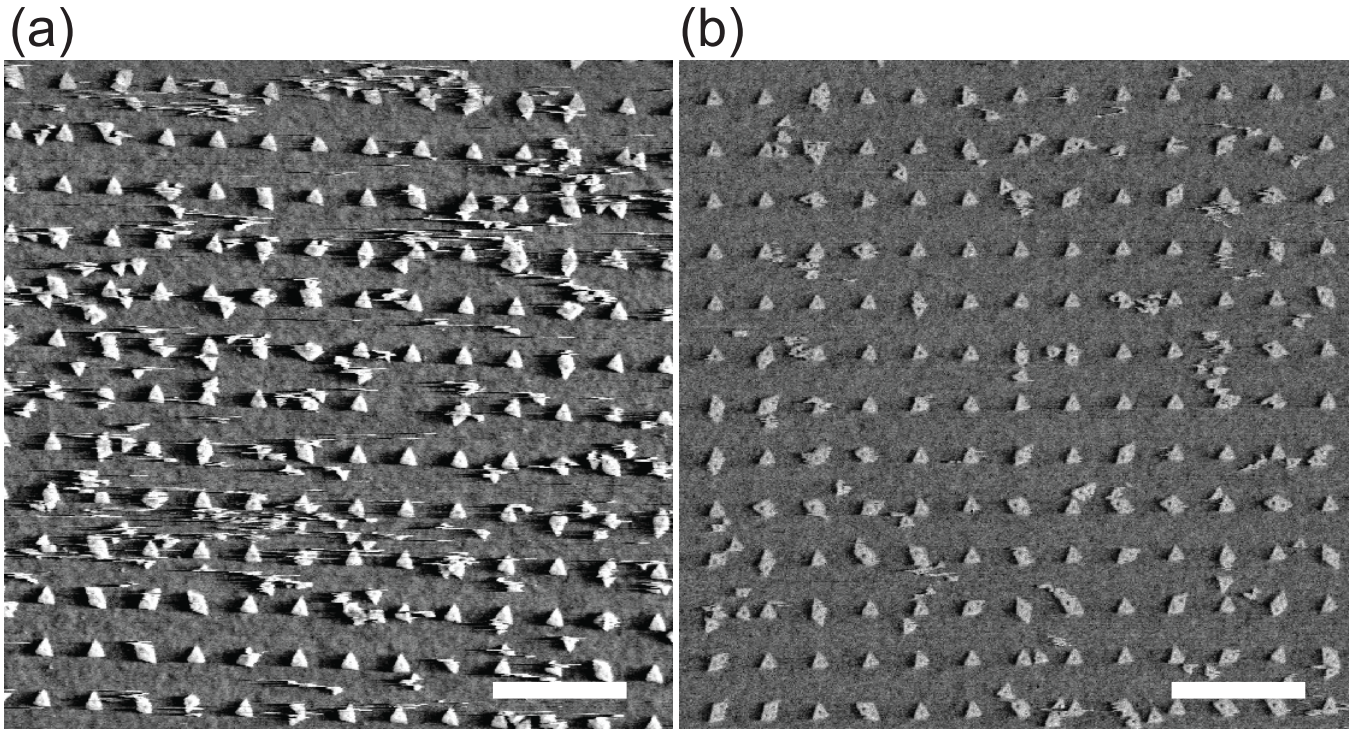

Figure S5. Preventing background binding with Tween 20. AFM image of a chip without (a) and with (b) the Tween 20 buffer wash which reduces the unintended binding of DNA origami onto the passivated background. Streaking in the background of (b) is much reduced when compared to (a). In order to exaggerate the effect over a shorter-than-usual 20 min incubation, a higher-than-optimal origami concentration (500 pM origami) and higher magnesium concentration (60 mM Mg^{2+}) were used (the buffer was 5 mM Tris at ph 8.35). Scale bar is 1μm.

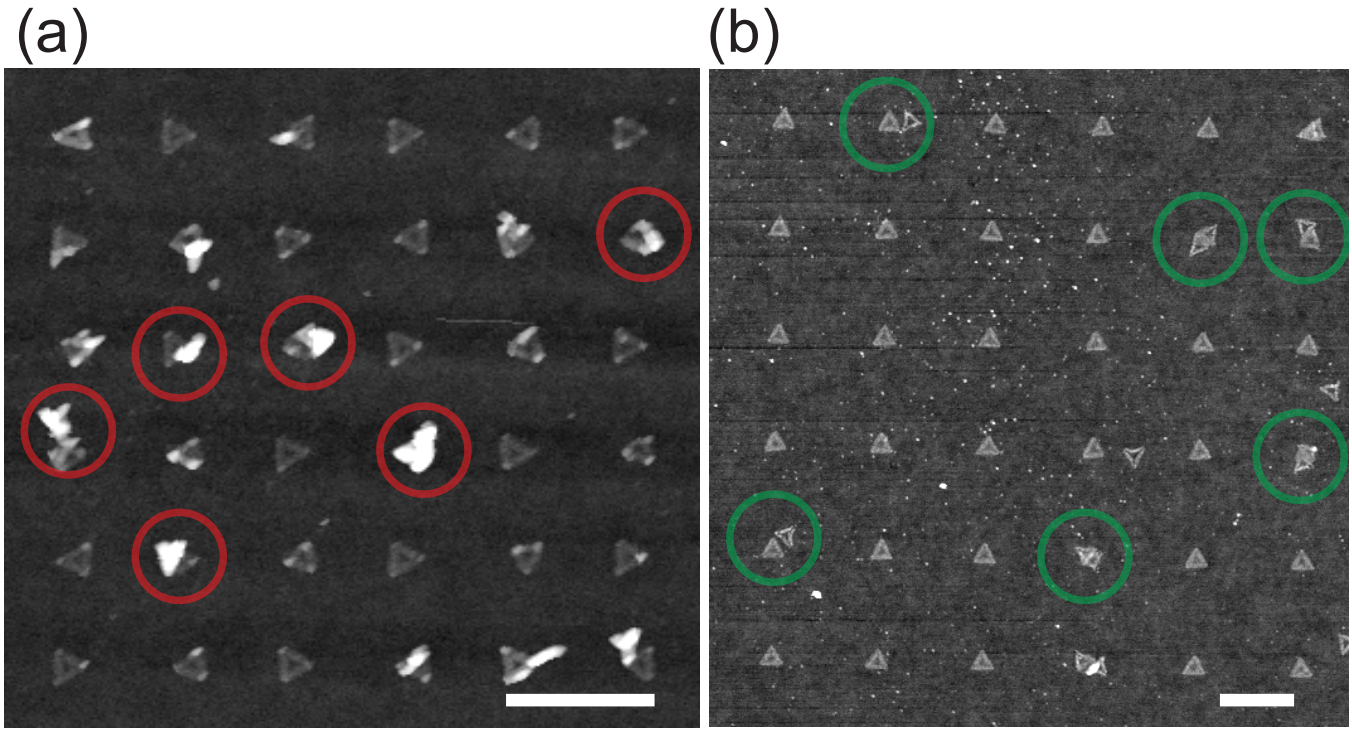

Figure S6. Dried origami arrays as a function of pH. Height images created using air tapping mode AFM of origami nanoarrays dried from pH 8.35 buffer (a) or after an additional 2 hours at an elevated pH of 9 (b). In (a), the parts of origami which extend over the passivated background are weakly bound. Thus second or third origami partially bound to a single site are drawn into the site by capillary forces and ball-up to form aggregates (red circles). The tips of individual origami which lie over the background similarly withdraw into the site upon drying and cause the corners of origami to give greater height contrast (appearing twice as thick as the rest of the origami). In (b), treatment at elevated pH has at least partially hydrolyzed the trimethyl silyl passivation later and the origami at multiply bound site are stably bound the surface. Thus little or no aggregation is observed; instead clusters of intact origami are seen (green circles). Similarly the corners of triangles are firmly bound to the surface and thus the origami present a normal shape. Scale bars: (a) 500 nm, (b) 400 nm.

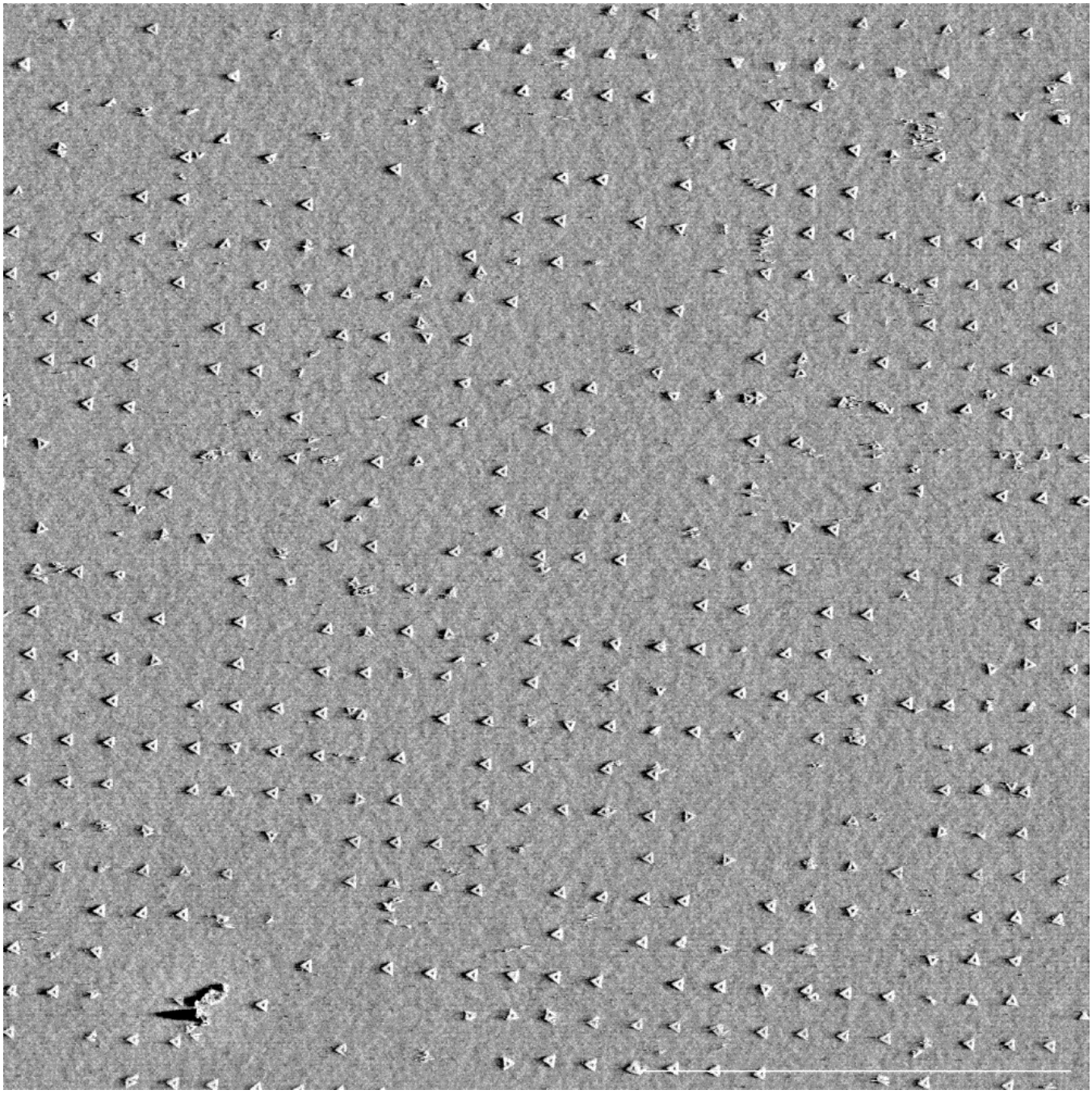

Figure S7. 55 pM origami, raw AFM. Other conditions are: 5 mM Tris, 35 mM Mg^{2+}, pH of 8.35, 60 min incubation, period of 400 nm.

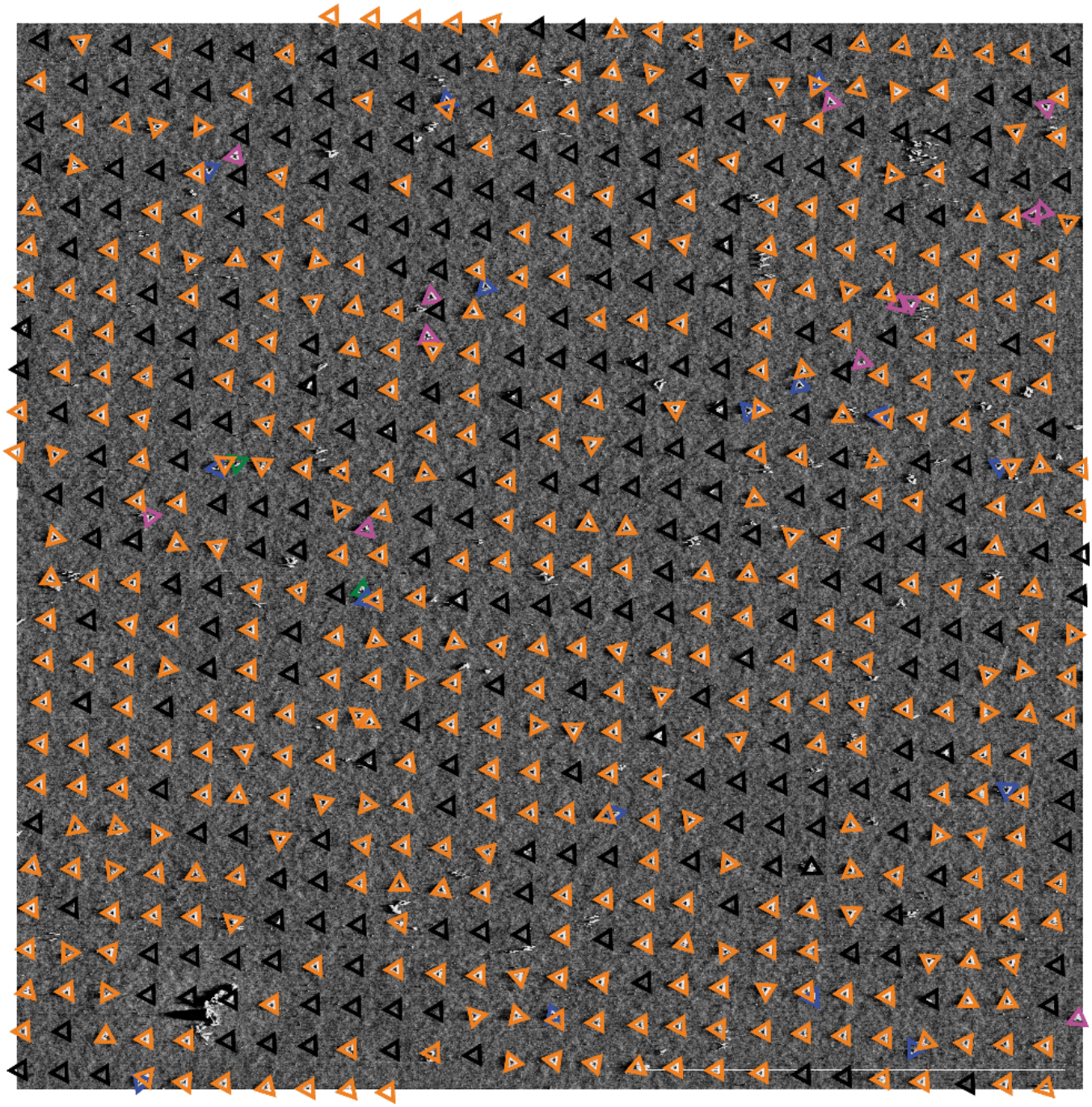

Figure S8. 55 pM origami, annotated AFM. Other conditions are: 5 mM Tris, 35 mM Mg^{2+}, pH of 8.35, 60 min incubation, period of 400 nm. Triangular outlines provide a classification of an origami and/or binding site: **empty binding site**, **first origami on a site**, **second origami on a site**, **third origami on a site**, or **origami bound to the background**.

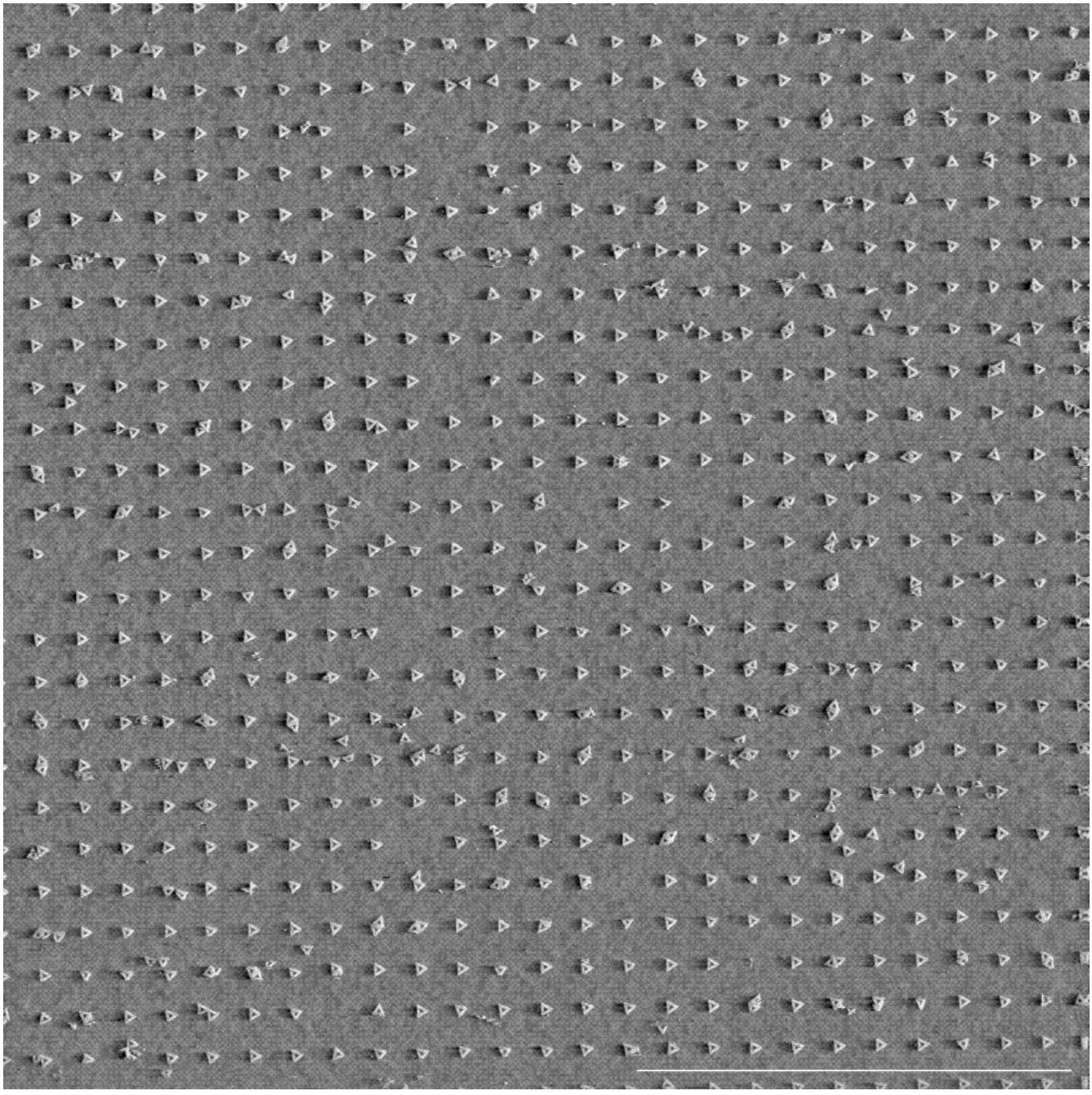

Figure S9. 110 pM origami, raw AFM. Other conditions are: 5 mM Tris, 35 mM Mg^{2+}, pH of 8.35, 60 min incubation, period of 400 nm.

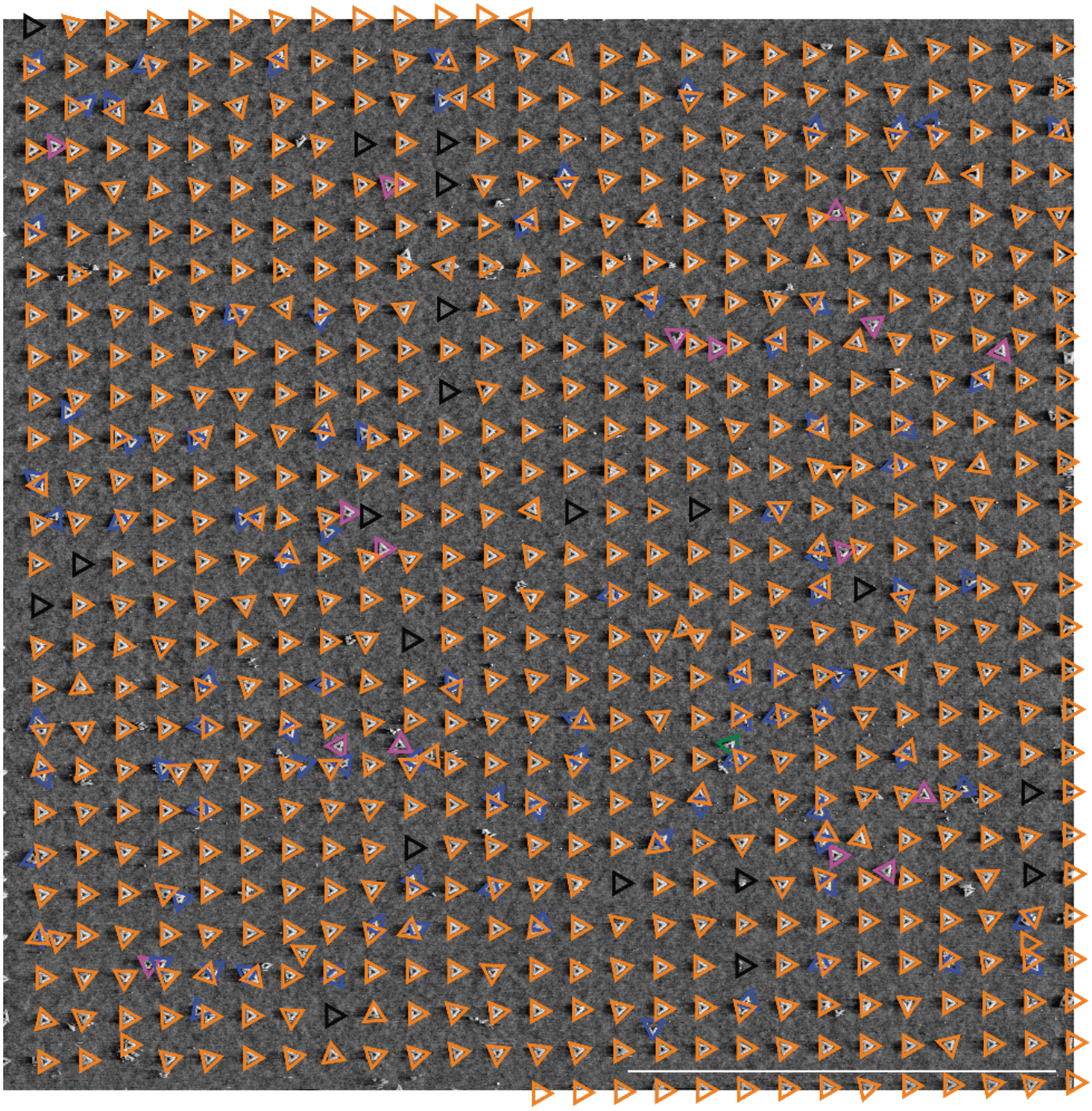

Figure S10. 110 pM origami, annotated AFM. Other conditions are: 5 mM Tris, 35 mM Mg^{2+}, pH of 8.35, 60 min incubation, period of 400 nm. Triangular outlines provide a classification of an origami and/or binding site: **empty binding site**, **first origami on a site**, **second origami on a site**, **third origami on a site**, or **origami bound to the background**.

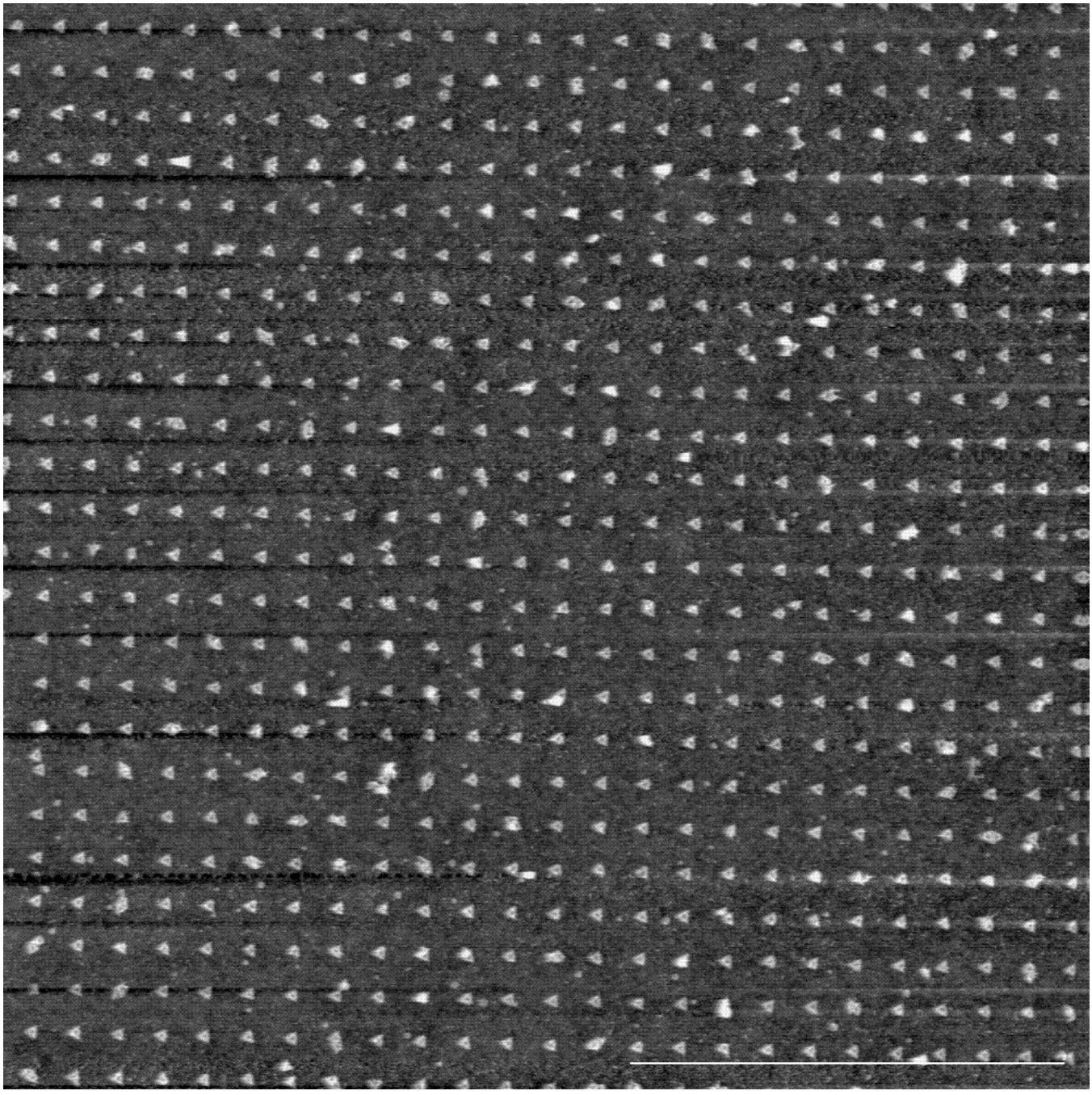

Figure S11. 175 pM origami, raw AFM. Other conditions are: 5 mM Tris, 35 mM Mg^{2+}, pH of 8.35, 60 min incubation, period of 400 nm.

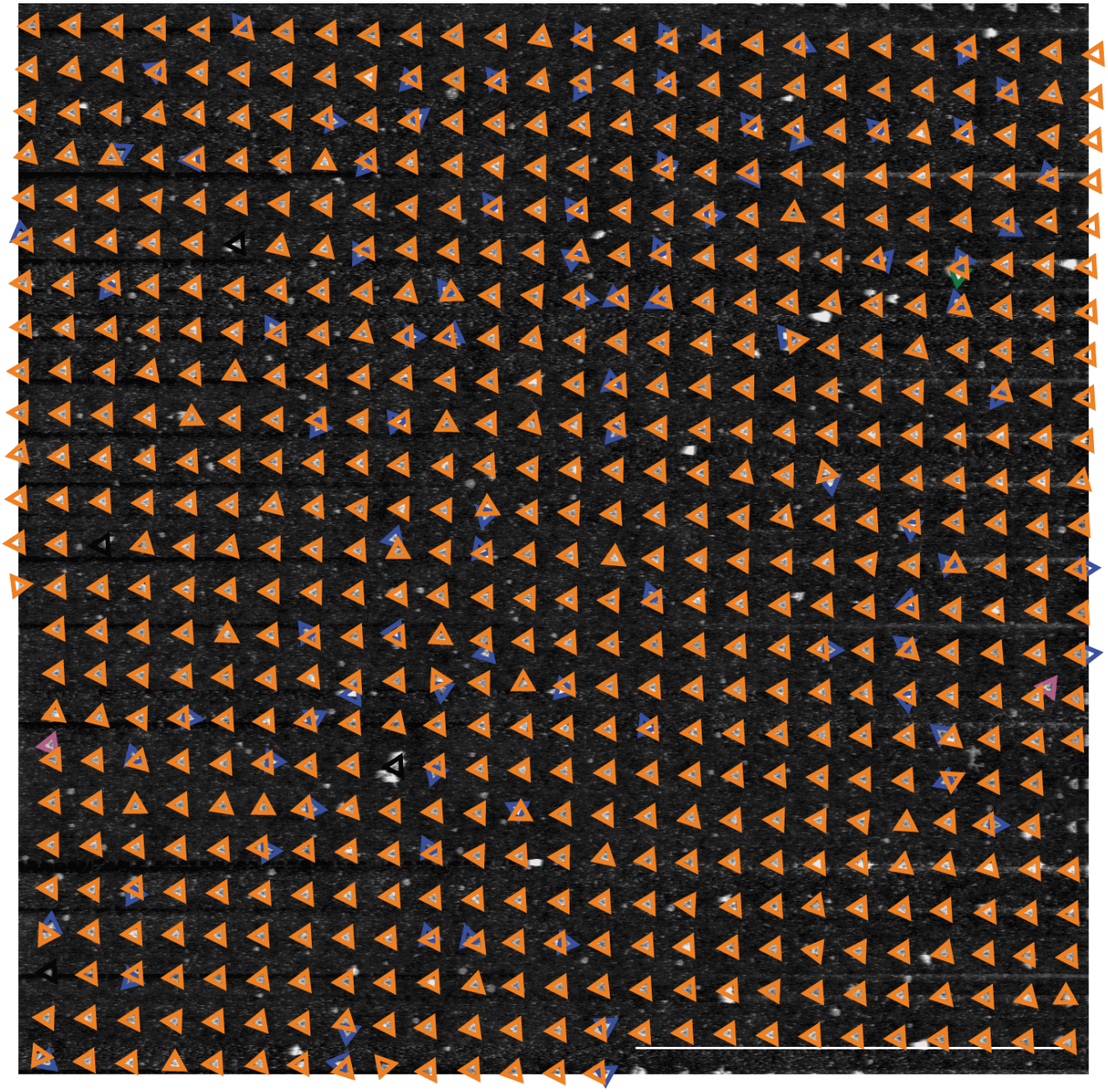

Figure S12. 175 pM origami, annotated AFM. Other conditions are: 5 mM Tris, 35 mM Mg^{2+}, pH of 8.35, 60 min incubation, period of 400 nm. Triangular outlines provide a classification of an origami and/or binding site: **empty binding site**, **first origami on a site**, **second origami on a site**, **third origami on a site**, or **origami bound to the background**.

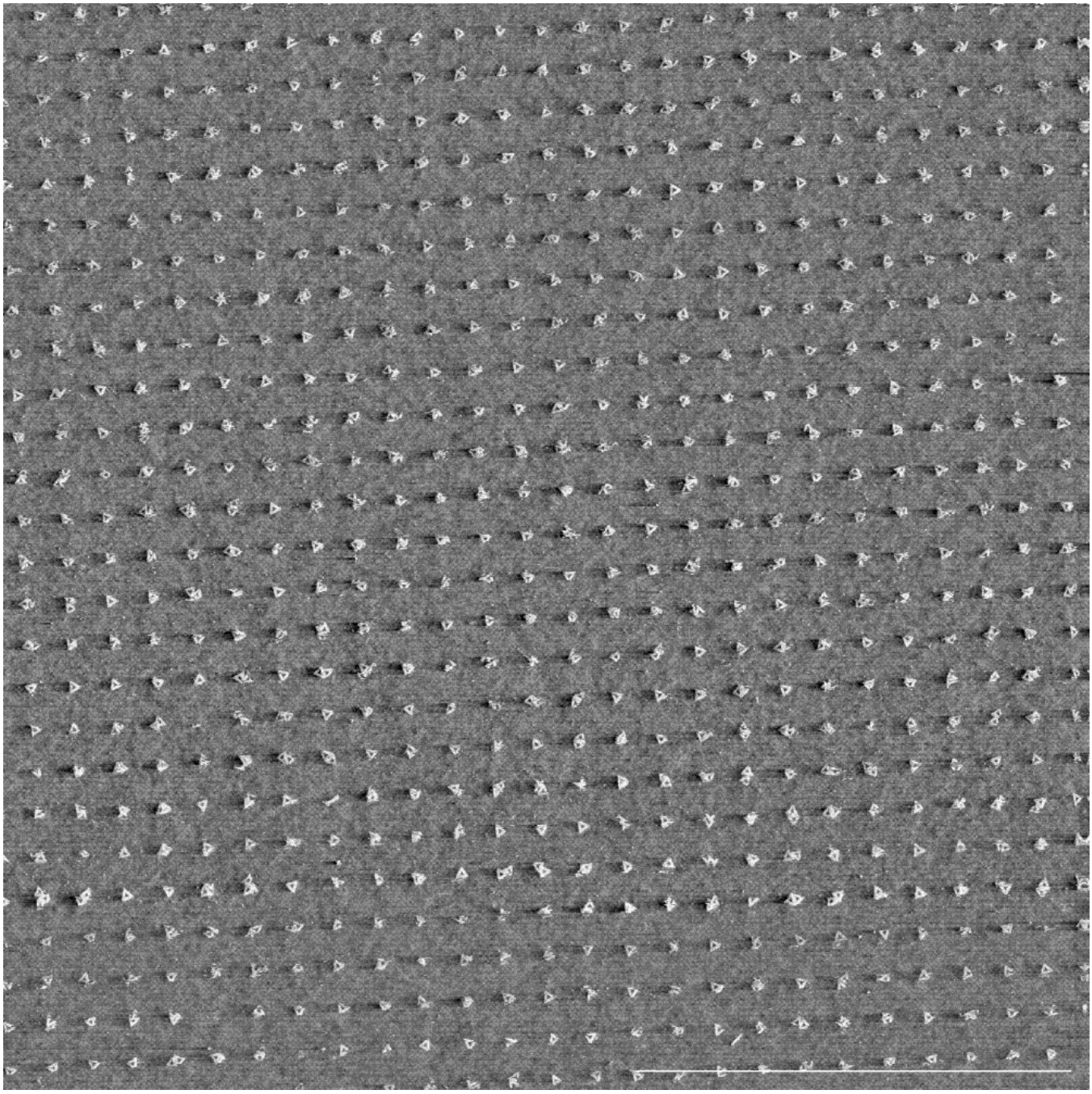

Figure S13. 220 pM origami, raw AFM. Other conditions are: 5 mM Tris, 35 mM Mg^{2+}, pH of 8.35, 60 min incubation, period of 400 nm.

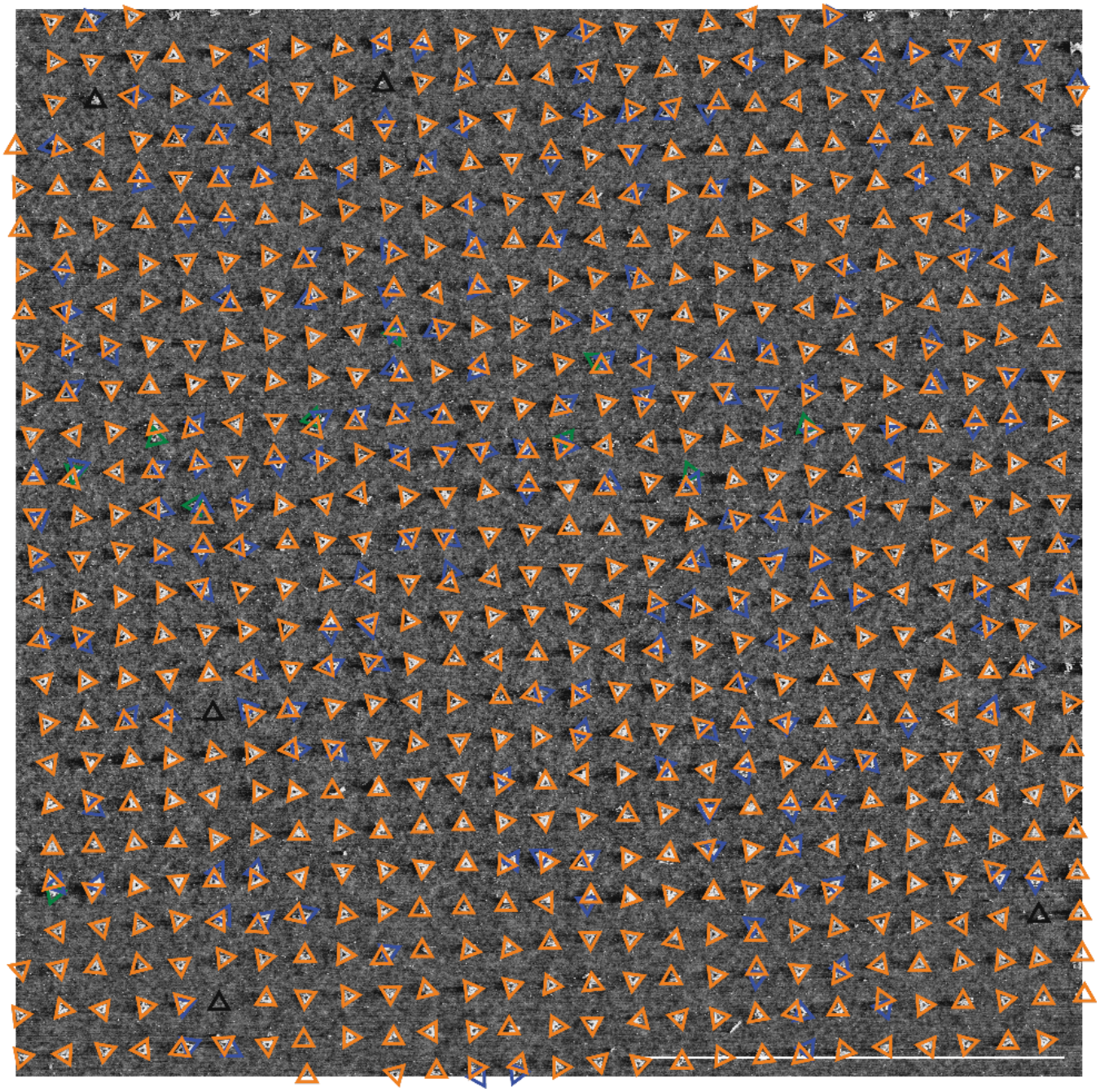

Figure S14. 220 pM origami, annotated AFM. Other conditions are: 5 mM Tris, 35 mM Mg^{2+}, pH of 8.35, 60 min incubation, period of 400 nm. Triangular outlines provide a classification of an origami and/or binding site: **empty binding site**, **first origami on a site**, **second origami on a site**, **third origami on a site**, or **origami bound to the background**.

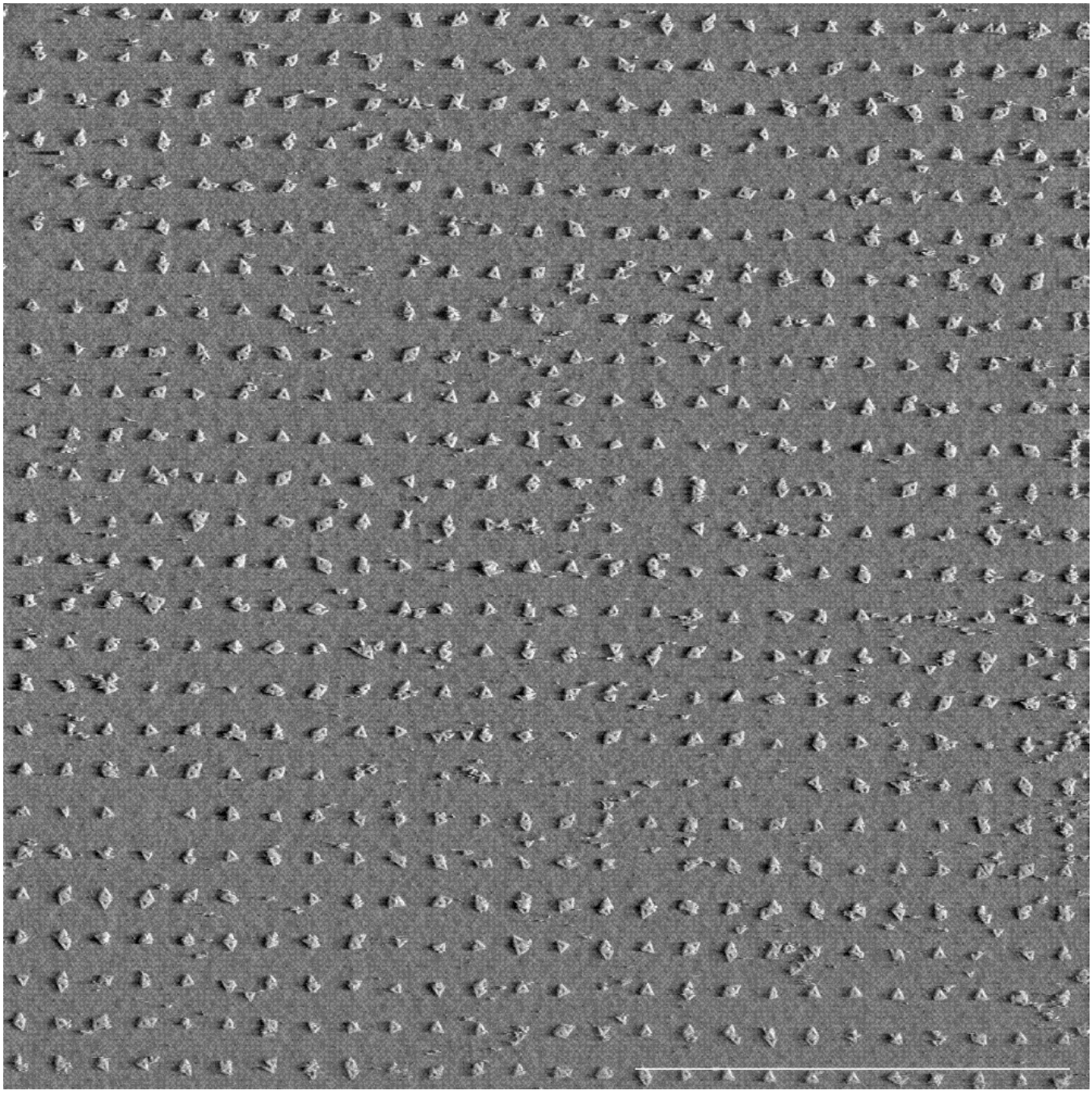

Figure S15. 400 pM origami, raw AFM. Other conditions are: 5 mM Tris, 35 mM Mg^{2+}, pH of 8.35, 60 min incubation, period of 400 nm.

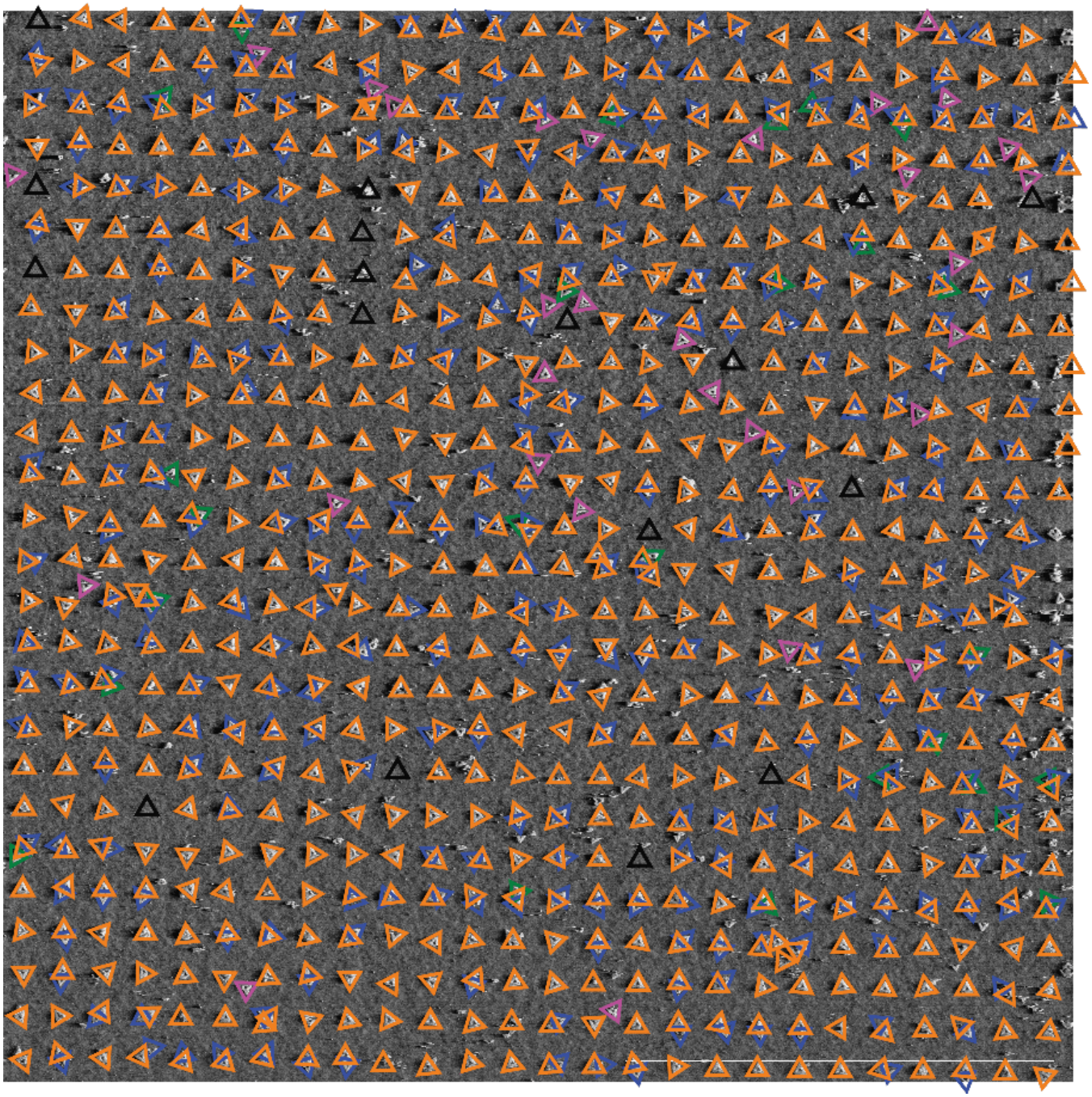

Figure S16. 400 pM origami, annotated AFM. Other conditions are: 5 mM Tris, 35 mM Mg^{2+}, pH of 8.35, 60 min incubation, period of 400 nm. Triangular outlines provide a classification of an origami and/or binding site: **empty binding site**, **first origami on a site**, **second origami on a site**, **third origami on a site**, or **origami bound to the background**.

Concentration (pM)	Filled	Single	Double	Triple	Background	Empty
55	63.25 ± 6	60.95 ± 6	2.305 ± 7	0.28 ± 0.2	1.87 ± 1	36.74 ± 3
110	97.07 ± 1.2	94.72 ± 5	2.34 ± 8	0.14 ± 0.1	2.19 ± 1	2.92 ± 2
175	99.36 ± 0.6	84.66 ± 6	14.6 ± 8	0.15 ± 0.1	0.31 ± 0.2	0.63 ± 0.4
220	99.21 ± 0.7	70.67 ± 3	28.5 ± 5	1.24 ± 1.2	0	0.78 ± 0.5
440	97.72 ± 2	55.77 ± 2	41.9 ± 4	3.95 ± 4	4.86 ± 2	2.27 ± 2

Figure S17. Results of varying origami concentration on nanoarray quality. The percentage site occupancy (with respect to number of binding sites) of origami in different states. Errors correspond to s.e.m from 3 separate experiments.

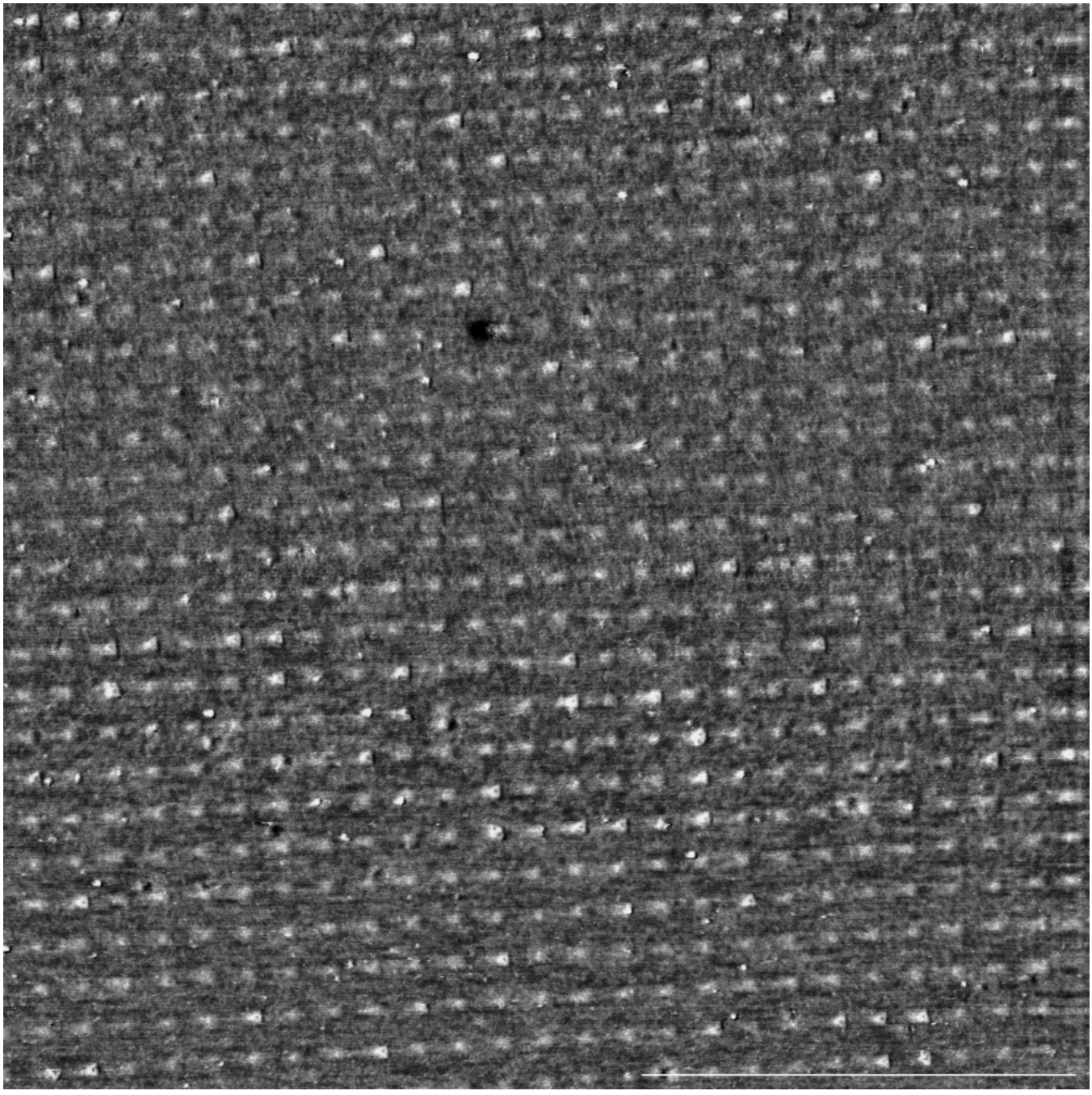

Figure S18. 25 mM Mg^{2+}, raw AFM. Other conditions are: 110 pM origami, 5 mM Tris, pH of 8.35, 60 min incubation, period of 400 nm.

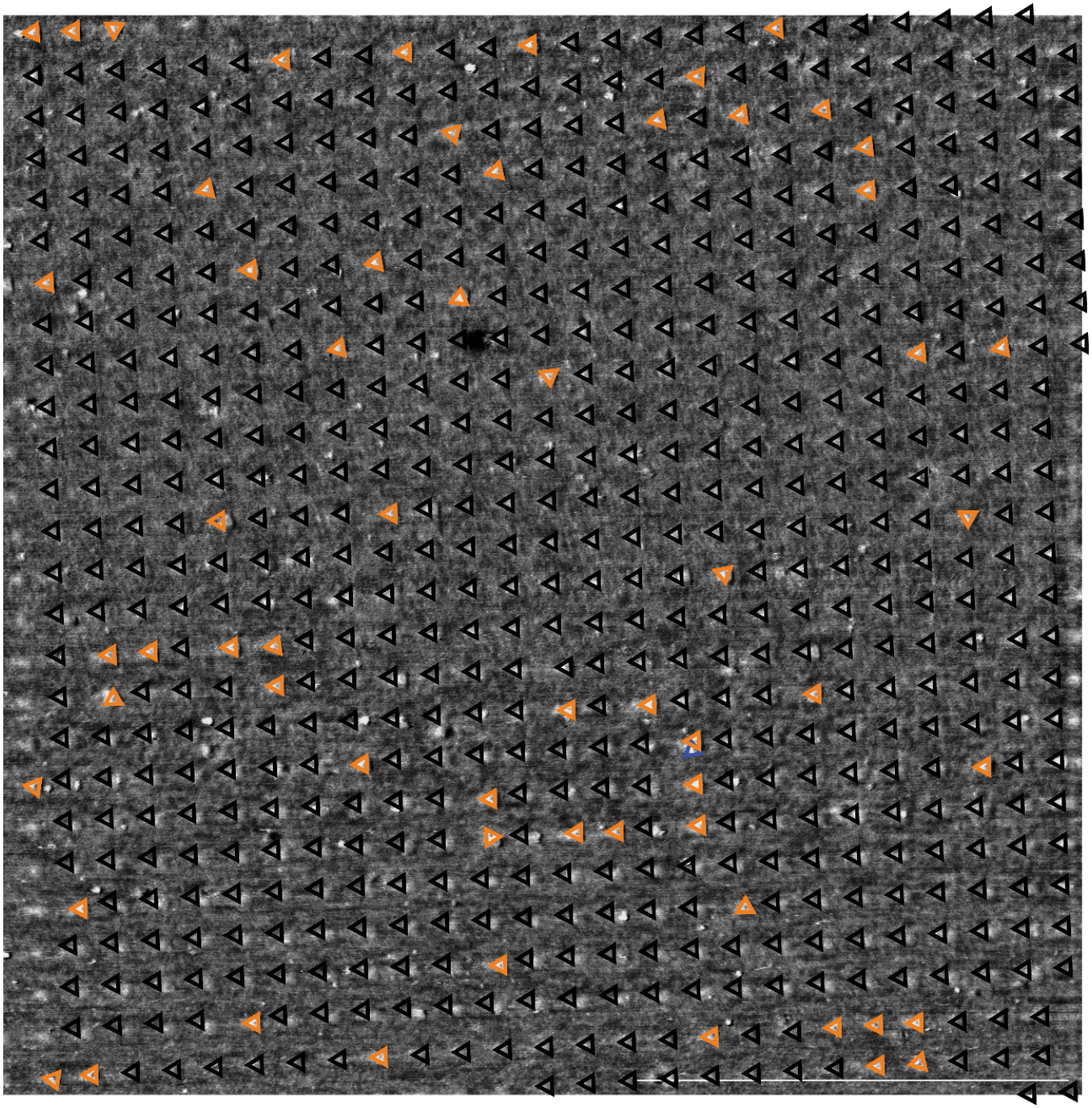

Figure S19. 25 mM Mg^{2+}, annotated AFM. Other conditions are: 110 pM origami, 5 mM Tris, pH of 8.35, 60 min incubation, period of 400 nm. Triangular outlines provide a classification of an origami and/or binding site: **empty binding site**, **first origami on a site**, **second origami on a site**, **third origami on a site**, or **origami bound to the background**.

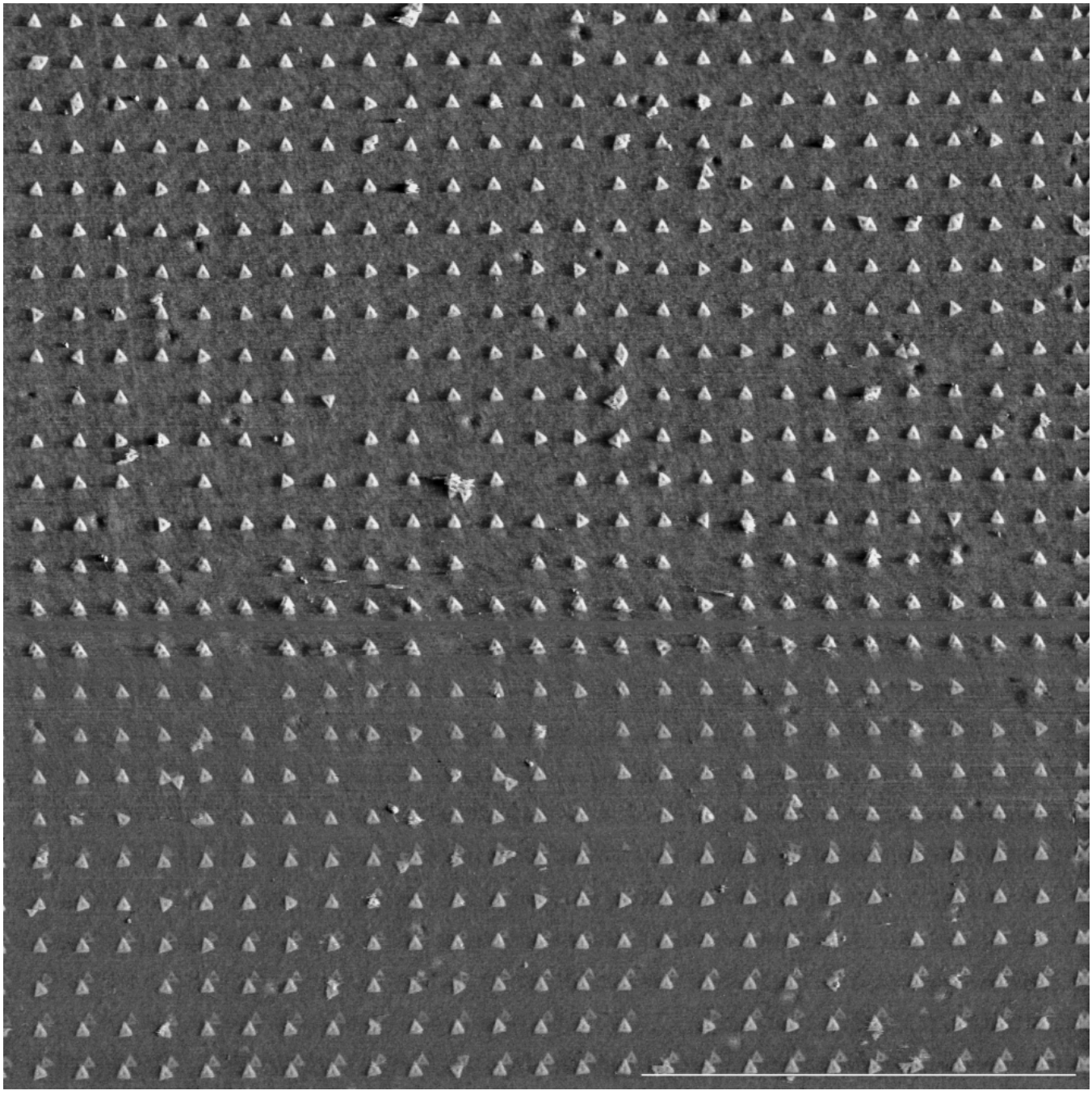

Figure S20. 35 mM Mg^{2+}, raw AFM. Other conditions are: 110 pM origami, 5 mM Tris, pH of 8.35, 60 min incubation, period of 400 nm.

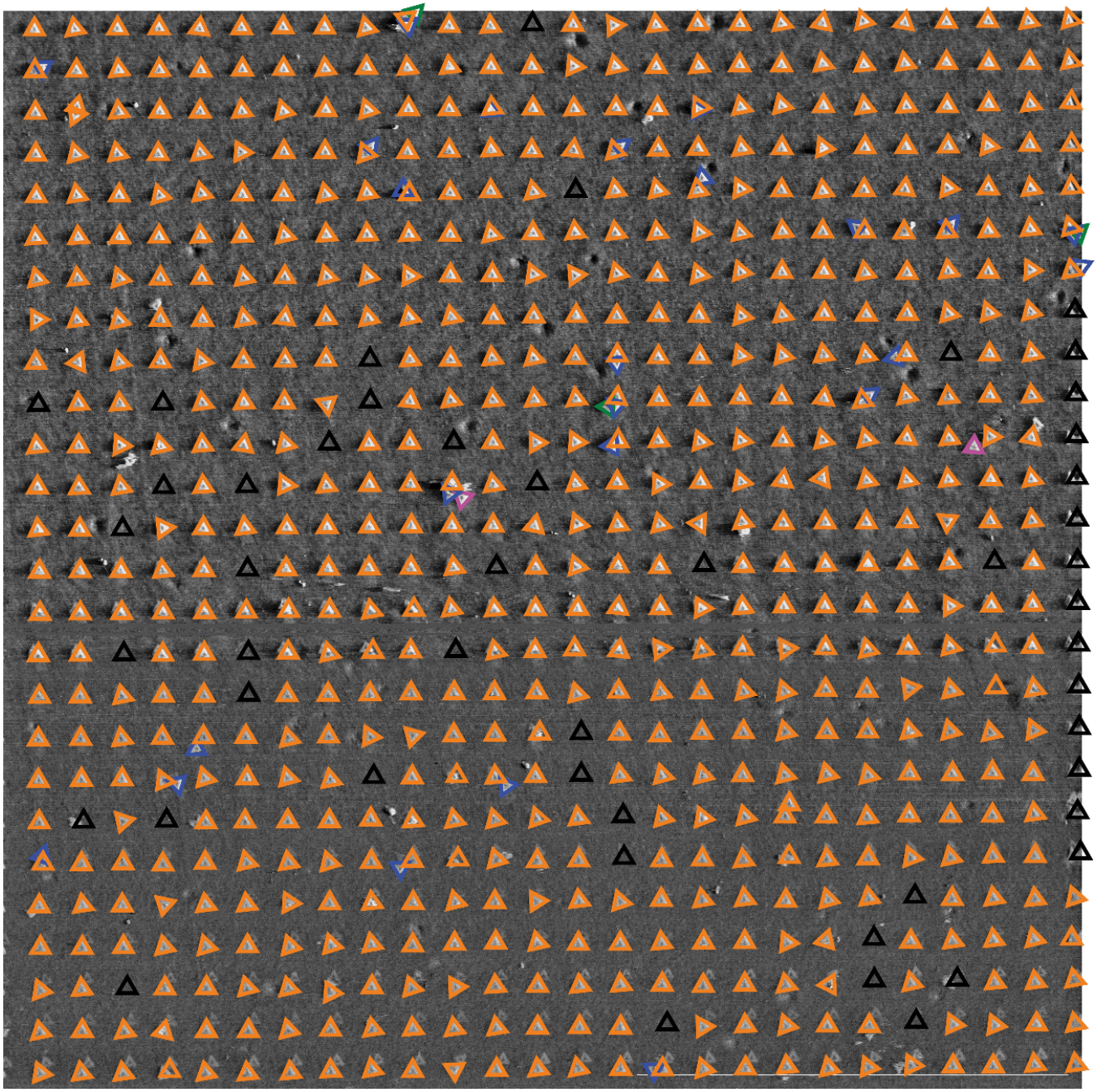

Figure S21. 35 mM Mg^{2+}, annotated AFM. Other conditions are: 110 pM origami, 5 mM Tris, pH of 8.35, 60 min incubation, period of 400 nm. Triangular outlines provide a classification of an origami and/or binding site: **empty binding site**, **first origami on a site**, **second origami on a site**, **third origami on a site**, or **origami bound to the background**.

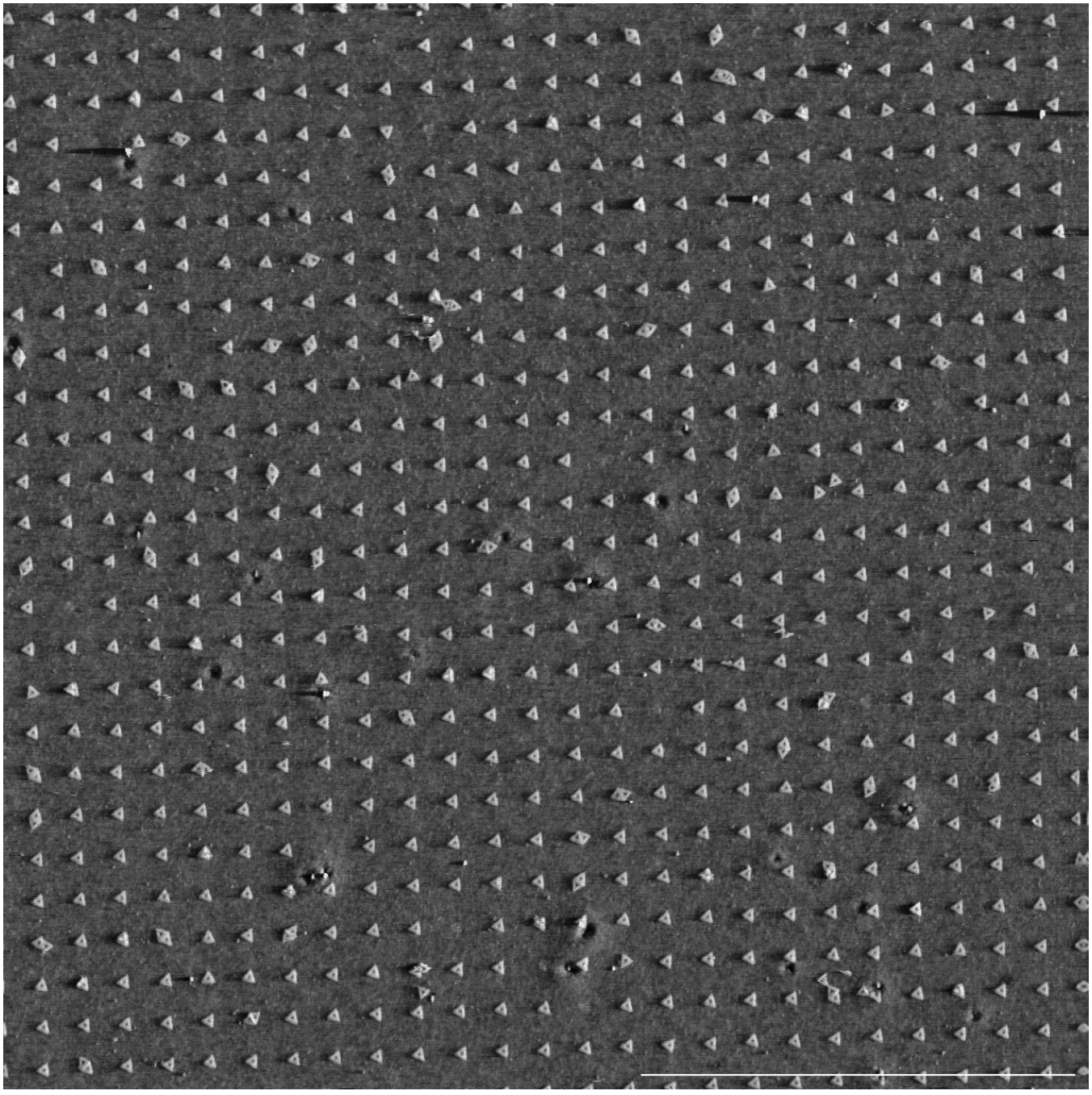

Figure S22. 42.5 mM Mg^{2+}, raw AFM. Other conditions are: 110 pM origami, 5 mM Tris, pH of 8.35, 60 min incubation, period of 400 nm.

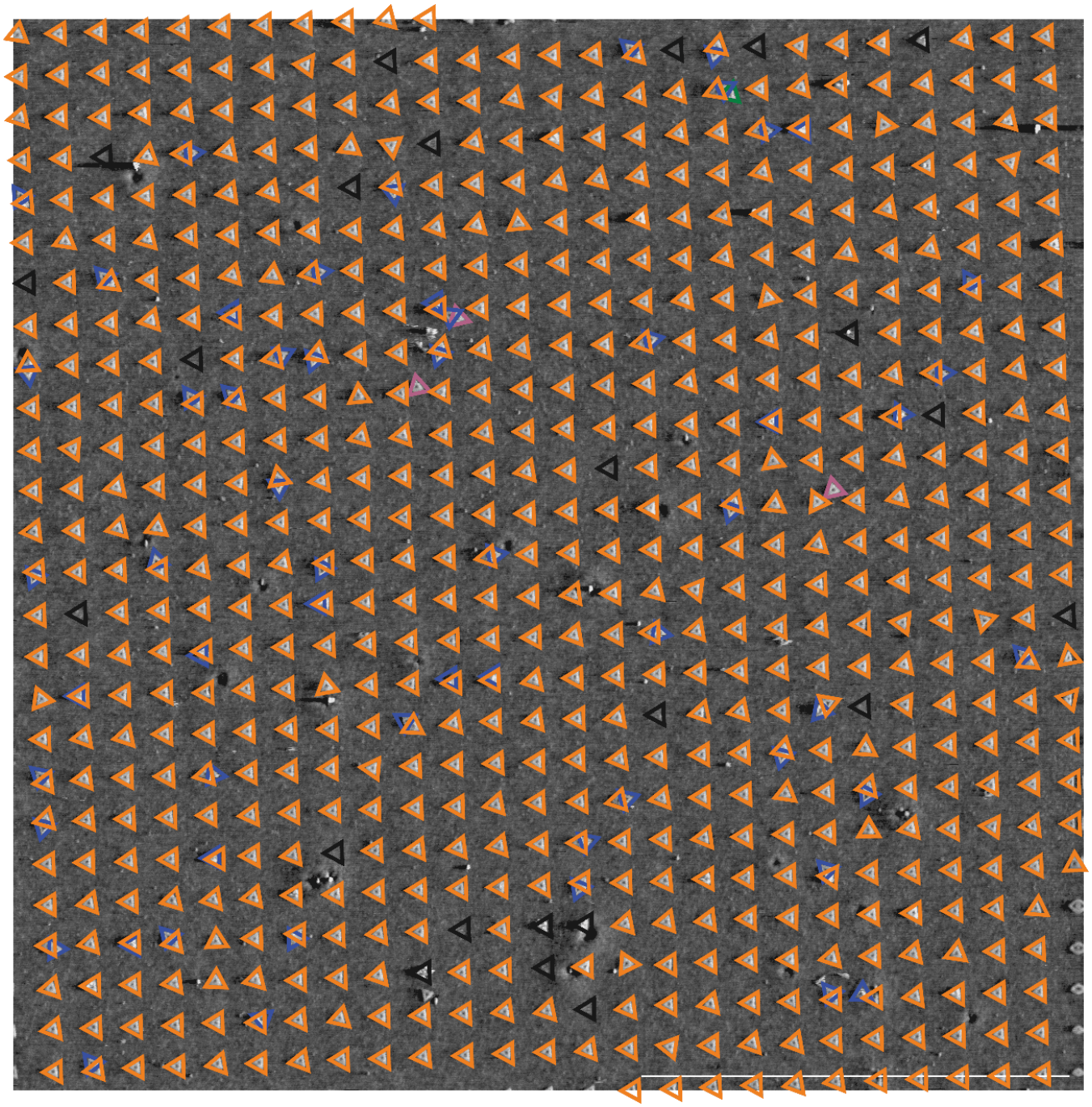

Figure S23. 42.5 mM Mg^{2+}, annotated AFM. Other conditions are: 110 pM origami, 5 mM Tris, pH of 8.35, 60 min incubation, period of 400 nm. Triangular outlines provide a classification of an origami and/or binding site: **empty binding site**, **first origami on a site**, **second origami on a site**, **third origami on a site**, or **origami bound to the background**.

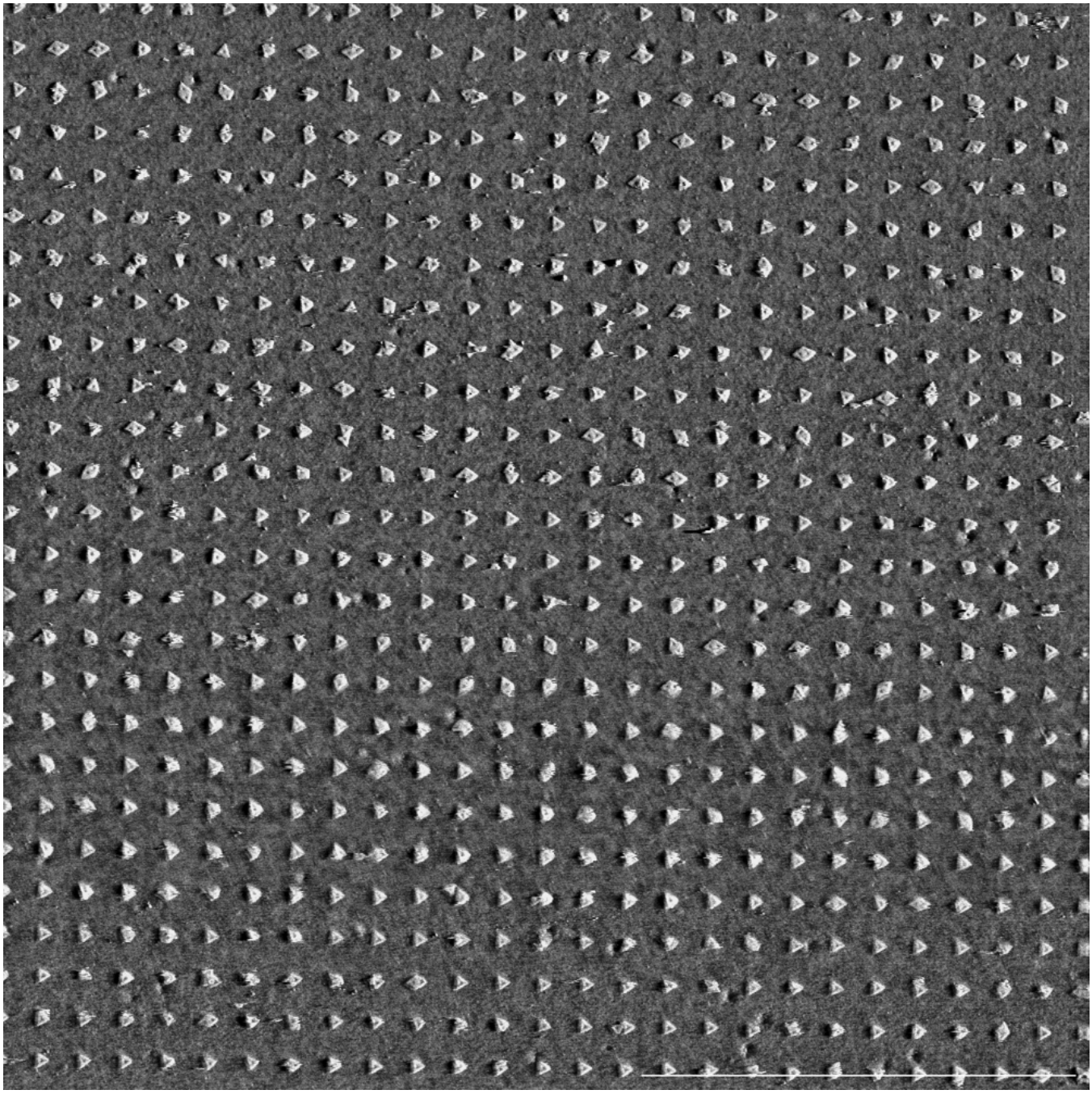

Figure S24. 60 mM Mg^{2+}, raw AFM. Other conditions are: 110 pM origami, 5 mM Tris, pH of 8.35, 60 min incubation, period of 400 nm.

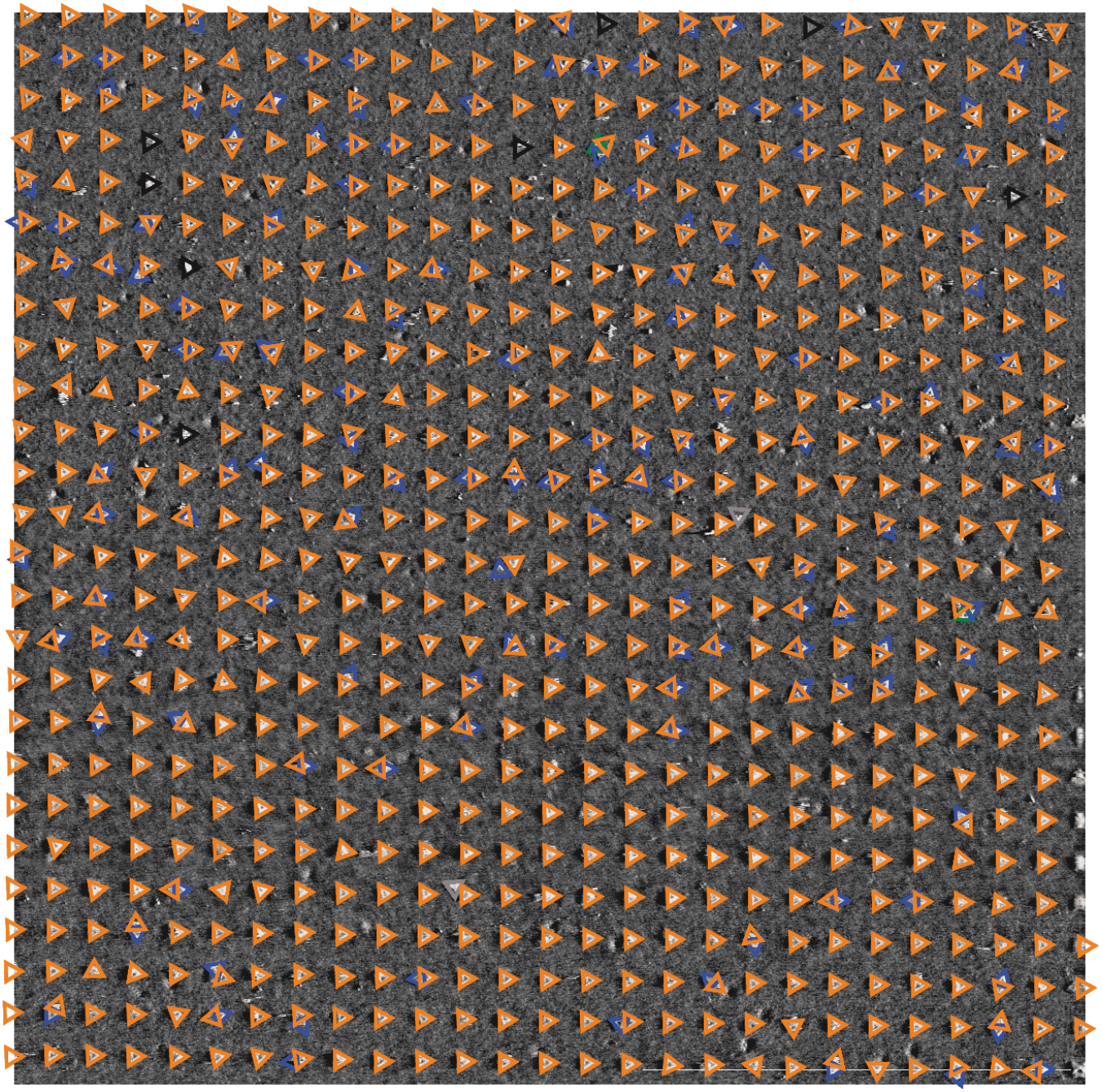

Figure S25. 60 mM Mg^{2+}, annotated AFM. Other conditions are: 110 pM origami, 5 mM Tris, pH of 8.35, 60 min incubation, period of 400 nm. Triangular outlines provide a classification of an origami and/or binding site: **empty binding site**, **first origami on a site**, **second origami on a site**, **third origami on a site**, or **origami bound to the background**.

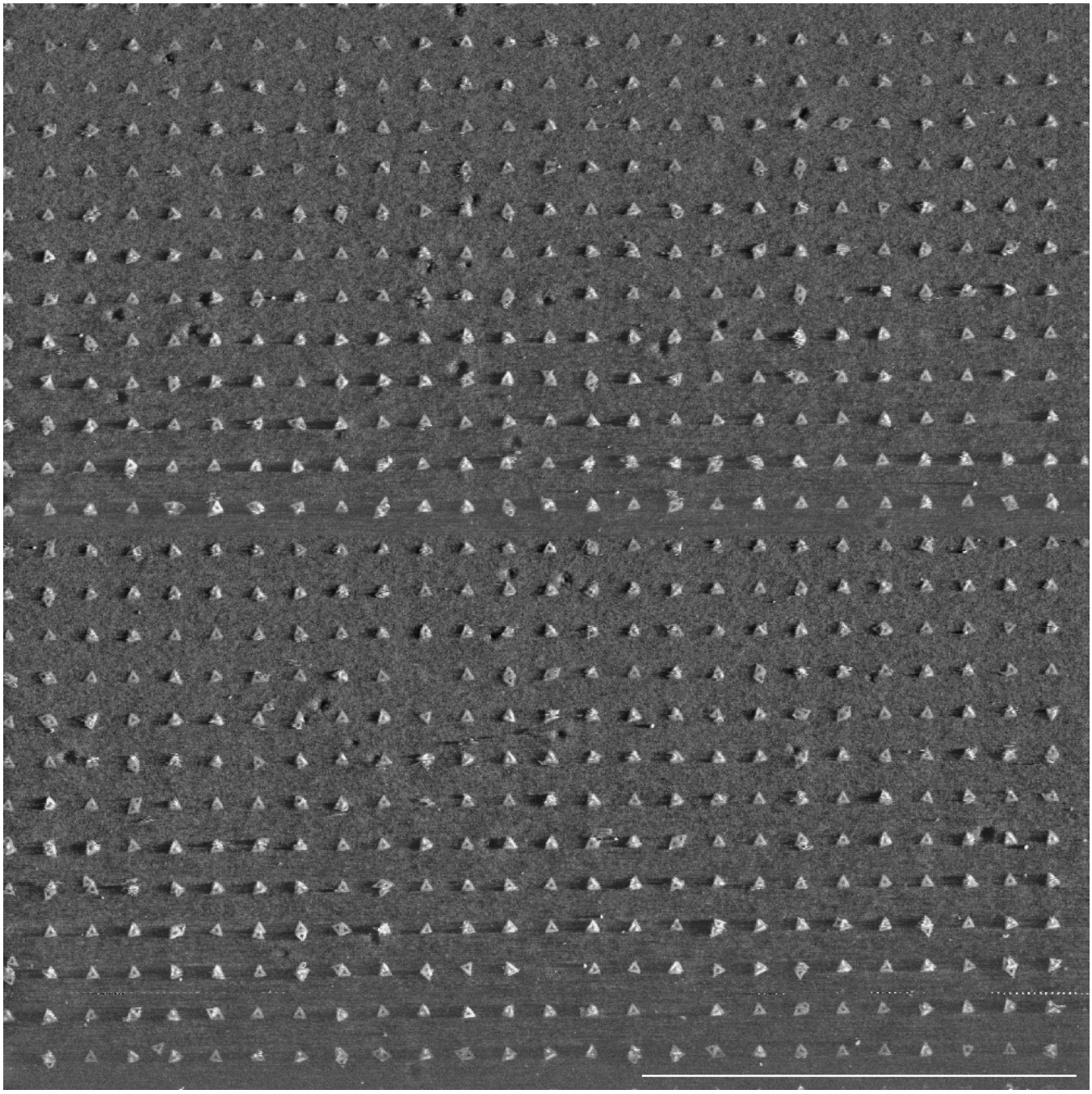

Figure S26. 80 mM Mg^{2+}, raw AFM. Other conditions are: 110 pM origami, 5 mM Tris, pH of 8.35, 60 min incubation, period of 400 nm.

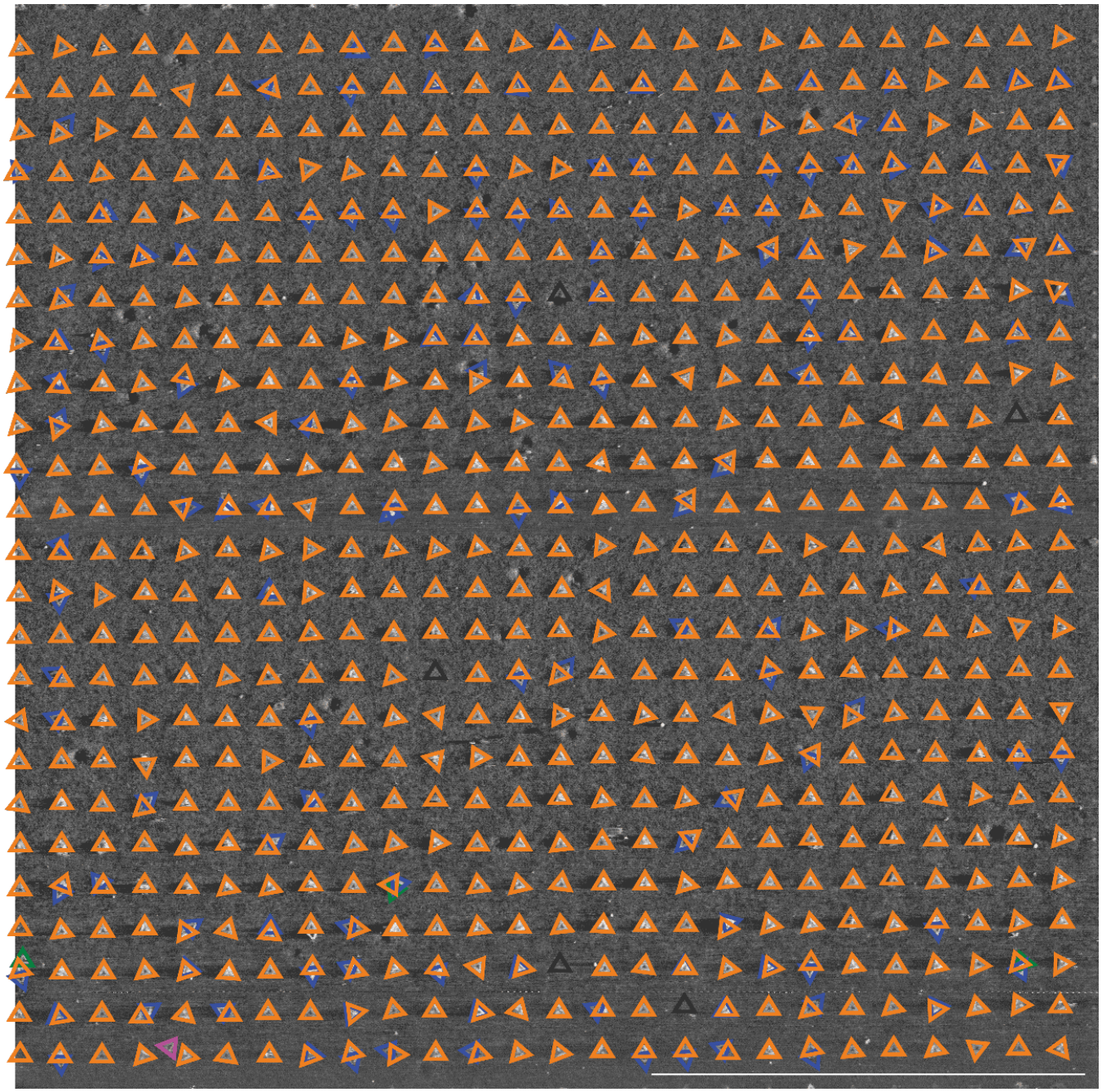

Figure S27. 80 mM Mg^{2+}, annotated AFM. Other conditions are: 110 pM origami, 5 mM Tris, pH of 8.35, 60 min incubation, period of 400 nm. Triangular outlines provide a classification of an origami and/or binding site: **empty binding site**, **first origami on a site**, **second origami on a site**, **third origami on a site**, or **origami bound to the background**.

Mg2+ Concentration (mM)	Filled	Single	Double	Triple	Background	Empty
12.5	0	0	0	0	0	100
25	9.20 ± 6	9.04 ± 8	0.15 ± 0.1	0	0	90.79 ± 1
35	92.77 ± 7	88.79 ± 7	3.53 ± 2.2	0.44 ± 0.2	0.292	7.22 ± 5
42.5	96.13 ± 4	87.36 ± 4	8.61 ± 7	0.14 ± 0.1	0.44	3.41 ± 2
60	98.82 ± 1.1	77.61 ± 2	20.91 ± 6	0.29 ± 0.2	0.29	1.17 ± 1
80	99.23 ± 0.8	76.65 ± 2	22.12 ± 5	0.46 ± 0.4	0.15	0.76 ± 0.5

Figure S28. Results of varying Mg^{2+} concentration on nanoarray quality. The percentage site occupancy (with respect to number of binding sites) of origami in different states. Errors correspond to s.e.m from 3 separate experiments.

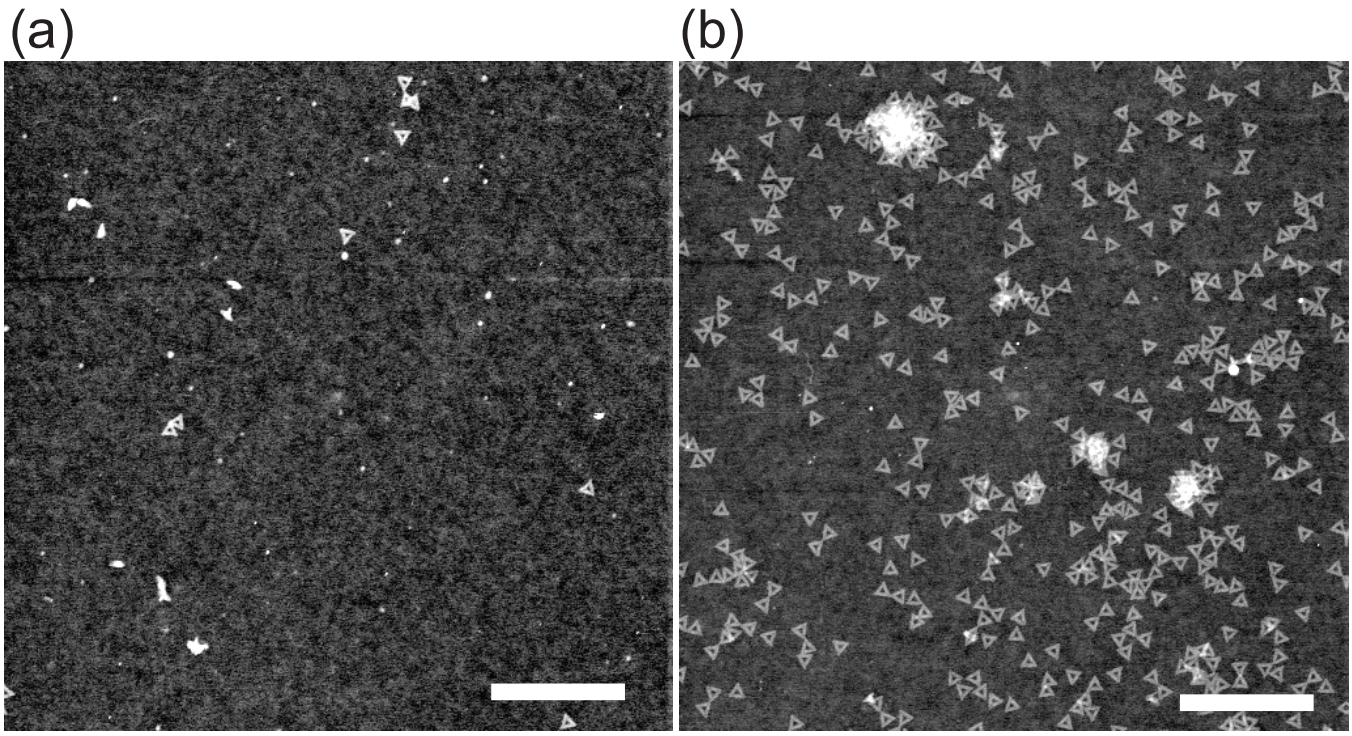

Figure S29. Mg^{2+} dependence of binding on unpatterned substrates. AFM of unpatterned SiO_2 substrates that were activated and exposed to solutions with origami at the same concentration (500 pM) but with two different Mg^{2+} concentrations: (a) 25 mM and (b) 35 mM. Thus the sharp transition in origami-surface binding is not limited to more stringent origami-binding site interactions, and it is not an artifact related to any of the processing steps involved in fabricating binding sites. Buffer conditions were otherwise standard (5 mM Tris, pH 8.35) but incubation time was only 20 minutes. Scale bar, 1μm.

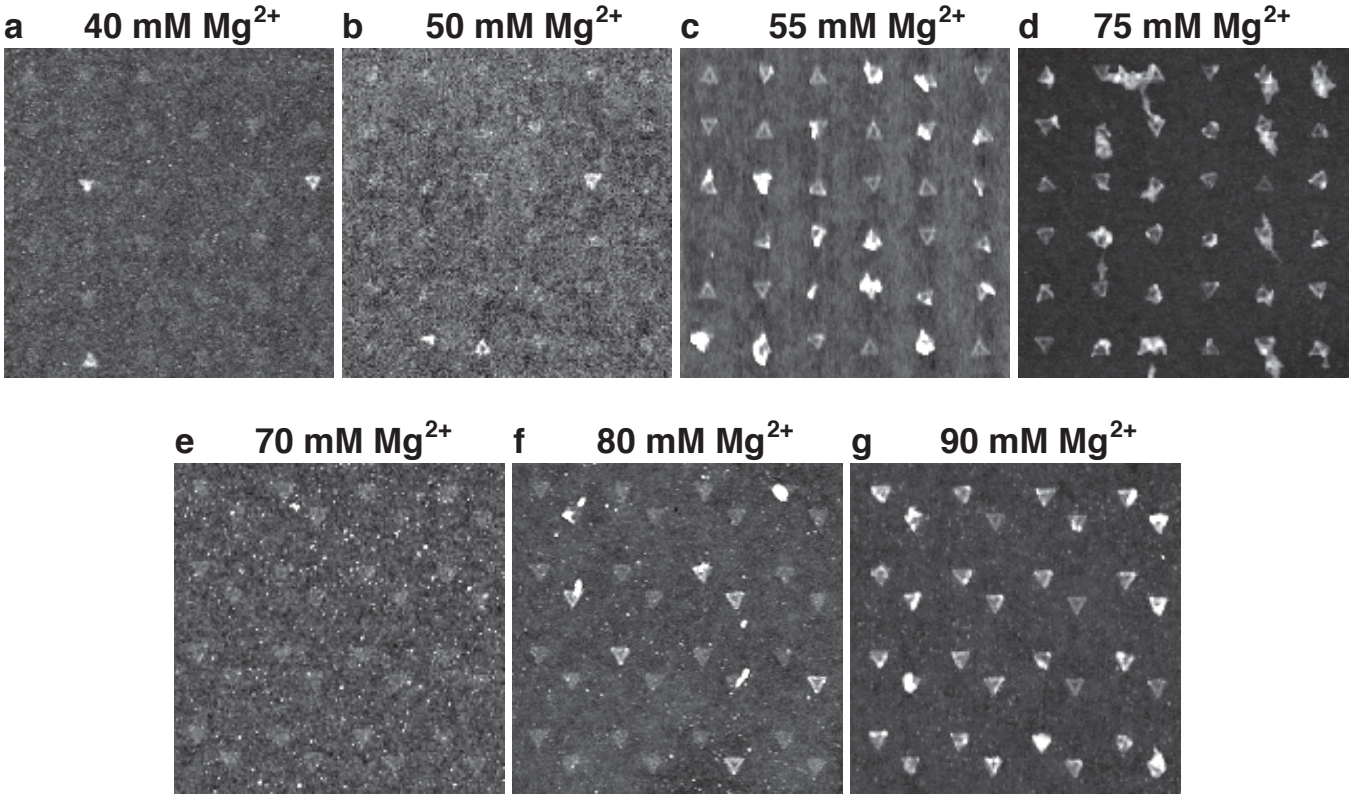

Figure S30. The concentration of Mg^{2+} required for high site occupancy varies with roughness. a–d RCA/HF cleaning procedure, roughness of processed wafer 5 Å by AFM. 55 mM Mg^{2+} required for 100% site occupancy. **e–g** RCA cleaning only, roughness of wafer before clean of 9-10Å by AFM. 90 mM Mg^{2+} for 100% site occupancy. All these samples are imaged dry, after an ethanol drying procedure, but without the new variation of using a high pH wash to hydrolyze the background. Thus all these images have the drying artifacts present in Fig. S6(a). Also, (a) and (b) have two different patterns of triangles than other placement substrates in this paper. In (a) every other binding site is rotated 180 degrees. In (b) binding sites occur as pairs of diagonally arrange sites.

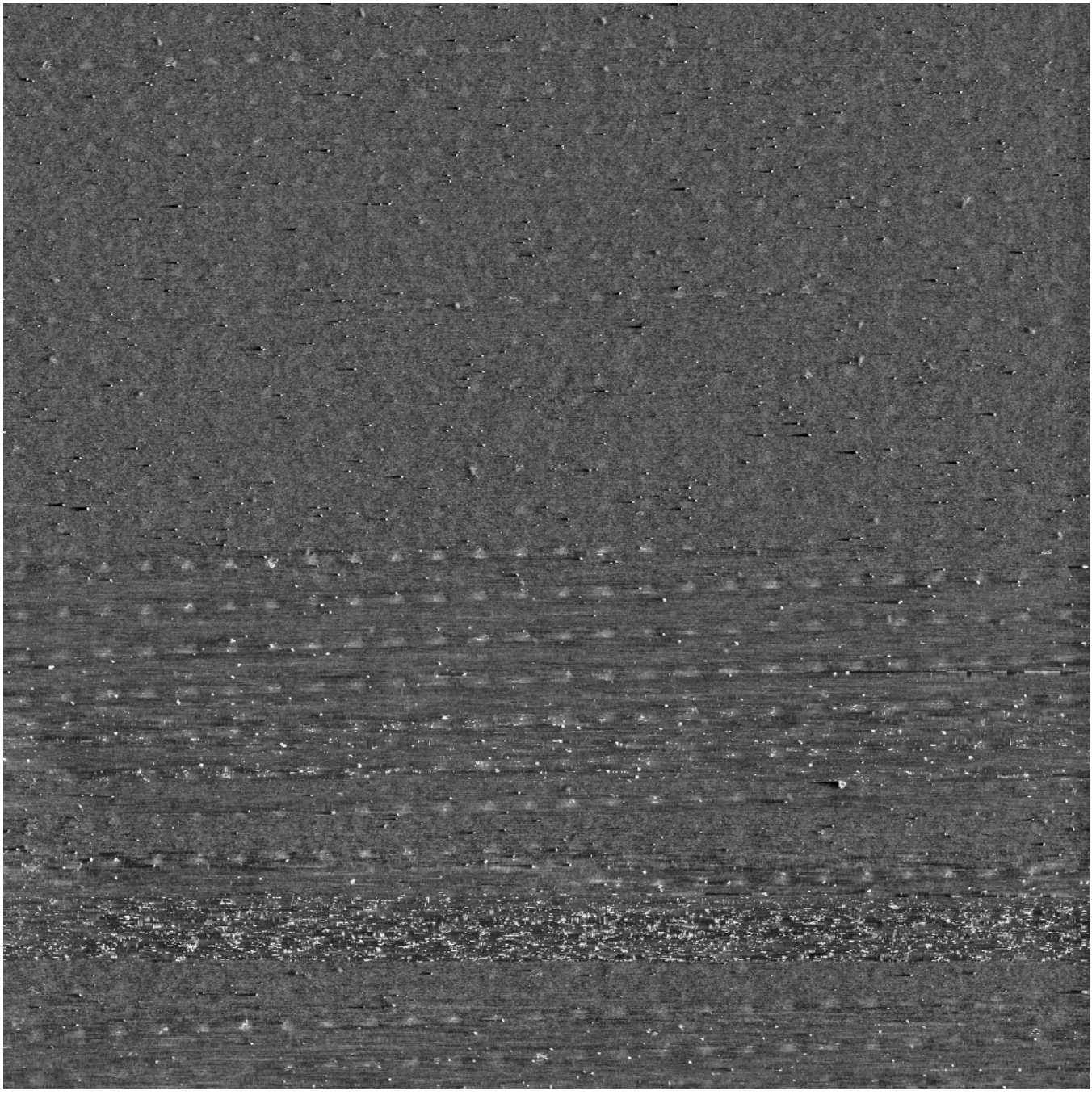

Figure S31. pH 7.1, raw AFM. Other conditions are: 5 mM Tris, 110 pM origami, 35 mM Mg^{2+}, 60 min incubation, period of 400 nm.

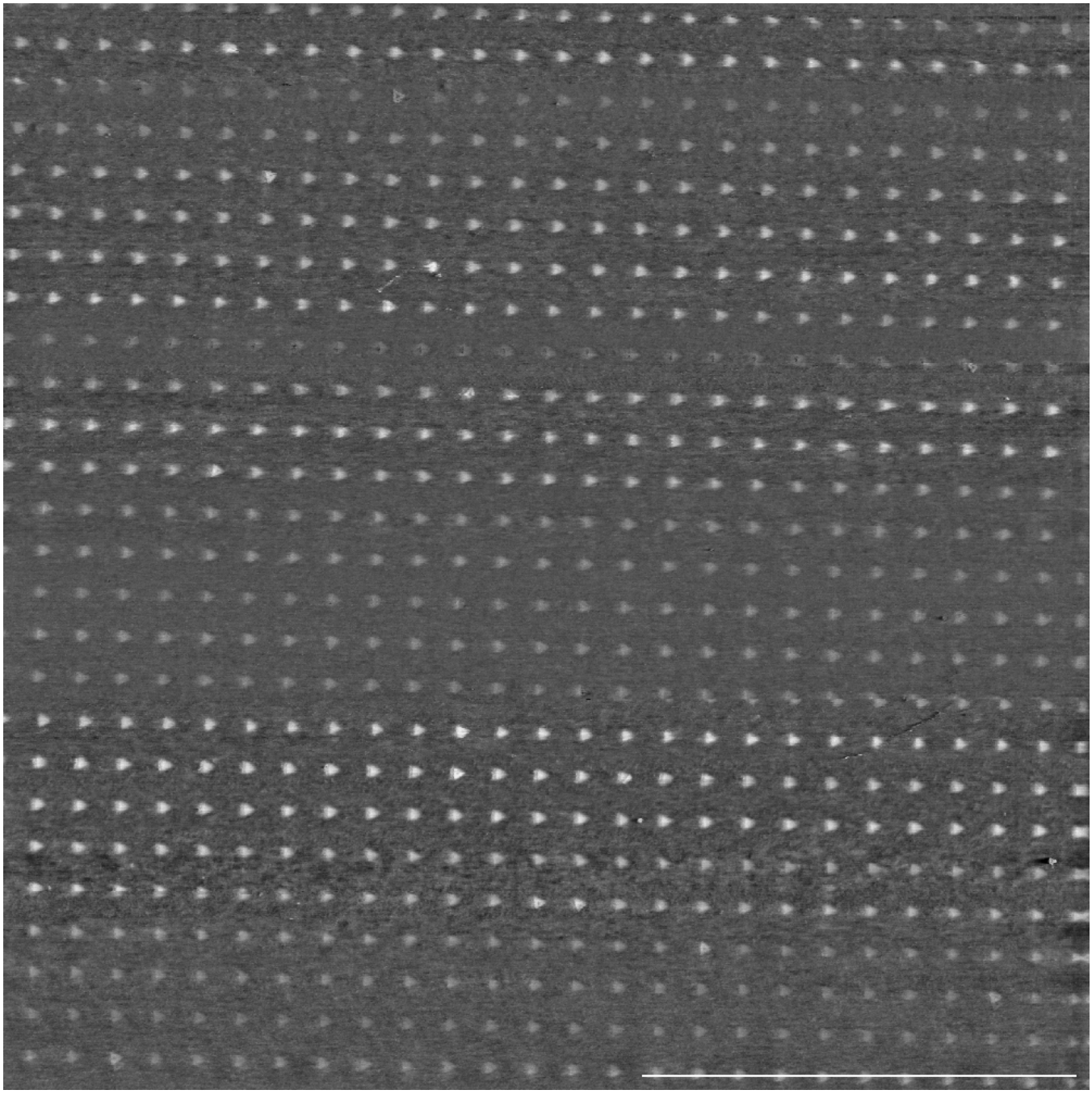

Figure S32. pH 7.5, raw AFM. Other conditions are: 5 mM Tris, 110 pM origami, 35 mM Mg^{2+}, 60 min incubation, period of 400 nm.

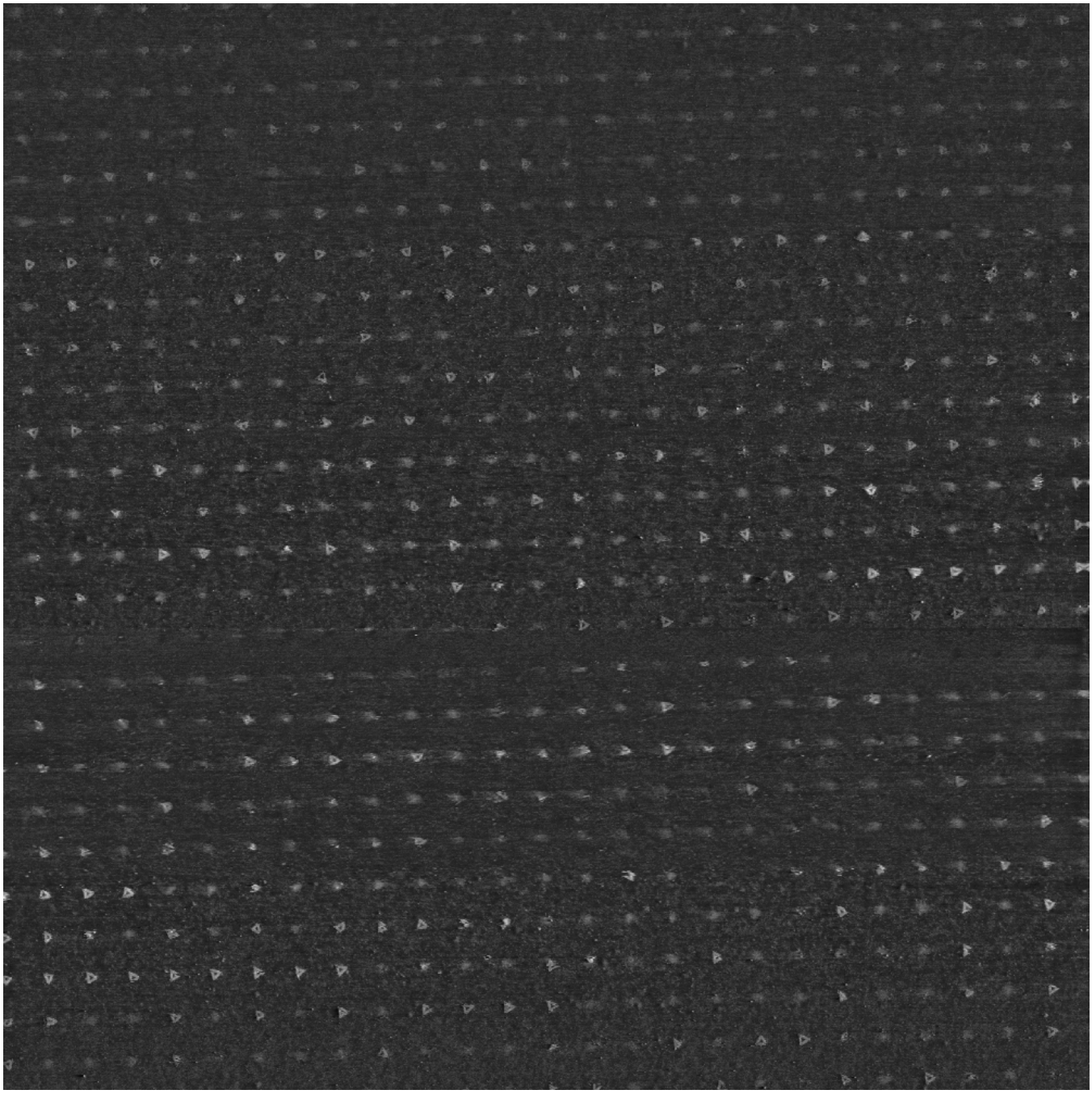

Figure S33. pH 7.8, raw AFM. Other conditions are: 5 mM Tris, 110 pM origami, 35 mM Mg^{2+}, 60 min incubation, period of 400 nm.

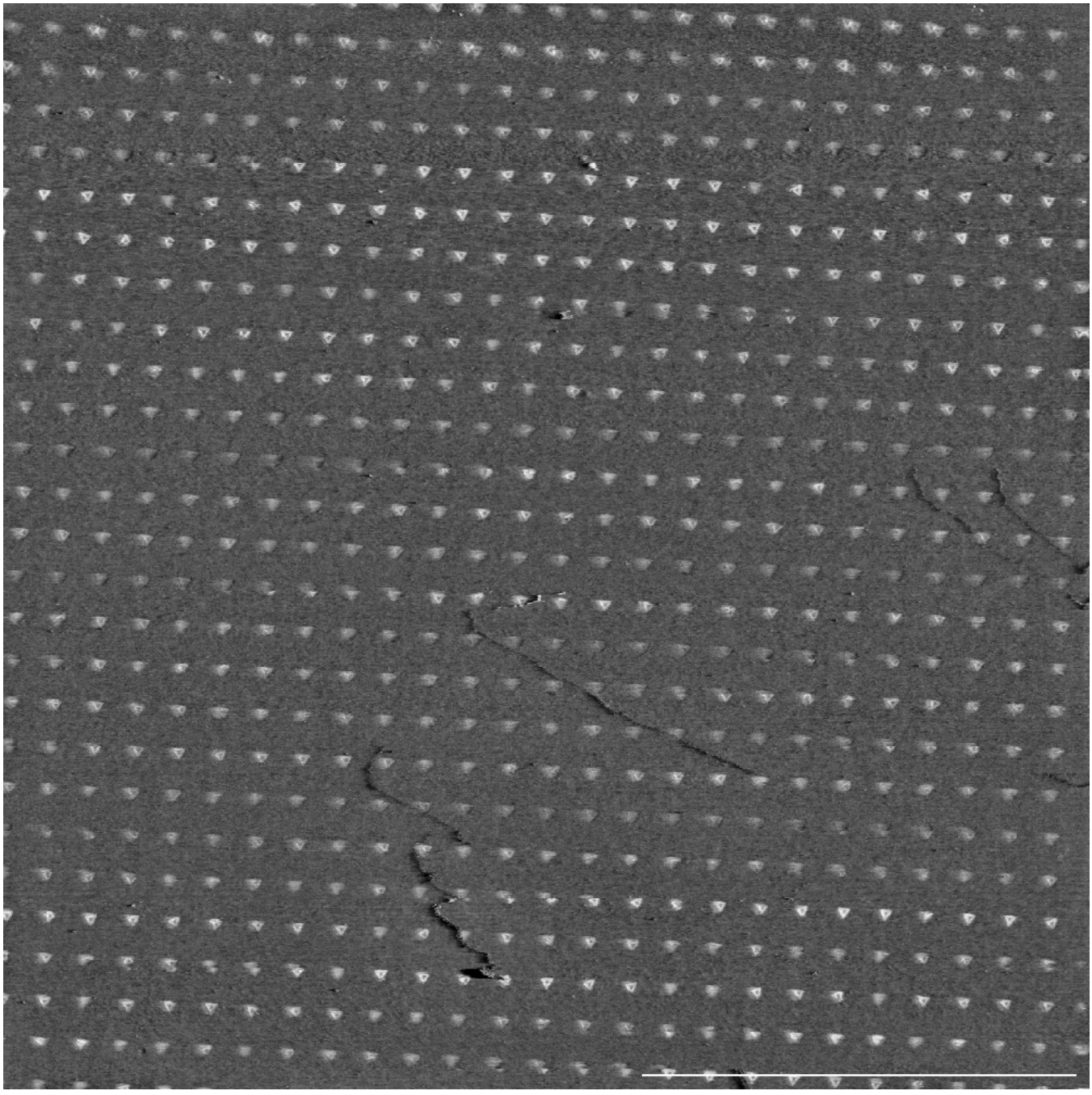

Figure S34. pH 8.0, raw AFM. Other conditions are: 5 mM Tris, 110 pM origami, 35 mM Mg^{2+}, 60 min incubation, period of 400 nm.

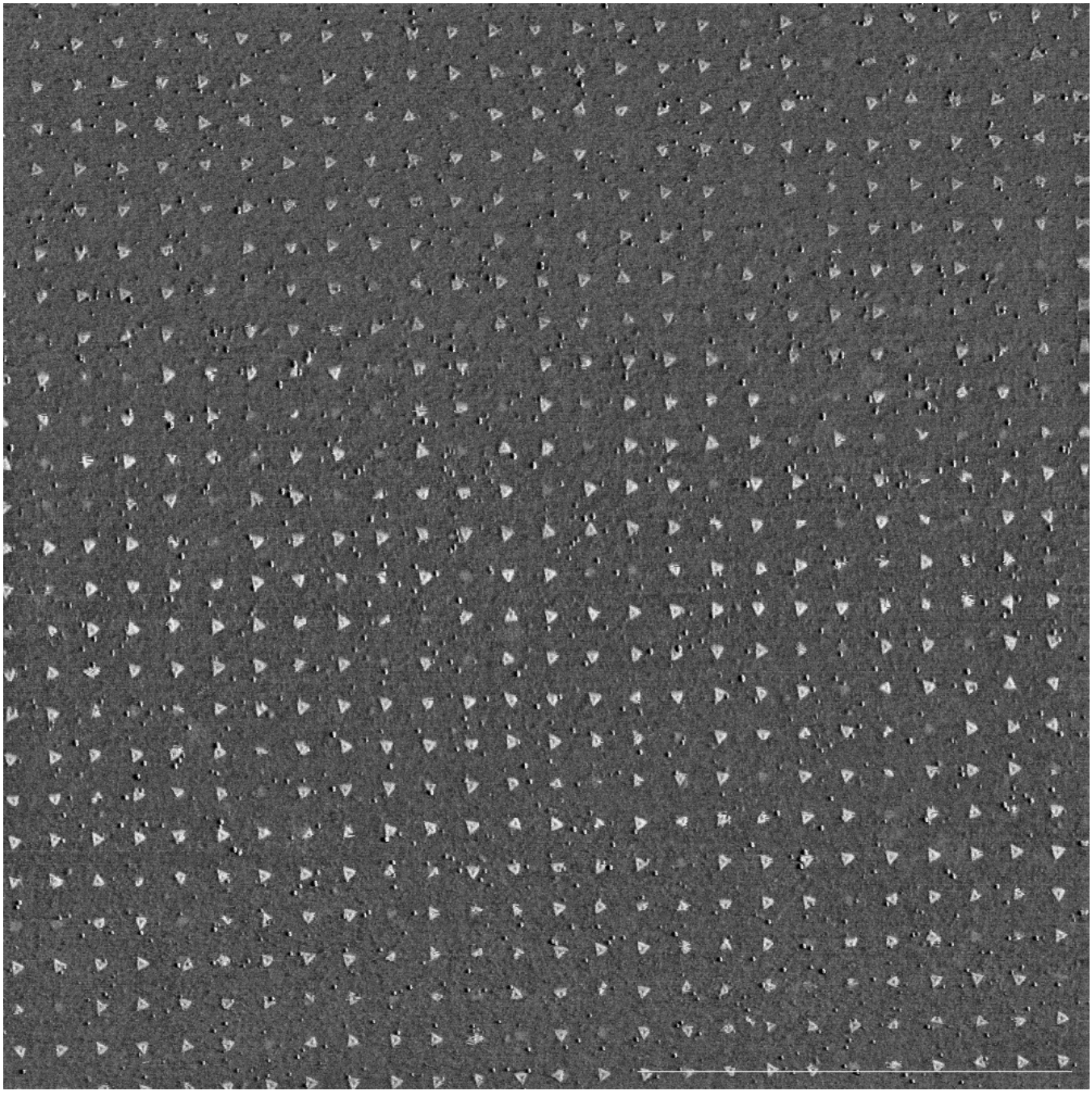

Figure S35. pH 8.16, raw AFM. Other conditions are: 5 mM Tris, 110 pM origami, 35 mM Mg^{2+}, 60 min incubation, period of 400 nm.

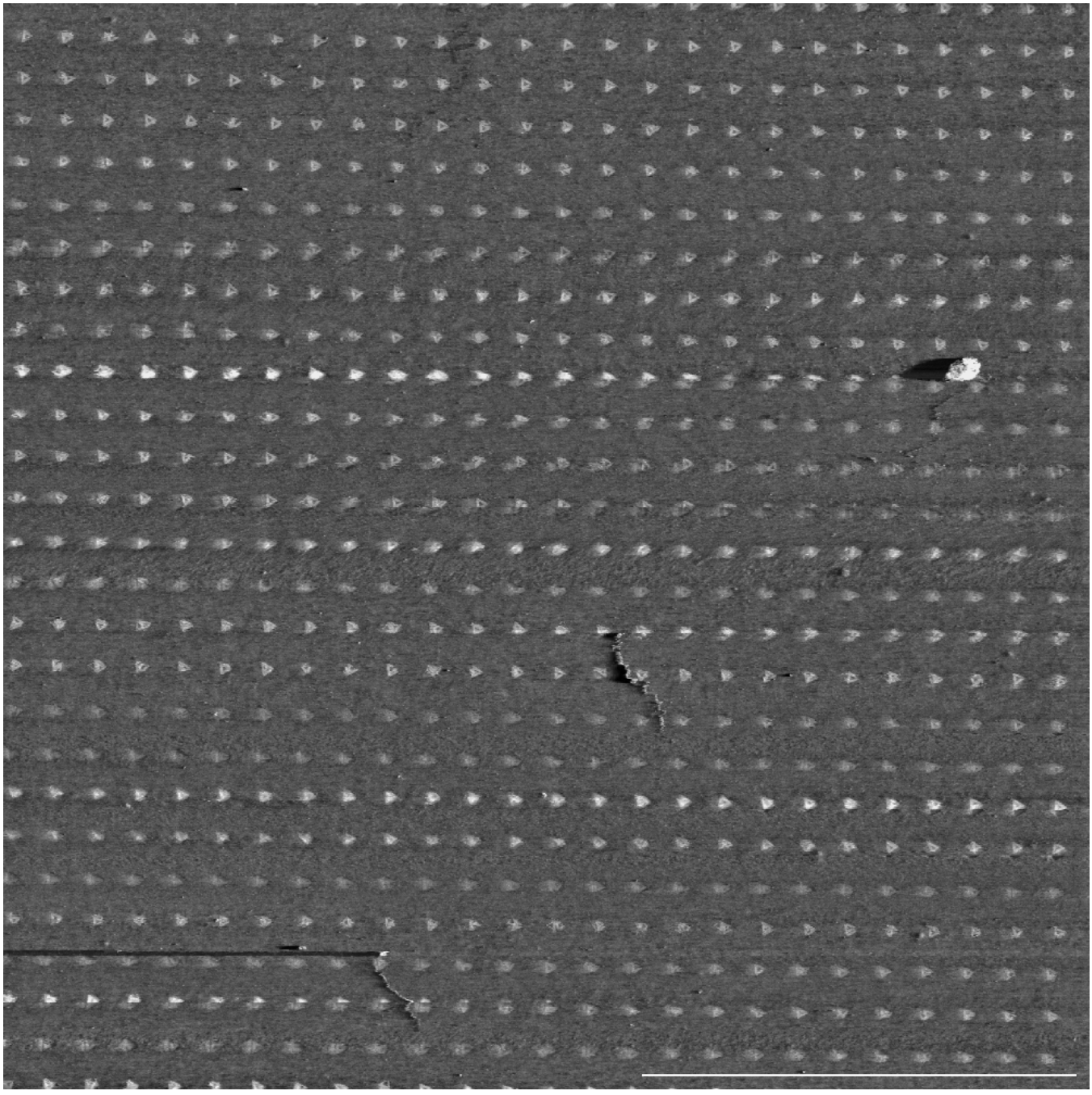

Figure S36. pH 8.5, raw AFM. Other conditions are: 5 mM Tris, 110 pM origami, 35 mM Mg^{2+}, 60 min incubation, period of 400 nm.

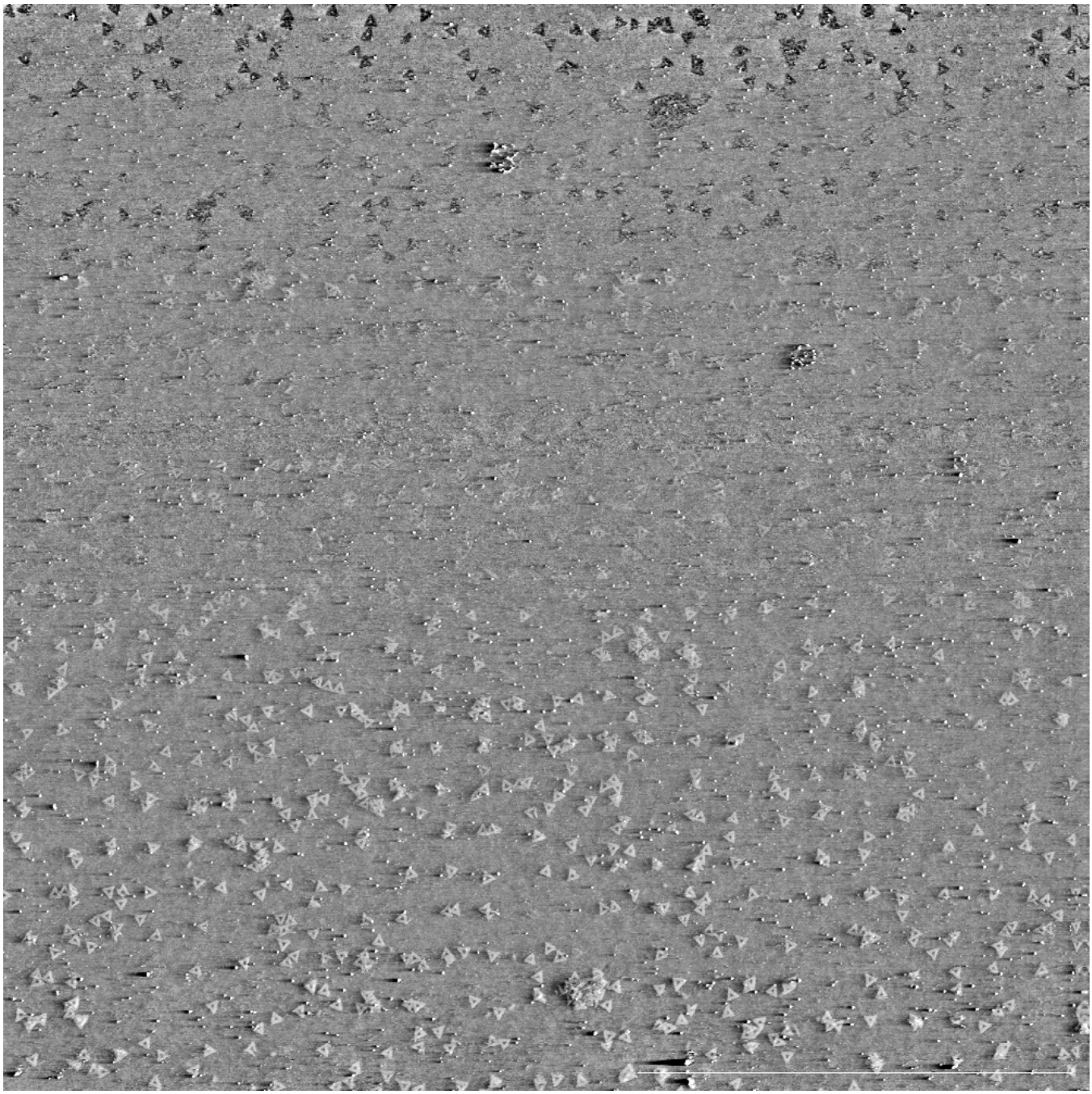

Figure S37. pH 9.2, raw AFM. Other conditions are: 5 mM Tris, 110 pM origami, 35 mM Mg^{2+}, 60 min incubation, period of 400 nm. The trimethyl silyl background passivation has hydrolyzed and origami bind frequently on the background.

pH	Filled	Single	Double	Triple	Background	Empty
7.1	0	0	0	0	0	100
7.5	1.89 ± 1	1.89 ± 0.5	0	0	0	98.10 ± 1
7.8	30.27 ± 4.5	29.96 ± 3	0.3012	0	0	69.72 ± 6
8	51.9 ± 8	51.9 ± 7	0	0	0	48.08 ± 4.5
8.16	88.82 ± 8	88.5 ± 4	0.29455	0	0	1.1 ± 1
8.3	97.07 ± 5	94.72 ± 5	2.34 ± 8	0.14 ± 0.1	2.92 ± 2	2.19 ± 1
8.4	95.17 ± 4.5	91.03 ± 7	4.13 ± 1	0	0	4.82 ± 1
8.8	97.67 ± 3	78.25 ± 8	19.41 ± 2	0	1	2 ± 1

Figure S38. Results of varying pH on nanoarray quality. The percentage site occupancy (with respect to number of binding sites) of origami in different states. Errors correspond to s.e.m from 3 separate experiments.

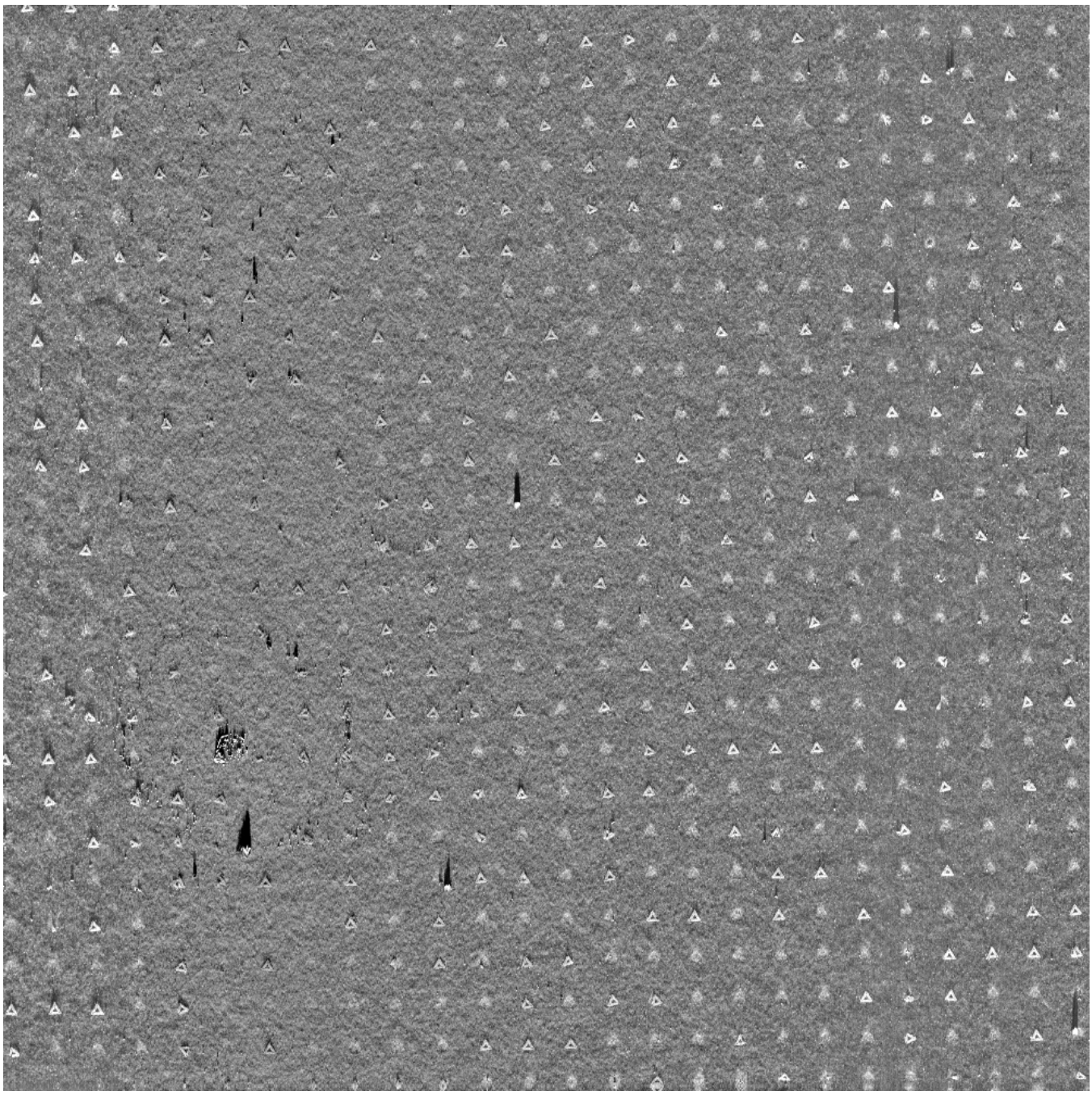

Figure S39. 5 minute incubation, raw AFM. Other conditions are: 5 mM Tris, 110 pM origami, 35 mM Mg^{2+}, pH 8.35, period of 400 nm.

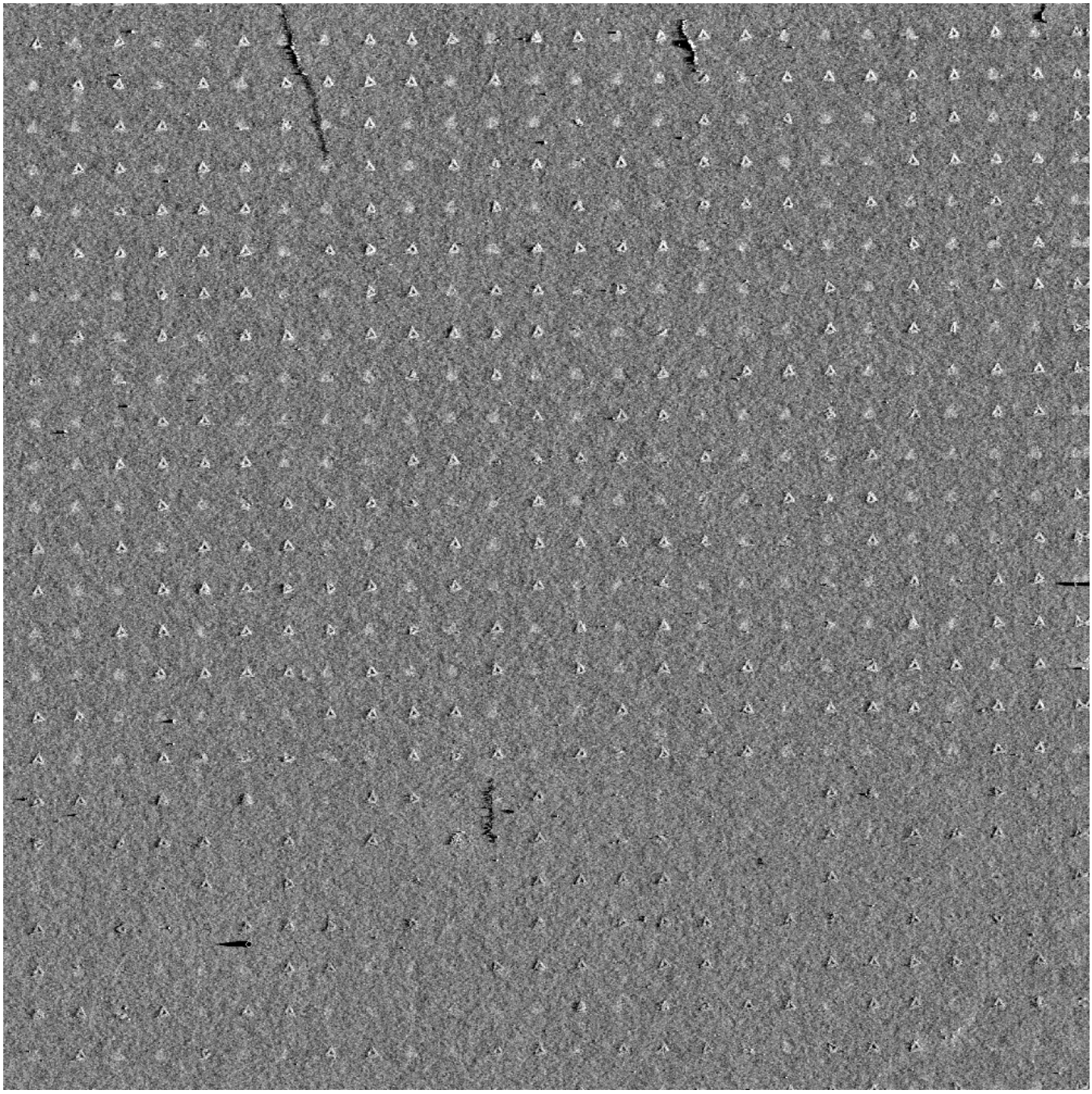

Figure S40. 10 minute incubation, raw AFM. Other conditions are: 5 mM Tris, 110 pM origami, 35 mM Mg^{2+}, pH 8.35, period of 400 nm.

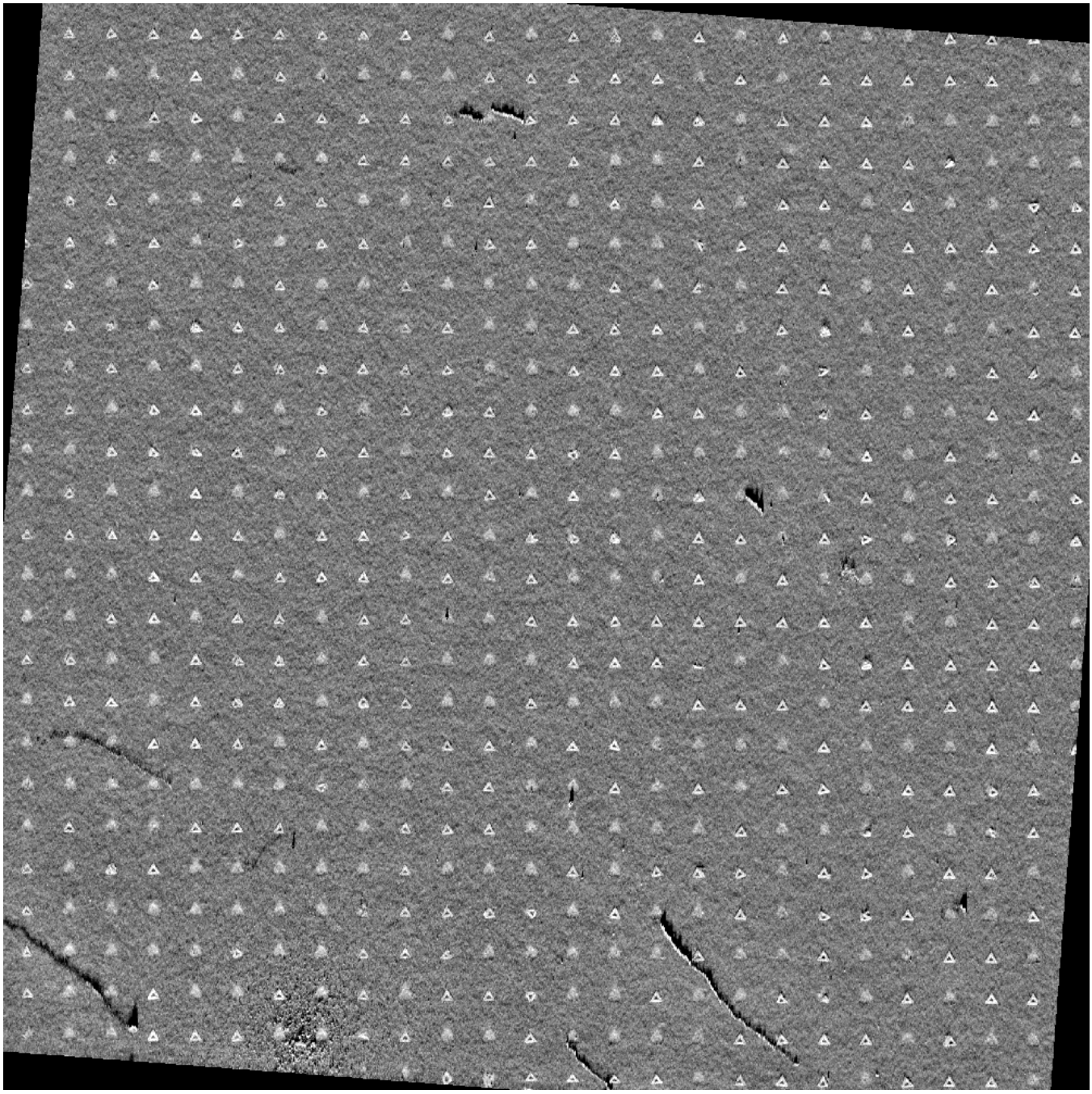

Figure S41. 20 minute incubation, raw AFM. Other conditions are: 5 mM Tris, 110 pM origami, 35 mM Mg^{2+}, pH 8.35, period of 400 nm.

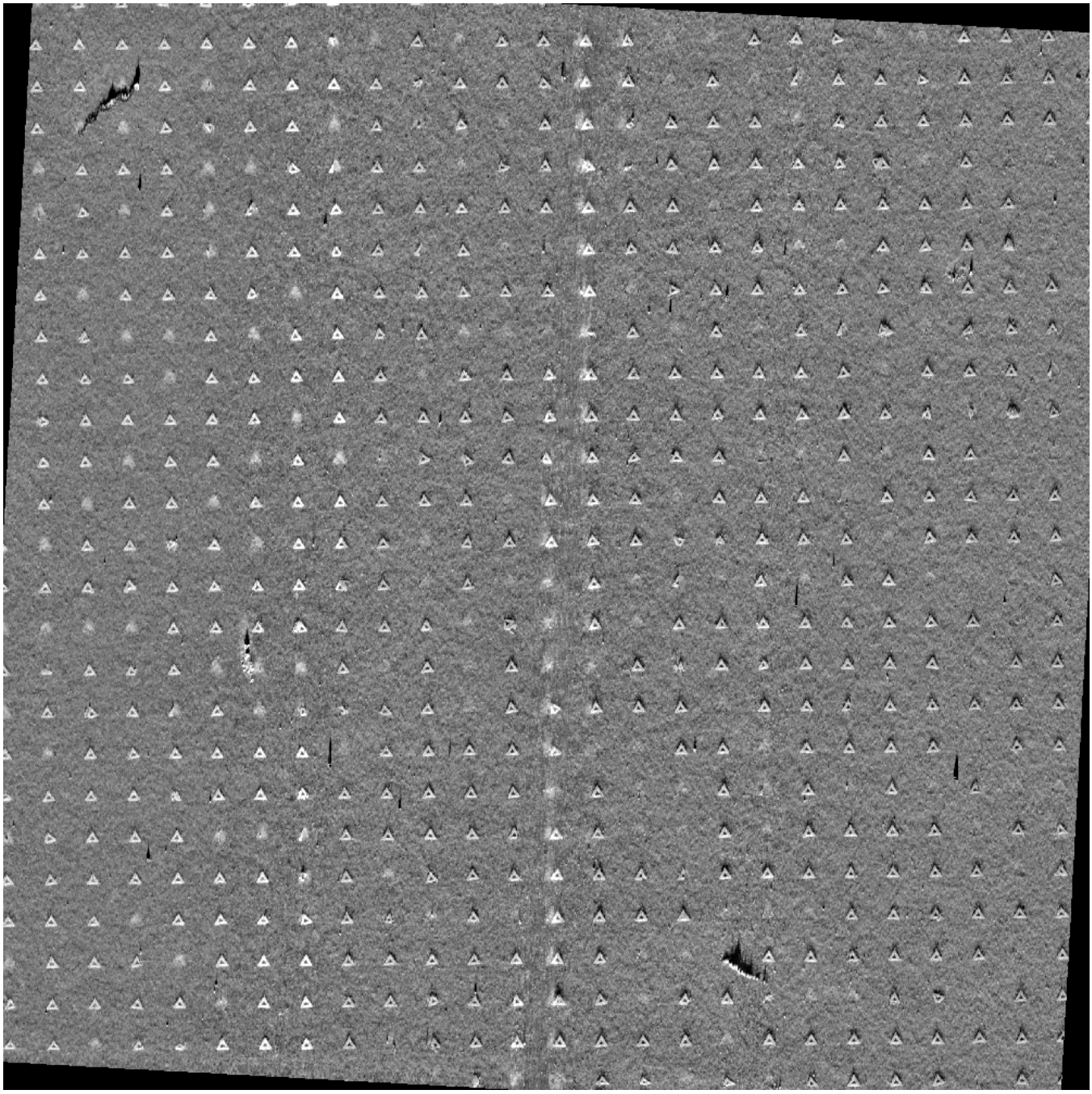

Figure S42. 30 minute incubation, raw AFM. Other conditions are: 5 mM Tris, 110 pM origami, 35 mM Mg^{2+}, pH 8.35, period of 400 nm.

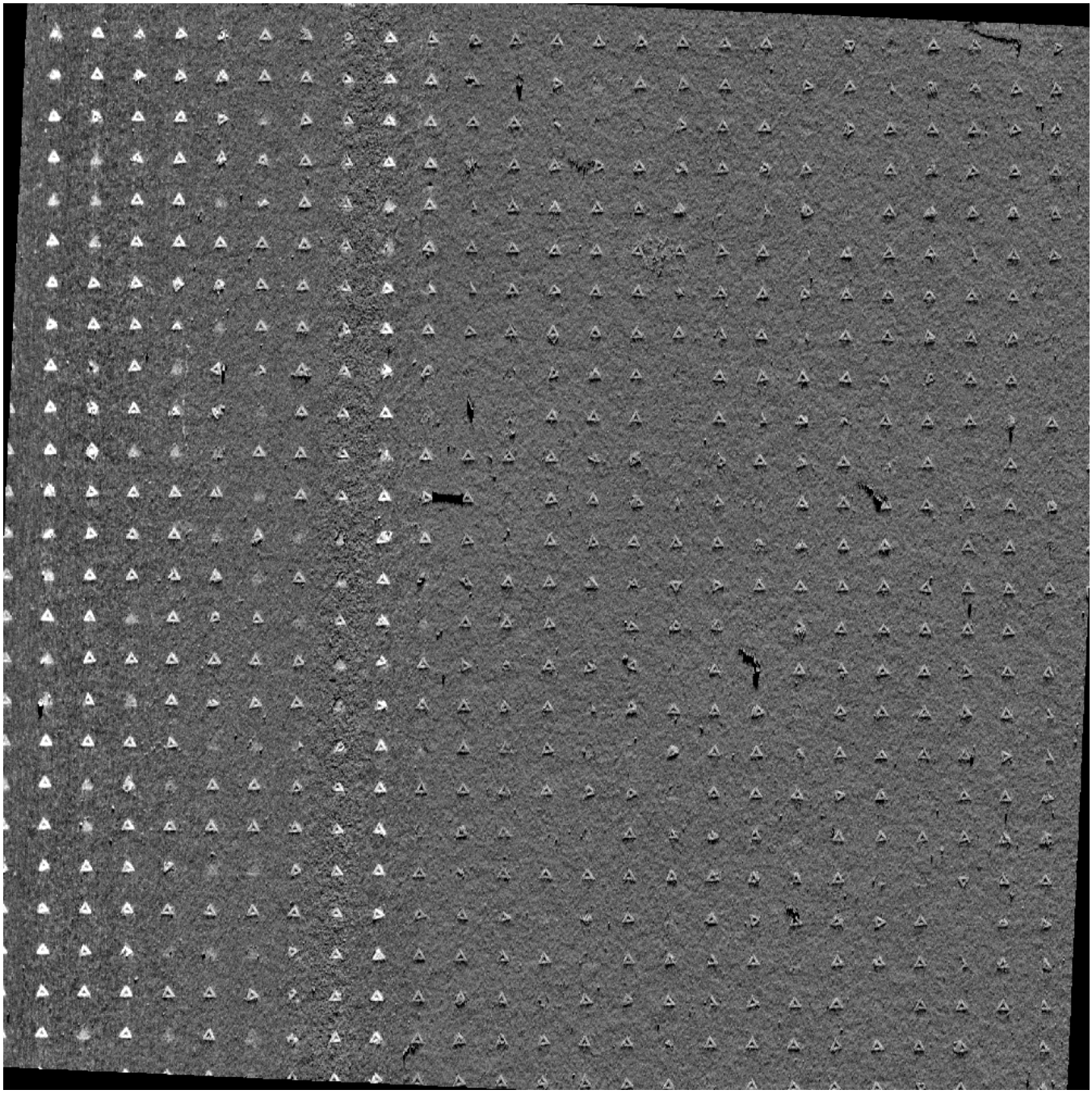

Figure S43. 45 minute incubation, raw AFM. Other conditions are: 5 mM Tris, 110 pM origami, 35 mM Mg^{2+}, pH 8.35, period of 400 nm.

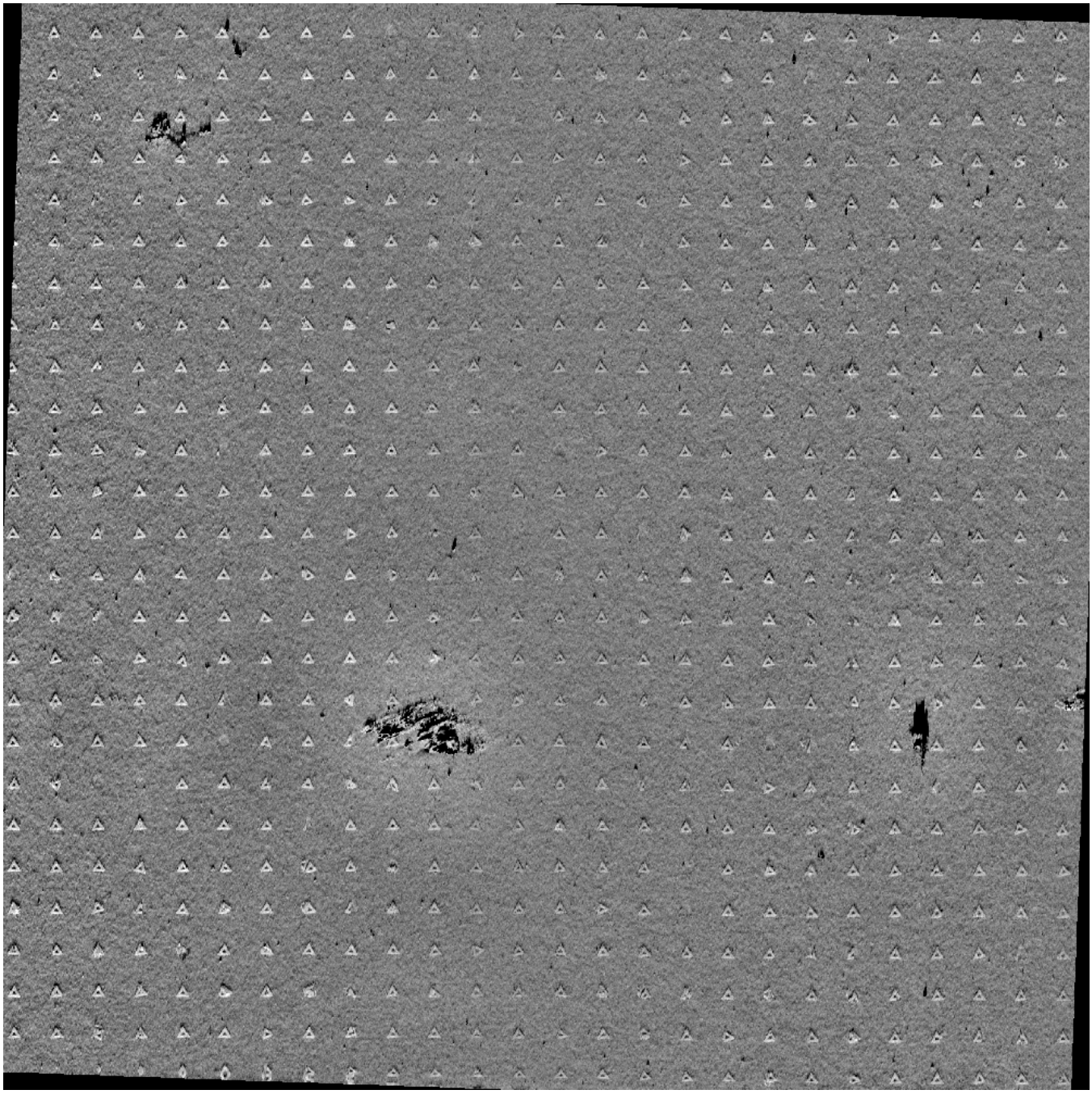

Figure S44. 60 minute incubation, raw AFM. Other conditions are: 5 mM Tris, 110 pM origami, 35 mM Mg^{2+}, pH 8.35, period of 400 nm.

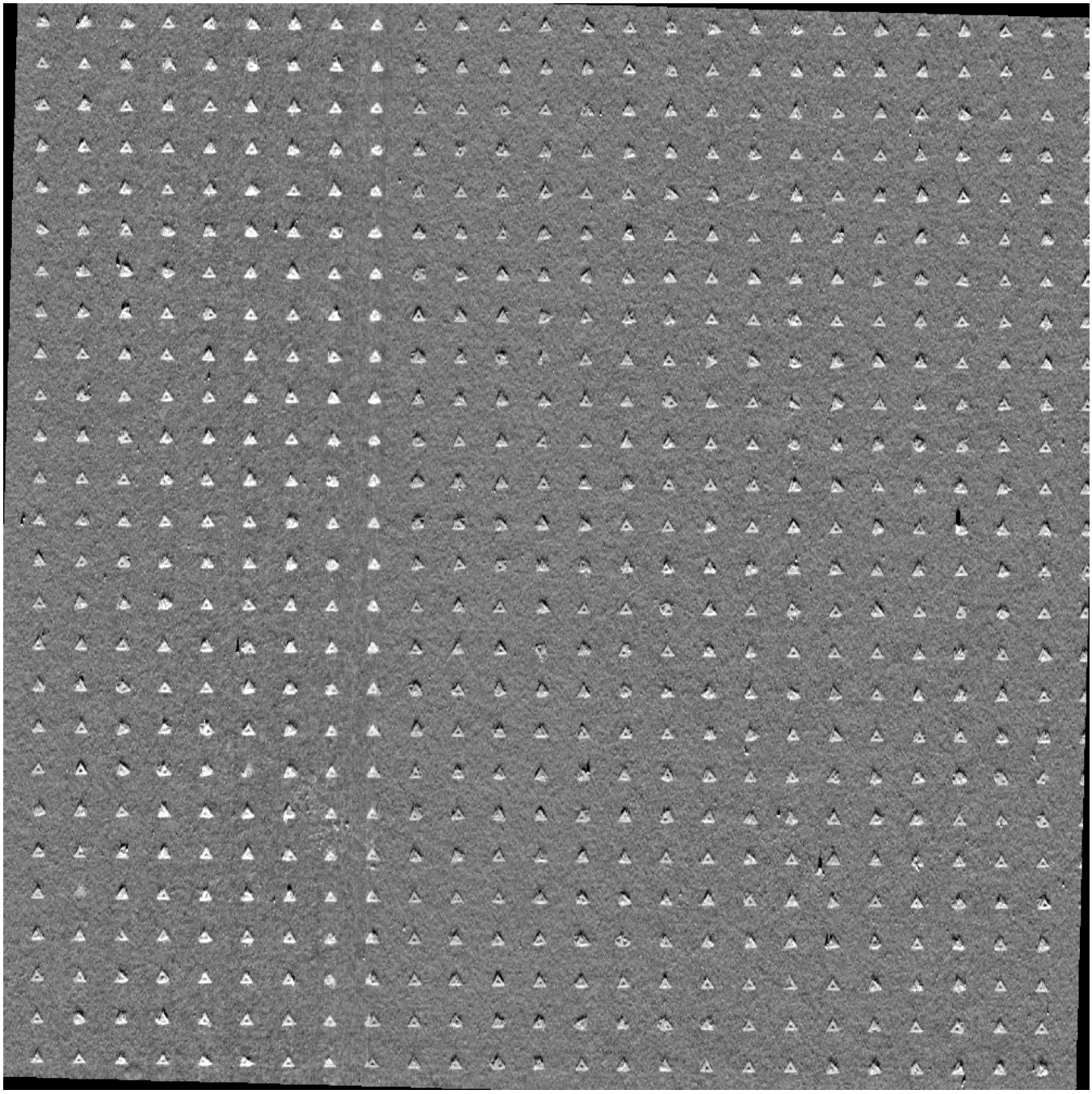

Figure S45. 120 minute incubation, raw AFM. Other conditions are: 5 mM Tris, 110 pM origami, 35 mM Mg^{2+}, pH 8.35, period of 400 nm.

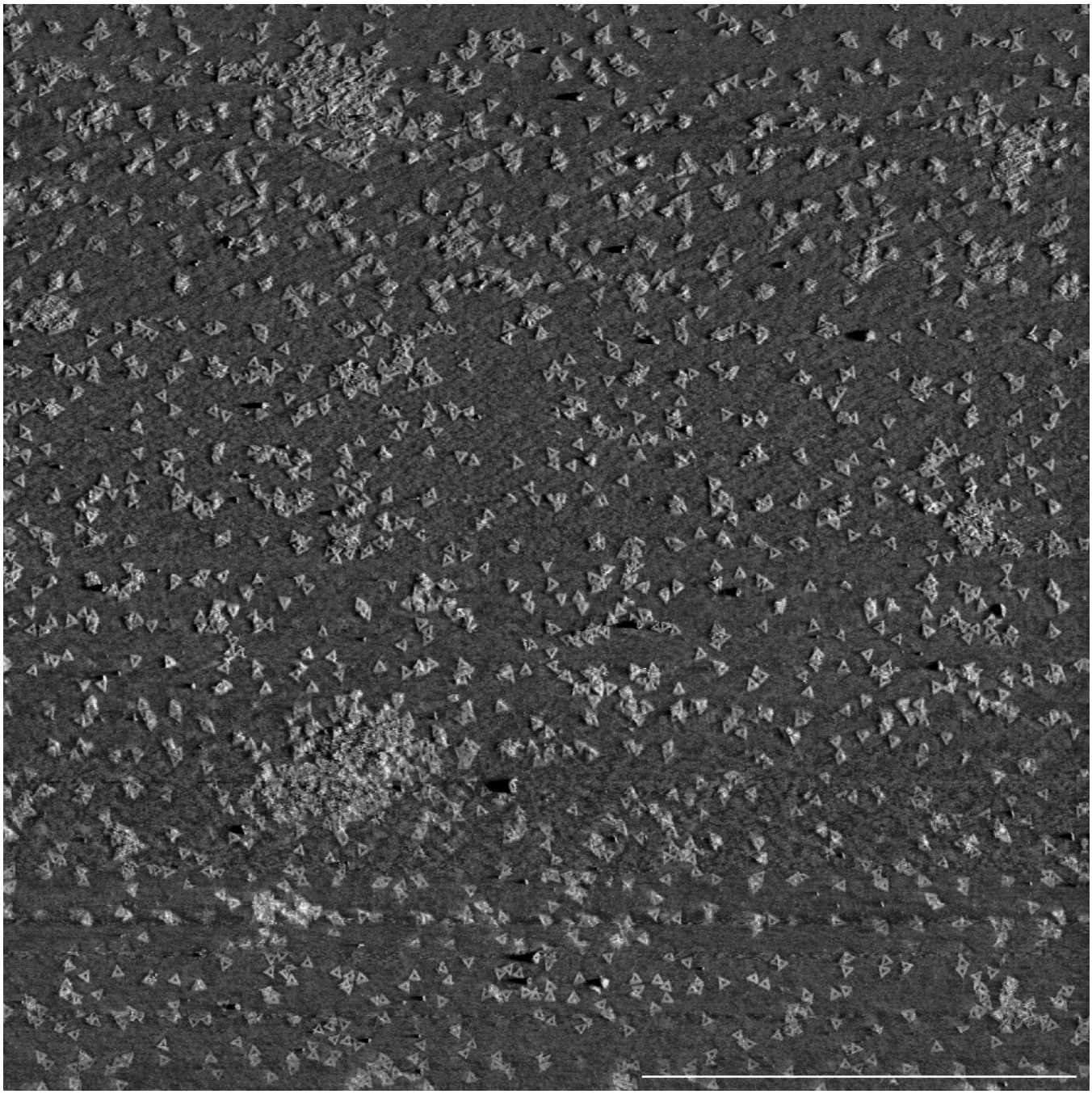

Figure S46. 480 minute incubation, raw AFM. Other conditions are: 5 mM Tris, 110 pM origami, 35 mM Mg^{2+}, pH 8.35, period of 400 nm. The trimethyl silyl background passivation has hydrolyzed and origami bind frequently on the background.

Incubation time(mins)	Filled	Single	Double	Triple	Background	Empty
5	39.17 ± 6	38.41 ± 8	0.7 + ± 0.3	0	0	60.8 ± 8
10	47.7 ± 7	46.0 ± 8	1.6 ± 1	0	0	52.3 ± 8
20	54.8 ± 6	52.8 ± 6	1.9 ± 0.9	0	0	45.1 ± 8
30	77.5 ± 5	75.7 ± 6	1.7 ± 1	0	0	22.5 ± 7
45	76 ± 6	72 ± 5	4 ± 2	0	0	24 ± 8
60	97.57 ± 4	95.14 ± 5	2.4 ± 2	0	0	2.4 ± 1
120	100	36 ± 8	48 ± 7	16 ± 4	0	0
480	100	0	0	0	0	0

Figure S47. Results of varying incubation time on nanoarray growth. The percentage site occupancy (with respect to number of binding sites) of origami in different states. Errors correspond to s.e.m from 3 separate experiments.

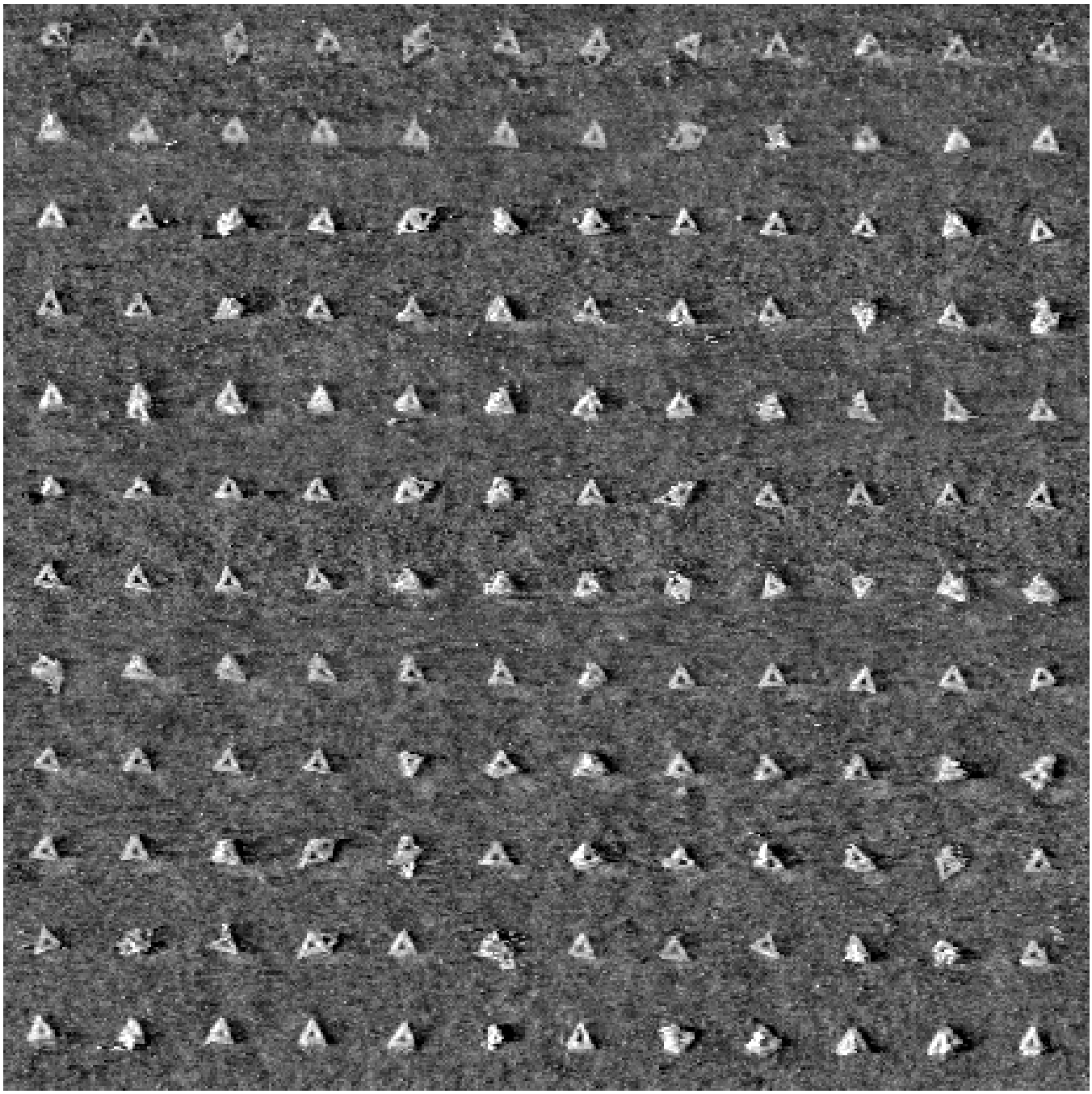

Figure S48. Placement on a nonconductive quartz substrate. Quartz placement substrates (suitable for TIRF microscopy) were fabricated with nanoimprint lithography, and origami were placed with 35 mM Mg^{2+} under standard conditions.

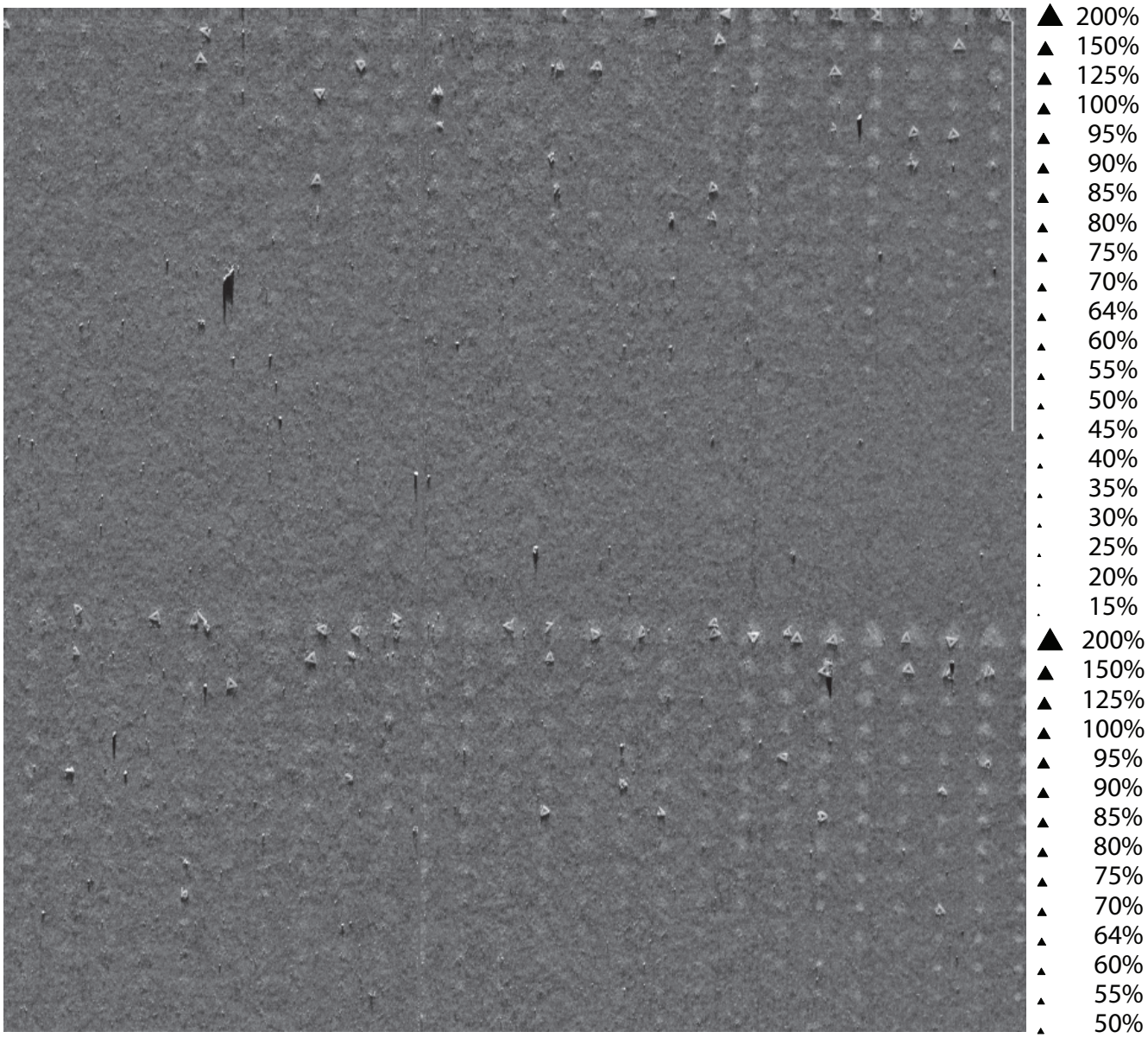

Figure S49. 25 mM Mg^{2+}, binding site size variation experiment. AFM of origami binding on a gradient of triangular binding sites whose sides range from 15% to 200% of the DNA origami edge length (127 nm). Buffer conditions: 5 mM Tris, pH 8.35.

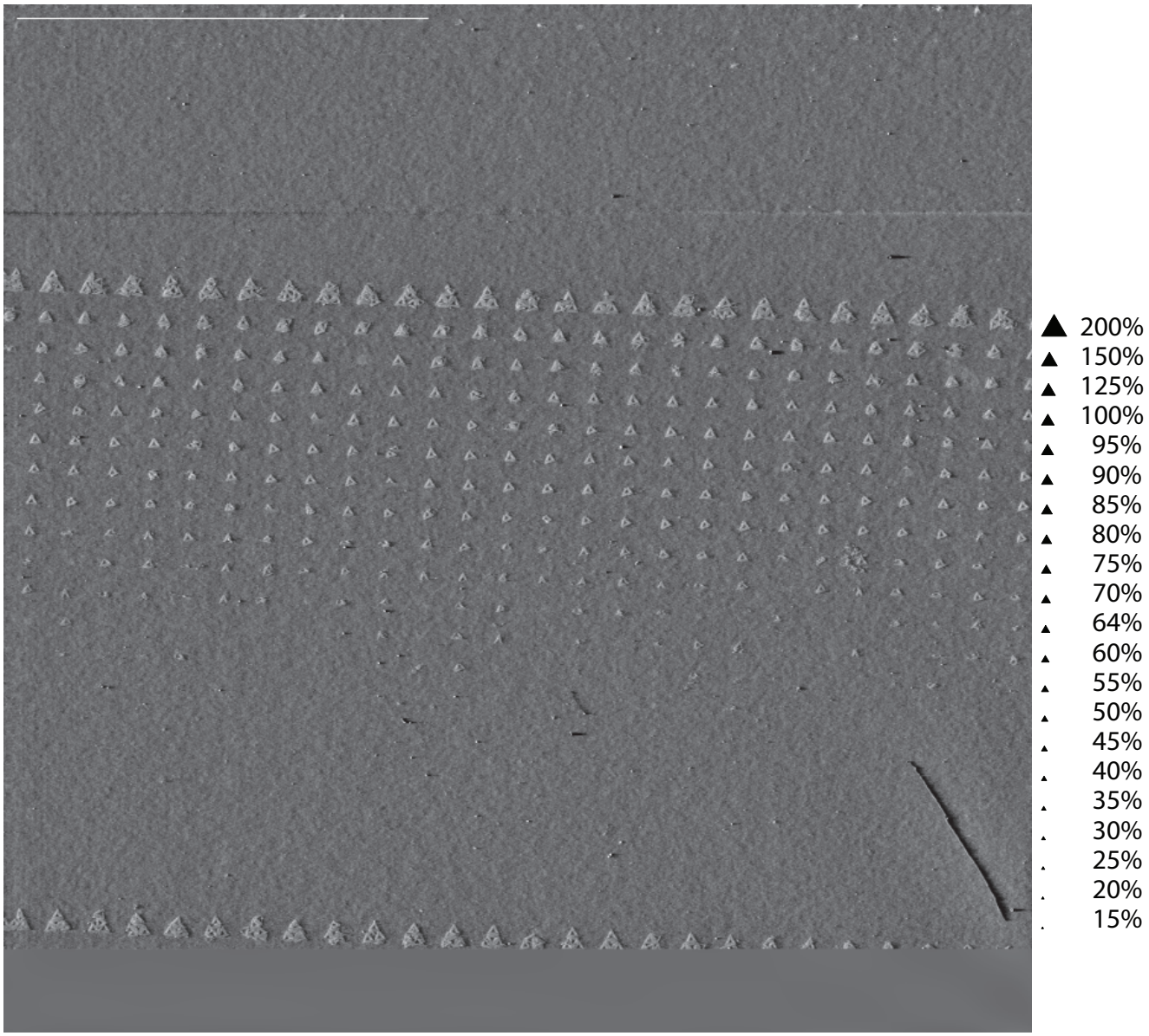

Figure S50. 35 mM Mg^{2+}, binding site size variation experiment. AFM of origami binding on a gradient of triangular binding sites whose sides range from 15% to 200% of the DNA origami edge length (127 nm). Buffer conditions: 5 mM Tris, pH 8.35.

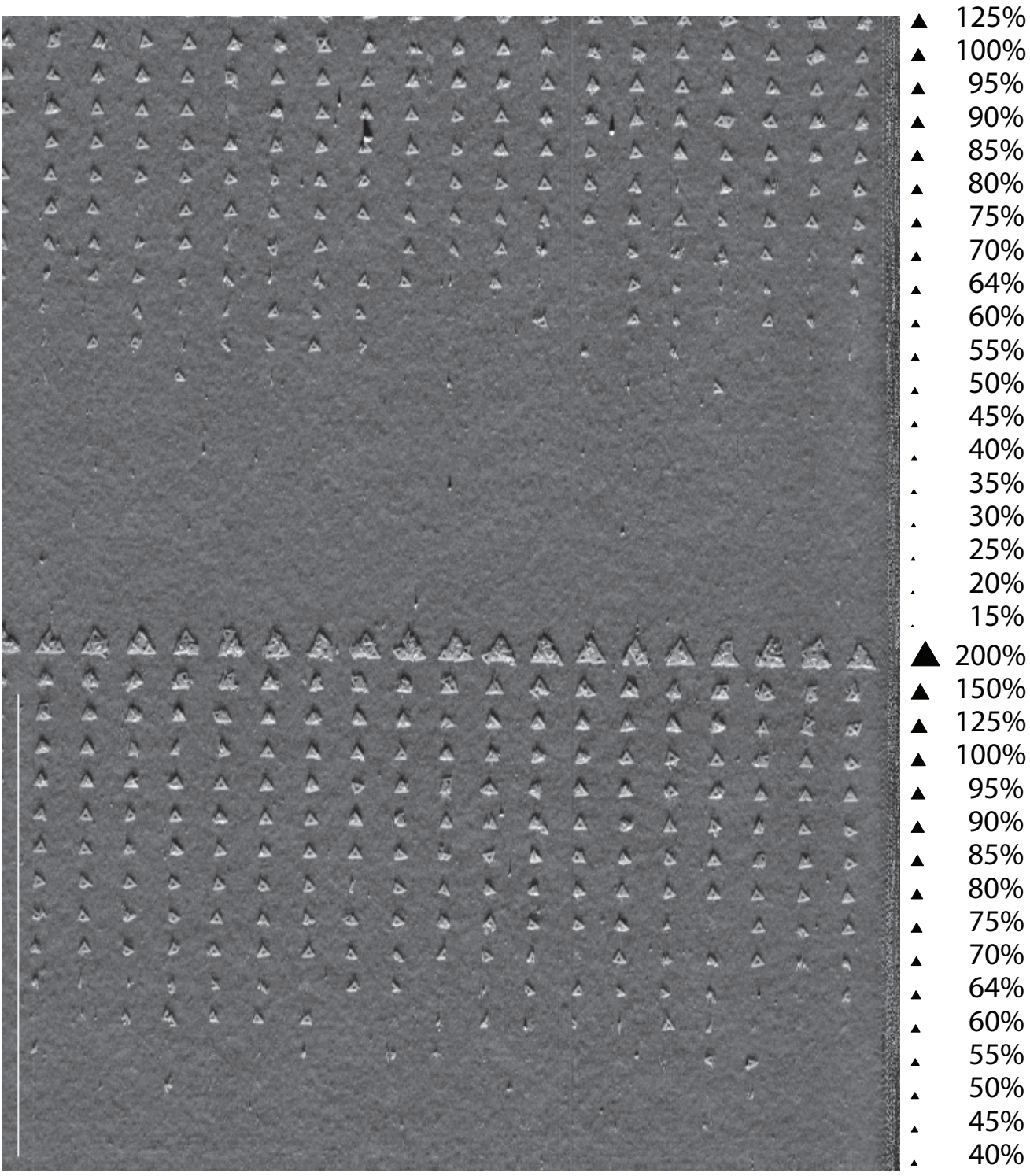

Figure S51. 40 mM Mg^{2+}, binding site size variation experiment. AFM of origami binding on a gradient of triangular binding sites whose sides range from 15% to 200% of the DNA origami edge length (127 nm). Buffer conditions: 5 mM Tris, pH 8.35.

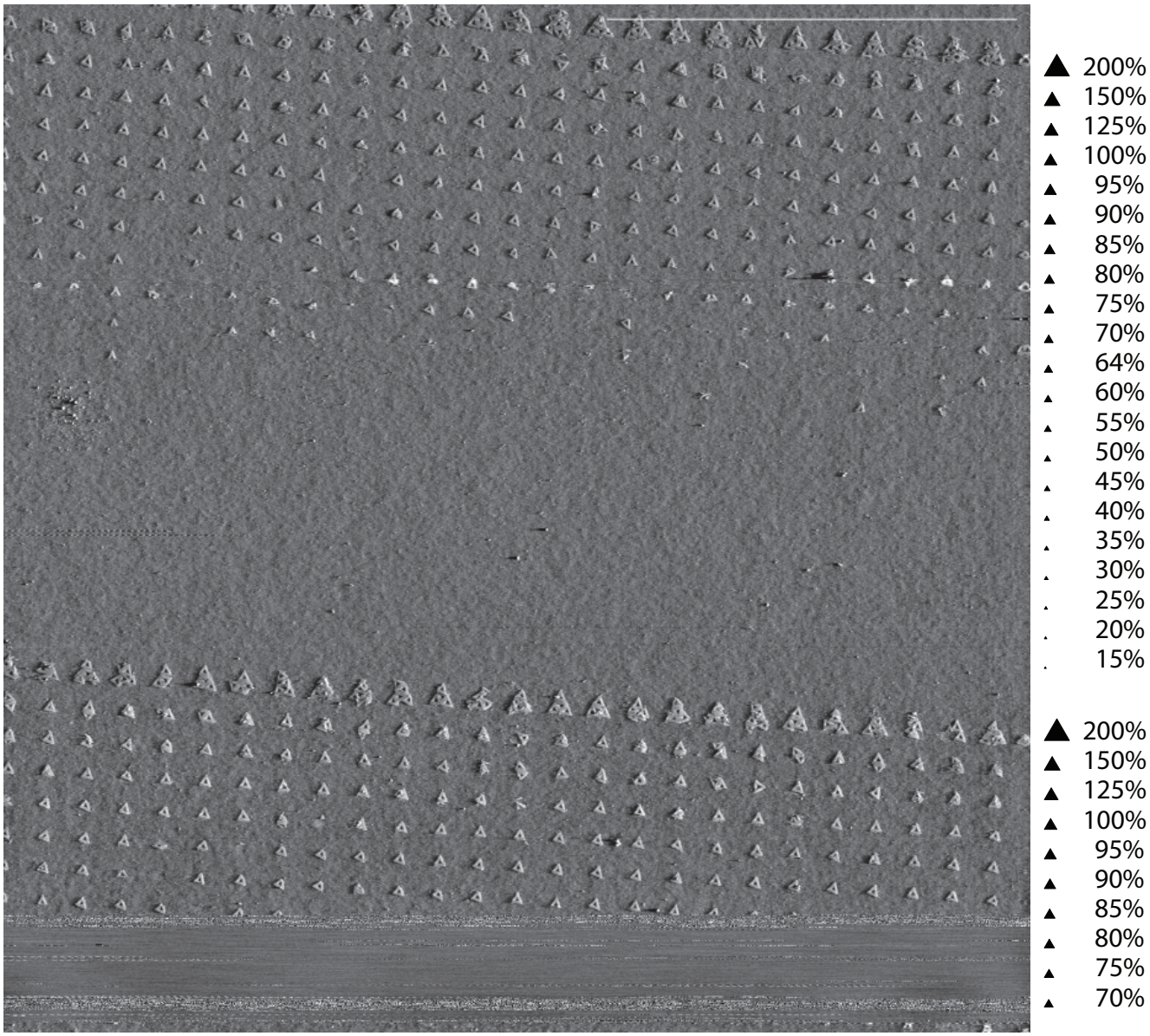

Figure S52. 50 mM Mg^{2+}, binding site size variation experiment. AFM of origami binding on a gradient of triangular binding sites whose sides range from 15% to 200% of the DNA origami edge length (127 nm). Buffer conditions: 5 mM Tris, pH 8.35.

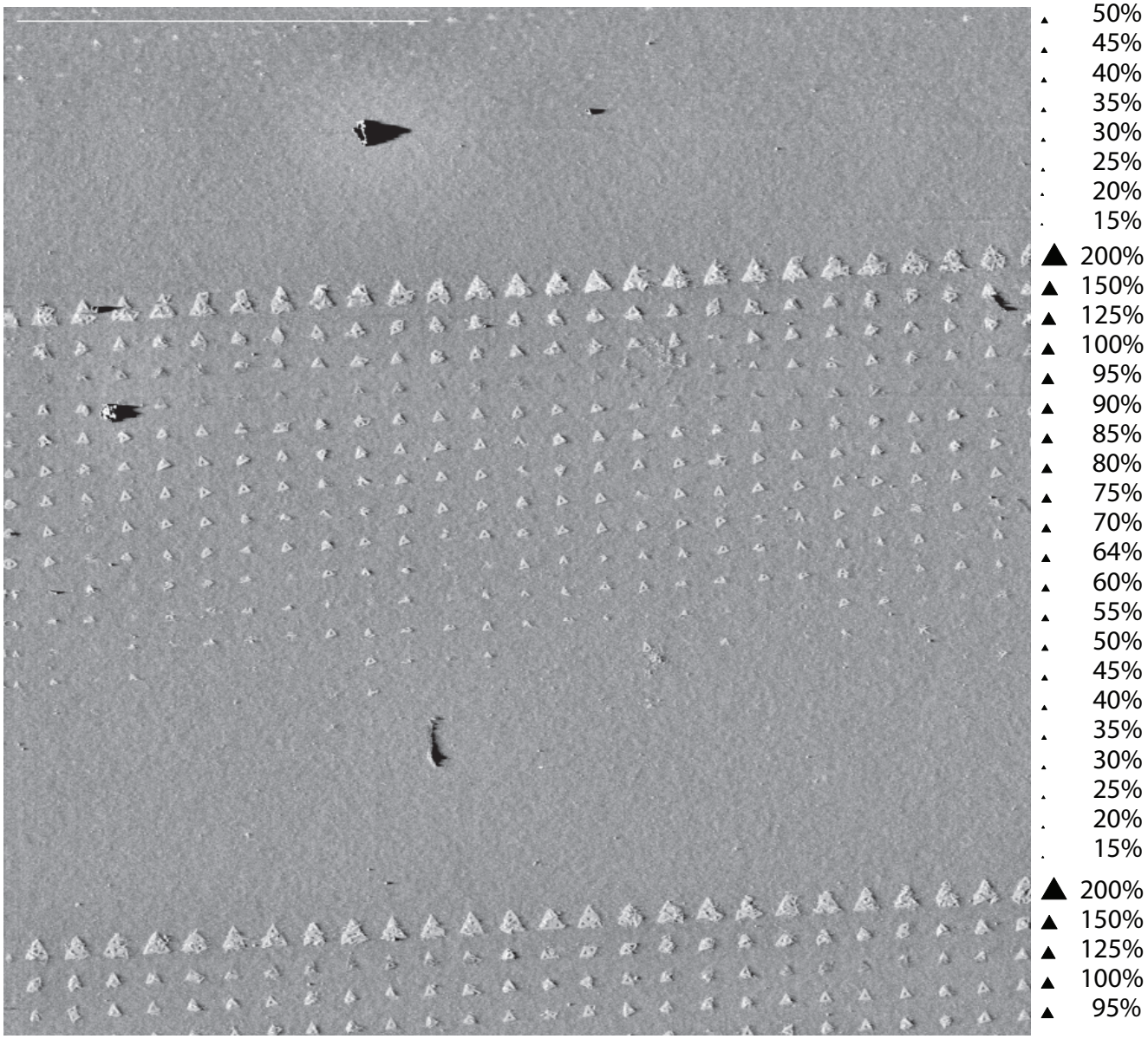

Figure S53. 60 mM Mg^{2+}, binding site size variation experiment. AFM of origami binding on a gradient of triangular binding sites whose sides range from 15% to 200% of the DNA origami edge length (127 nm). Buffer conditions: 5 mM Tris, pH 8.35.

Size of Binding site	25mM	s.e.m.	35mM	s.e.m.	40mM	s.e.m.	50mM	s.e.m.	60mM	s.e.m.
200	17	14	100	0	100	0	100	0	100	0
150	13	7.5	100	0	100	0	100	0	100	0
125	14	6.5	99	1.5	100	0	100	0	100	0
100	11	7	98	2	100	0	97	3	100	0
95	12	6	98	2	100	0	96	4	100	0
90	10	1.5	96	0	100	0	97	1.5	100	0
85	7	3	100	0	100	0	95	5	100	0
80	5	5	100	0	100	0	92	2	100	0
75	0	0	90	2	97	4.5	73	7.5	97	4.5
70	2	3	86	2	85	3.5	59	10.5	85	3.5
65	0	0	56	4	68	6	47	11	68	6
60	0	0	25	3.5	44	12	33	17	44	12
55	0	0	14	5	36	10	8	12	36	10
50	0	0	0	0	19	5	0	0	19	5
45	0	0	0	0	1	1.5	0	0	1	1.5
40	0	0	0	0	0	0	0	0	0	0
35	0	0	0	0	0	0	0	0	0	0
30	0	0	0	0	0	0	0	0	0	0
25	0	0	0	0	0	0	0	0	0	0
20	0	0	0	0	0	0	0	0	0	0
15	0	0	0	0	0	0	0	0	0	0

Figure S54. Results of the binding site size variation experiment. The percentage site occupancy for each binding site of a particular size. Errors correspond to s.e.m. from 3 separate experiments.

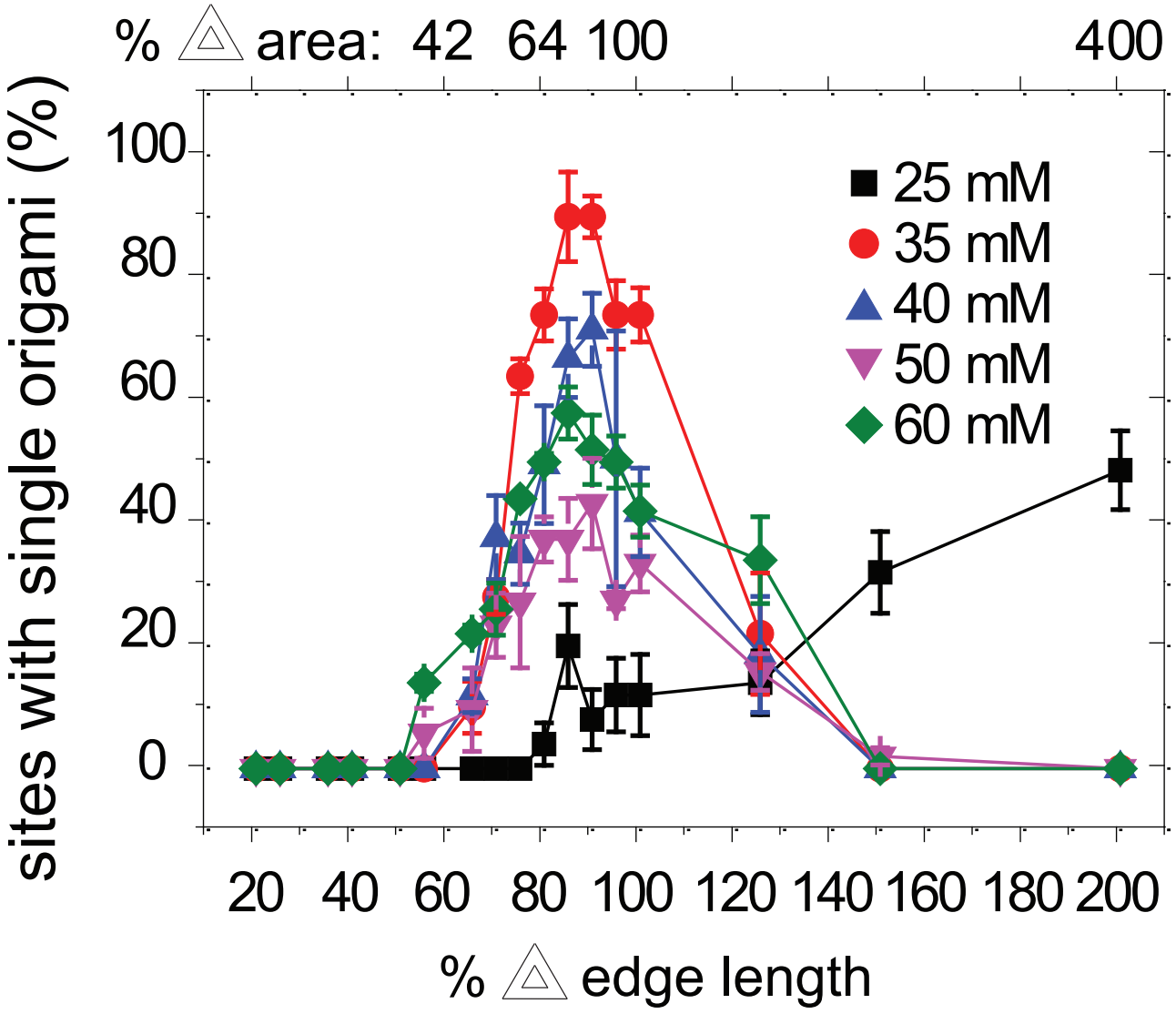

Figure S55. Single origami binding as a function of binding site size. The percentage of sites having a single origami which can be completely resolved by AFM. Sites with multiple origami or partially imaged origami were not counted. Single origami binding events are maximized (90%) for binding sites that are slightly undersized (85–90% of a full origami edge length). Errors correspond to s.e.m. from 3 separate experiments.

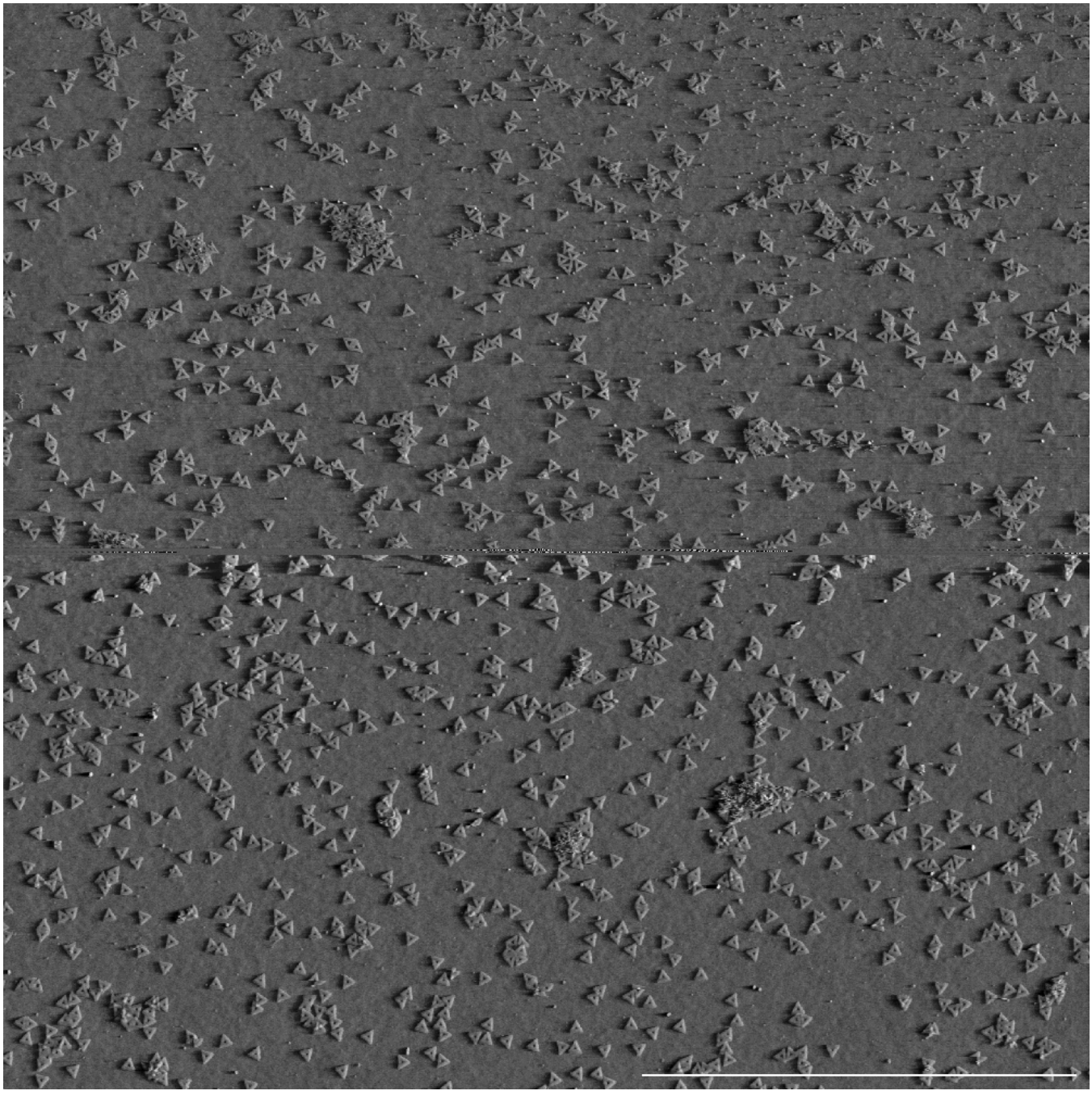

Figure S56. 0 nm period, binding site spacing variation experiment. Other conditions were 110 pM origami, 5 mM Tris, 35 mM Mg^{2+}, pH 8.35

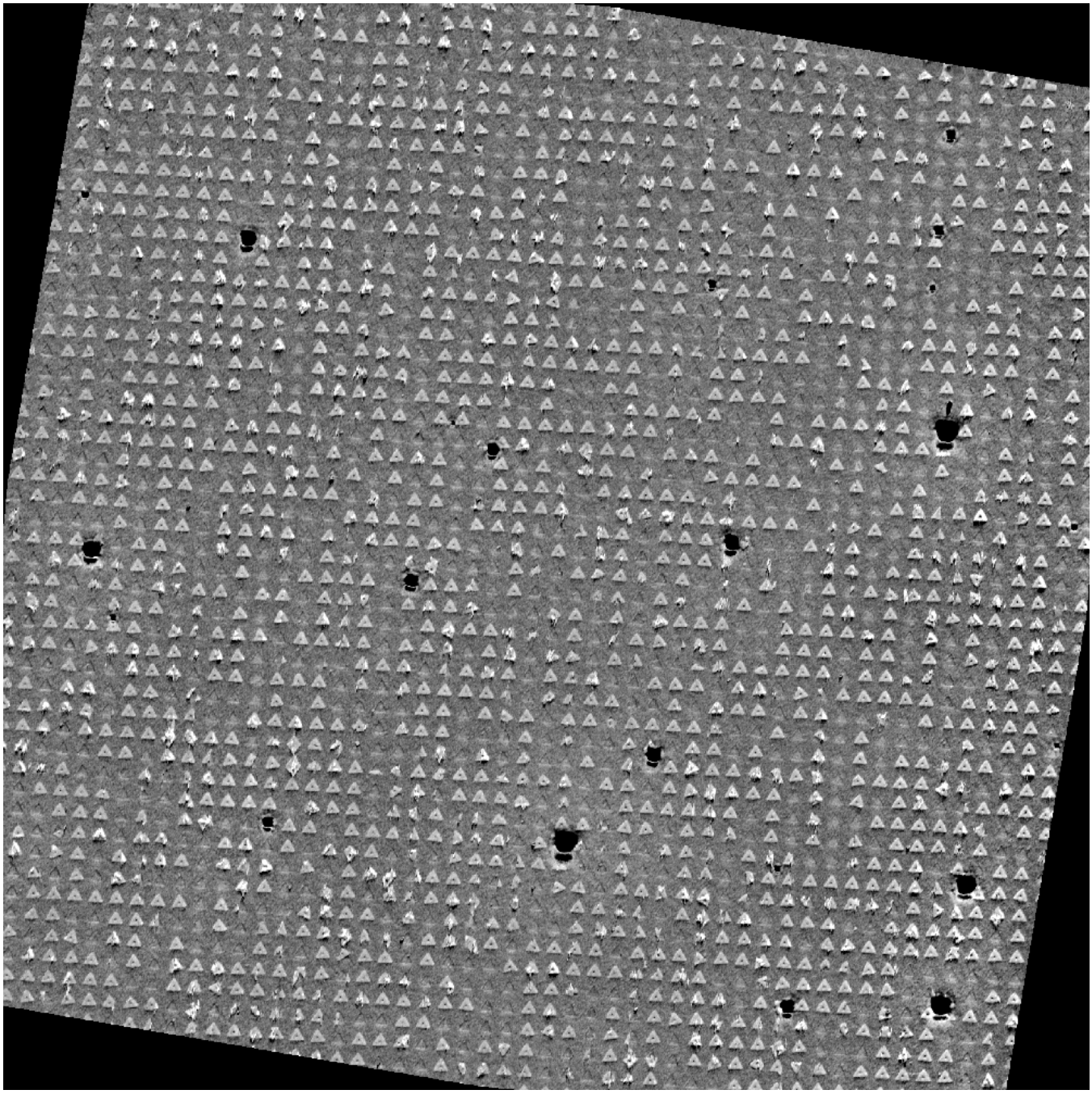

Figure S57. 200 nm period, binding site spacing variation experiment. Other conditions were 110 pM origami, 5 mM Tris, 35 mM Mg^{2+}, pH 8.35

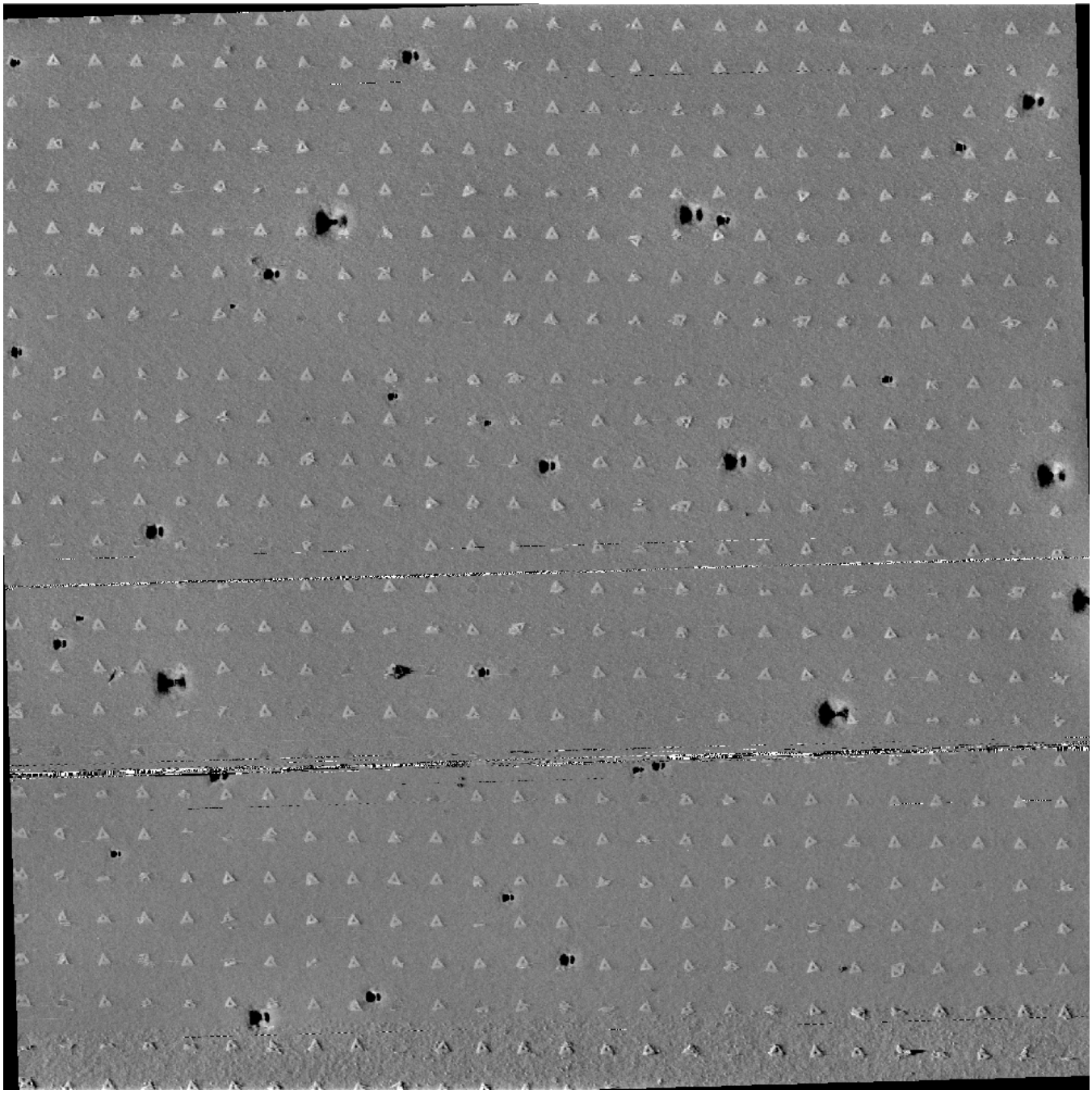

Figure S58. 400 nm period, binding site spacing variation experiment. Other conditions were 110 pM origami, 5 mM Tris, 35 mM Mg^{2+}, pH 8.35

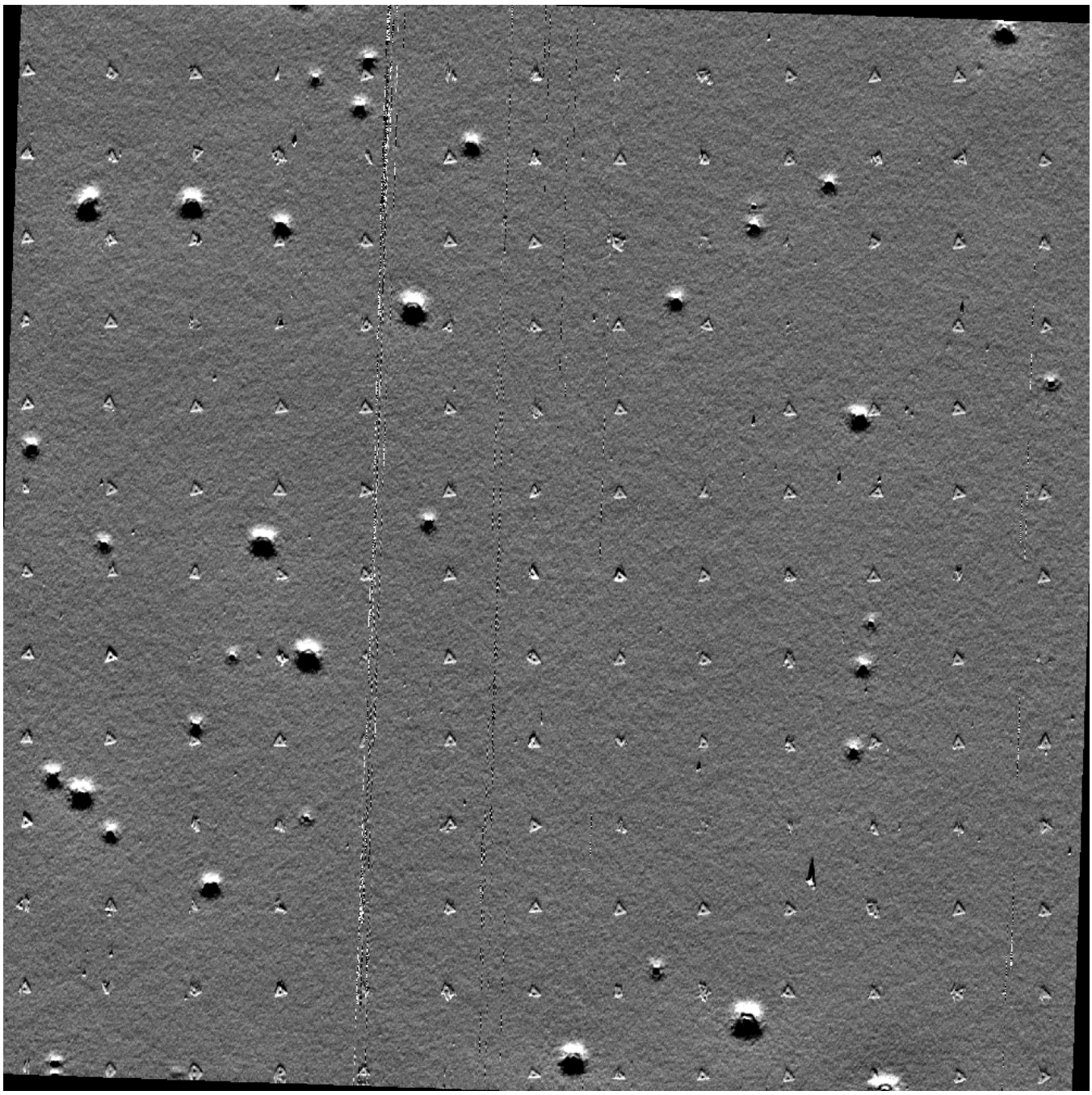

Figure S59. 800 nm period, binding site spacing variation experiment. Other conditions were 110 pM origami, 5 mM Tris, 35 mM Mg^{2+}, pH 8.35

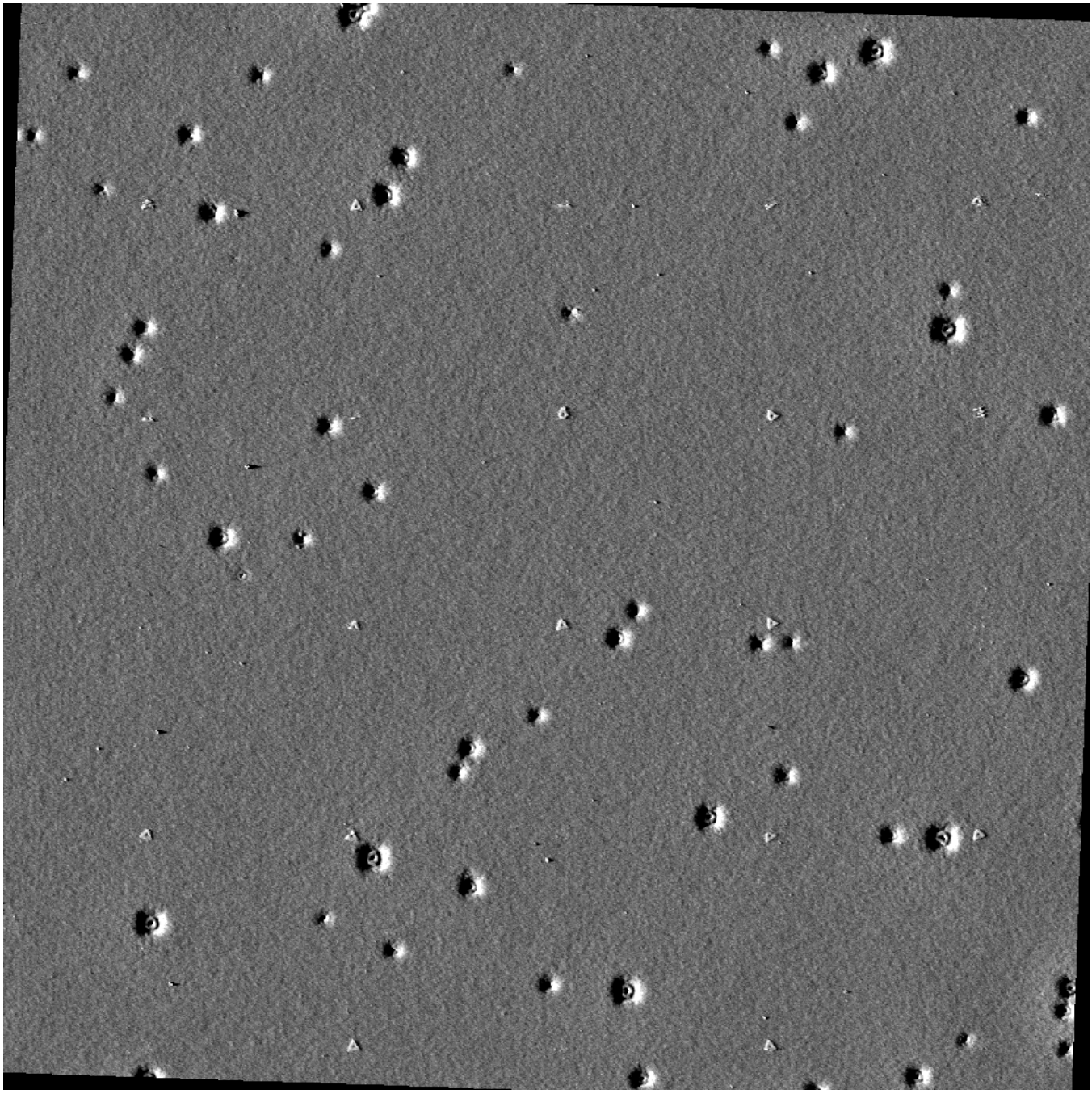

Figure S60. 2000 nm period, binding site spacing variation experiment. Other conditions were 110 pM origami, 5 mM Tris, 35 mM Mg^{2+}, pH 8.35

Period of grid	Filled	Single	Double	Empty
0	24.79675	24.79675	0	75.20325
200	71.07438	61.15702	9.91736	28.92562
400	100	76	24	0
800	88	80	8	12
2000	72	72	0	28

Figure S61. Results of varying binding site spacing (period). The percentage site occupancy as a function the spacing between binding sites. 0 nm data was taken on a $117\mu\mathrm{m}\times117\mu\mathrm{m}$ square whose area matched that of experiments with individual binding sites.

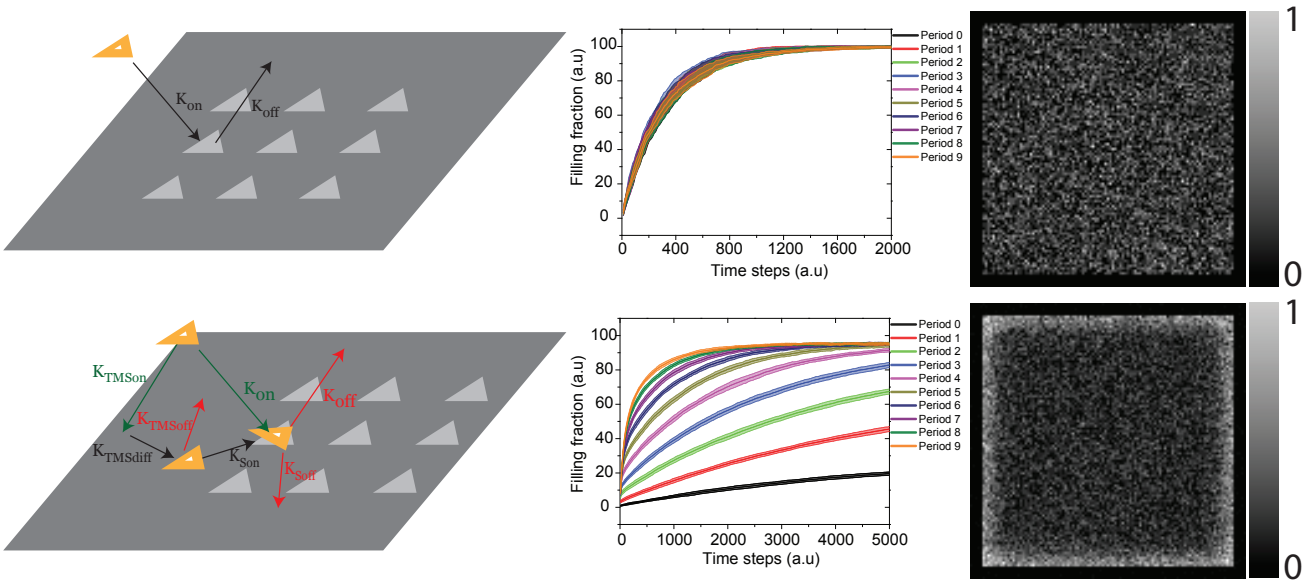

Figure S62. Simulation of origami binding with exclusively 3D or 2D diffusion. **a**–**d** 3D diffusion, model and simulation results. **d**–**f** 2D diffusion, model and simulation results. **a** has the same assumptions as the Langmuir model. Only reactions and rate constants for origami arriving and departing a binding site from solution are diagrammed, but the arrow for k_{Soff} is red to indicate that we are considering the limit of almost irreversible binding (1/100,000 chance of an origami falling off per simulated time step). **d** shows new reactions that are possible if one considers binding to the background and surface diffusion from the background to binding sites. Green and black arrows are part of the simulation but red arrows indicate rate constants taken to be zero in our simulation. Binding to the background from solution is irreversible but allows 2D diffusion. The short arrow for rate constant k_{Soff} is meant to indicate that binding to a binding site is either irreversible (**e**), or "nearly irreversible" (**f**). For simulations used to generate **f**, "nearly irreversible" was implemented by setting the rate constant for origami leaving a binding site to be 200 times lower than the rate constant for origami leaving a background site. **b**,**e** Site occupancy as a function of simulated time steps. Ten simulation runs were made for each of ten different spacings of binding sites, from period 0 to 9, which indicates the number of lattice units between sites. The width of the traces indicates the variability over the ten runs. Period 0 indicates close-packed sites, which models the large square regions used in our surface diffusion experiments. **c**,**f** Averages of 25 final states of period 0 simulations for 3D and 2D respectively. These plots represent the probability of finding an origami at a particular site over 25 simulations, and these plots are analogous to the data (Supplementary Fig. S63f) that was smoothed to generate the probability map in Fig. 3h. Note the high probability of finding an origami near the edge of the array for the 2D simulation in **f**; compare to Fig. 3h which similarly assigns a high probability of finding origami at positions near the edge of the large square.

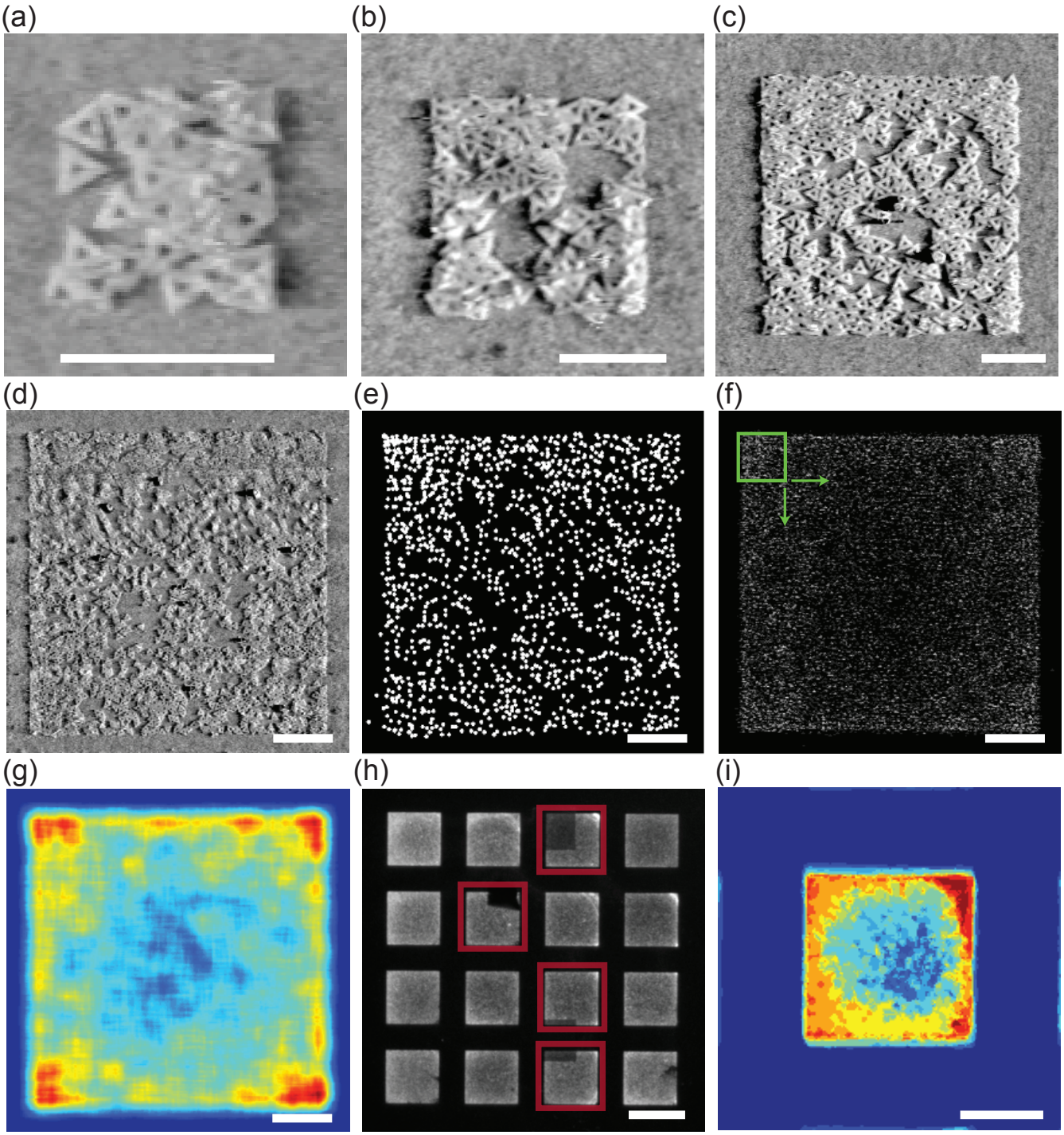

Figure S63. Spatially heterogenous binding of origami to large activated square. (a), 500 nm square activated window. (b), 1 micron square activated window. (c), 2 micron square activated window. (d), 5 micron square activated window. (e), positions of origami from (d) digitized with 2 nm precision, represented as a 2500 $\times$ 2500 element array. (f), average of 25 arrays like those in (e). (g), Probability map generated by averaging a 1 micron moving window (green) on (f). Edges and corners of the window have slight artifacts due to smoothing, for example corners are rounded. Dark red indicates a probability of 1.0 and dark blue 0.0. The highest probability in this map is roughly 0.9. (h), An optical analog of the AFM experiment performed with fluorescent origami on 20 μm$\times$ 20μm activated squares. Red outlines indicate squares excluded from analysis because of large artifacts, some of which derive from fiducial markers. (i), The average of intensities for 12 squares cut out and aligned from (h). Scale bars: (a)–(c), 500 nm; (d)–(g), 1 μm; (h), 20 μm; (i), 10 μm

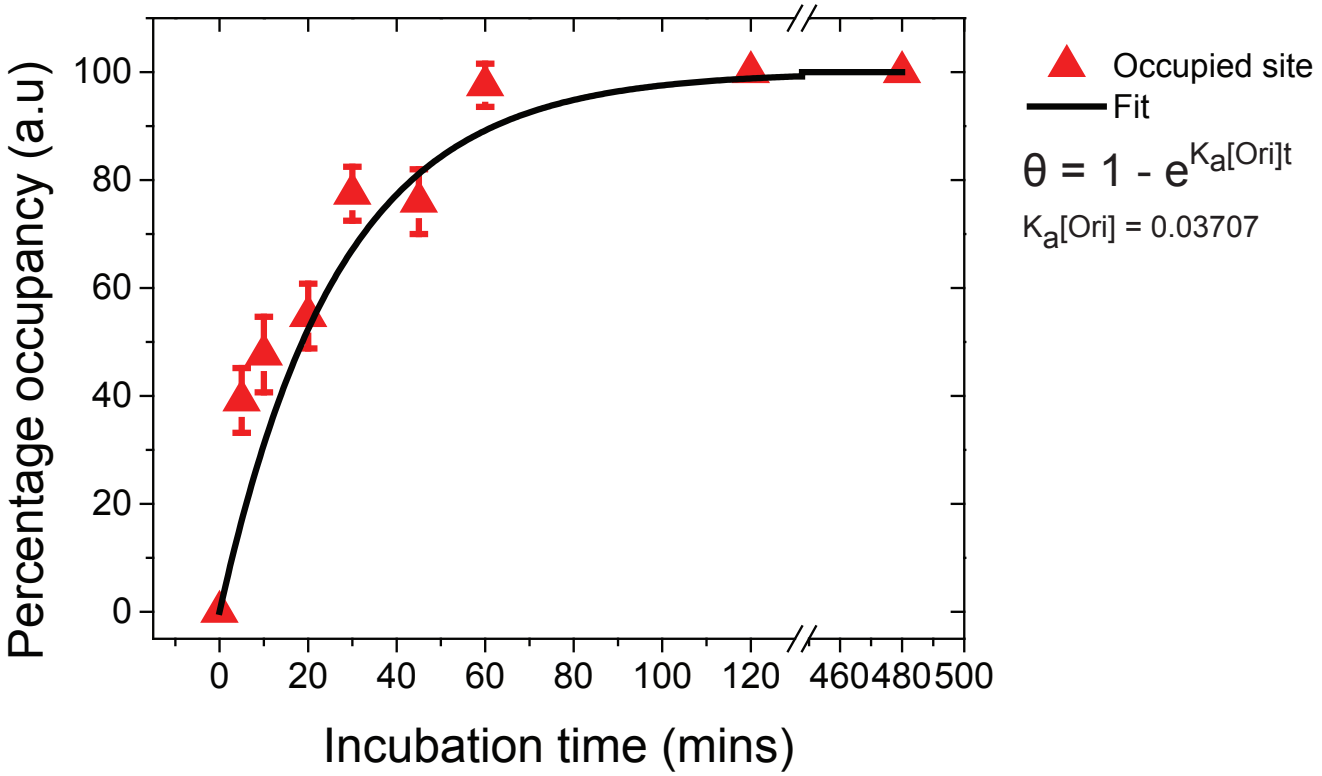

Figure S64. Fit of Langmuir adsorption to experimental placement kinetics. Least squares was used to fit an exponential growth curve to data from our incubation time experiments. $R^2 = 0.95$, adjusted $R^2 = 0.94$ and RMSE $= 5.9$ percentage points and the range of the data is 100 percentage points. Kinetic data is site occupancy data (the red trace) from Fig. 2m in the main paper. Error bars are s.e.m.

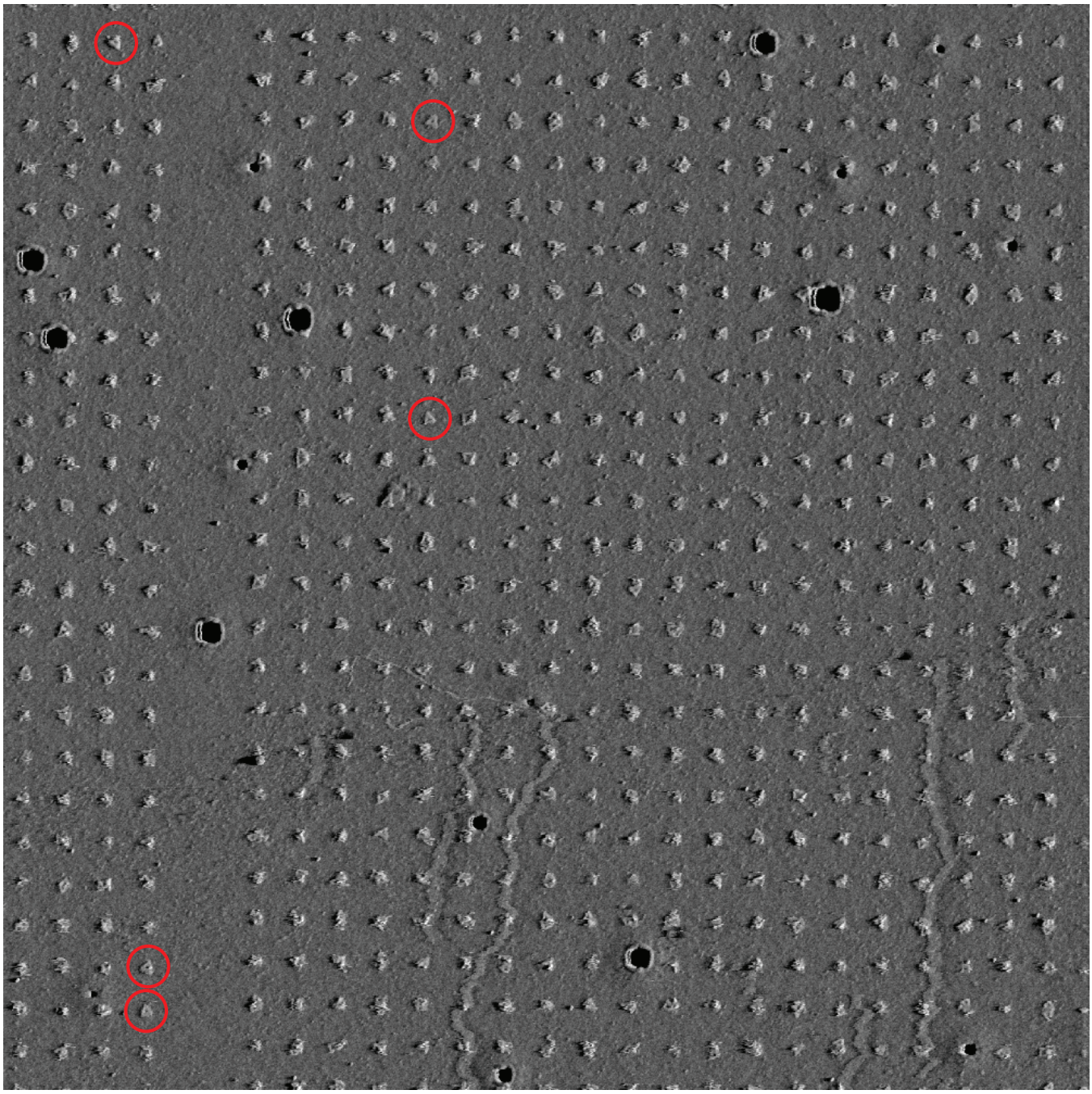

Figure S65. Placement on amine-functionalizd binding sites (Method 2). AFM of origami nanoarrays that have been assembled on chips with positively charged binding sites, created by treating standard binding sites with aminopropyl silatrane. Almost all sites contain aggregates of multiple origami; a few sites circled in red have distinct single origami.

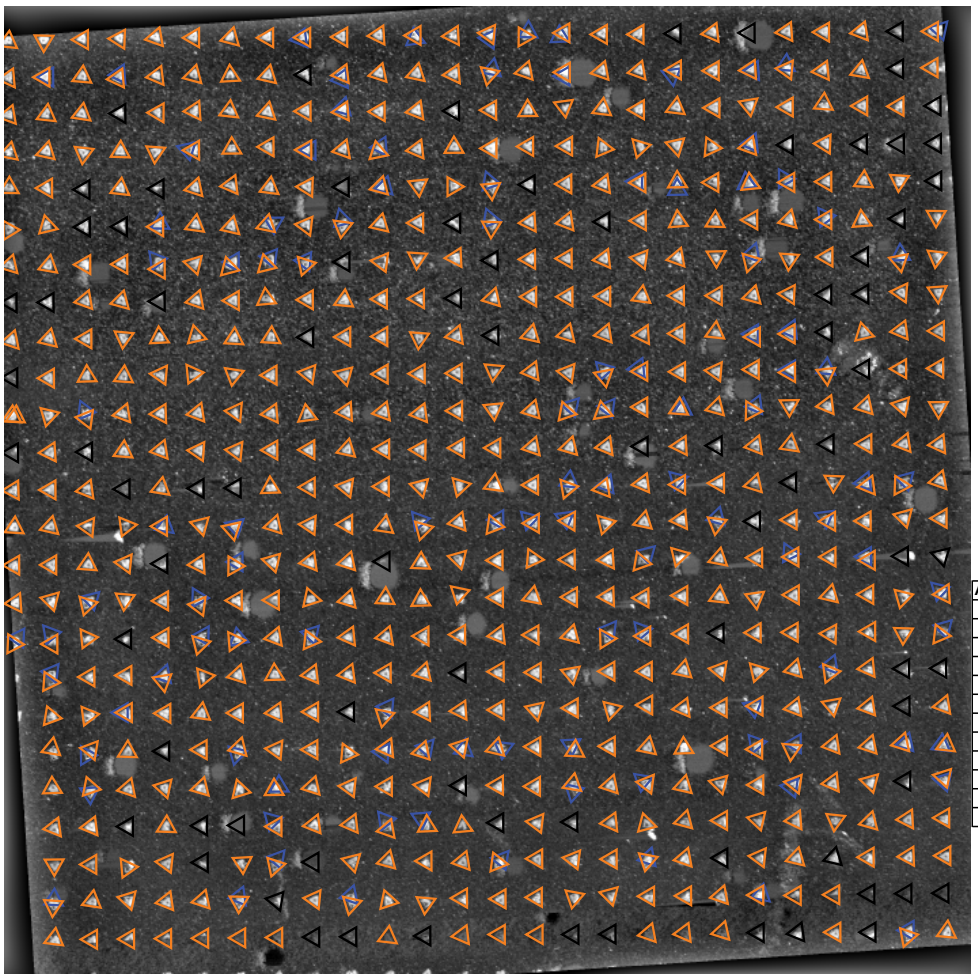

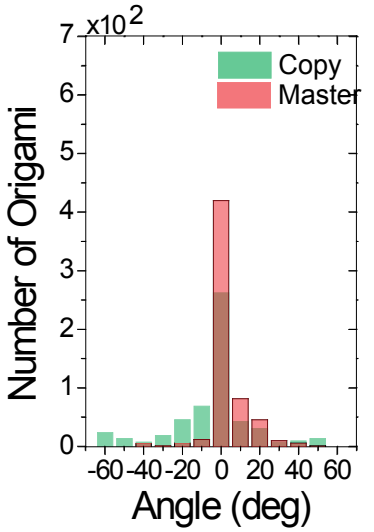

Angle	Number of origami	Number of origami
-60	22	0
-50	7	0
-40	7	5
-30	19	1
-20	46	6
-10	69	12
0	261	422
10	41	82
20	25	46
30	0	10
40	0	6
50	0	1

Figure S66. Microcontact printing onto aminated substrates (Method 3). AFM of DNA origami nanoarrays that have been microcontact printed from a standard placement chip (the master) to an amine-functionalized chip (the copy). Origami were placed on the master using standard placement (Method 1) with 42.5 mM Mg^{2+} (conditions were otherwise standard: 110 pM origami, pH 8.35, 5 mM Tris, 60 min incubation). AFM verifying placement quality on the master chip is shown in Fig. S22. Above, AFM of the copy chip in 1 $\times$ PBS buffer is shown.

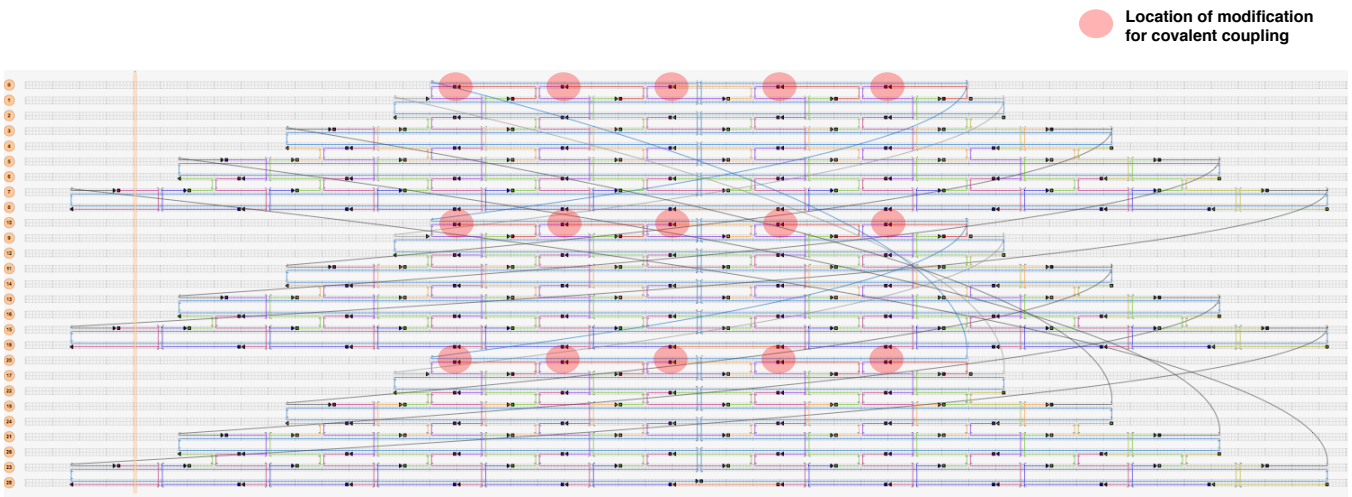

Figure S 67. Design of amine-functionalized DNA origami. Red dots indicate positions functionalized with amines. 18-T linkers extensions were made to the 5′ end of the purple staples underneath the red dots. 21-A strands with 3′ amine modifications were then hybridized to these extensions. This staple diagram derives from caDNAno, amine-functionalization positions were added by hand. The ratio of amino-modifed strands to poly-T-modified staples used in our experiments dictated that, on average, 10 of the 15 possible modification sites were amino-modified (see synthesis of these origami on page 3).

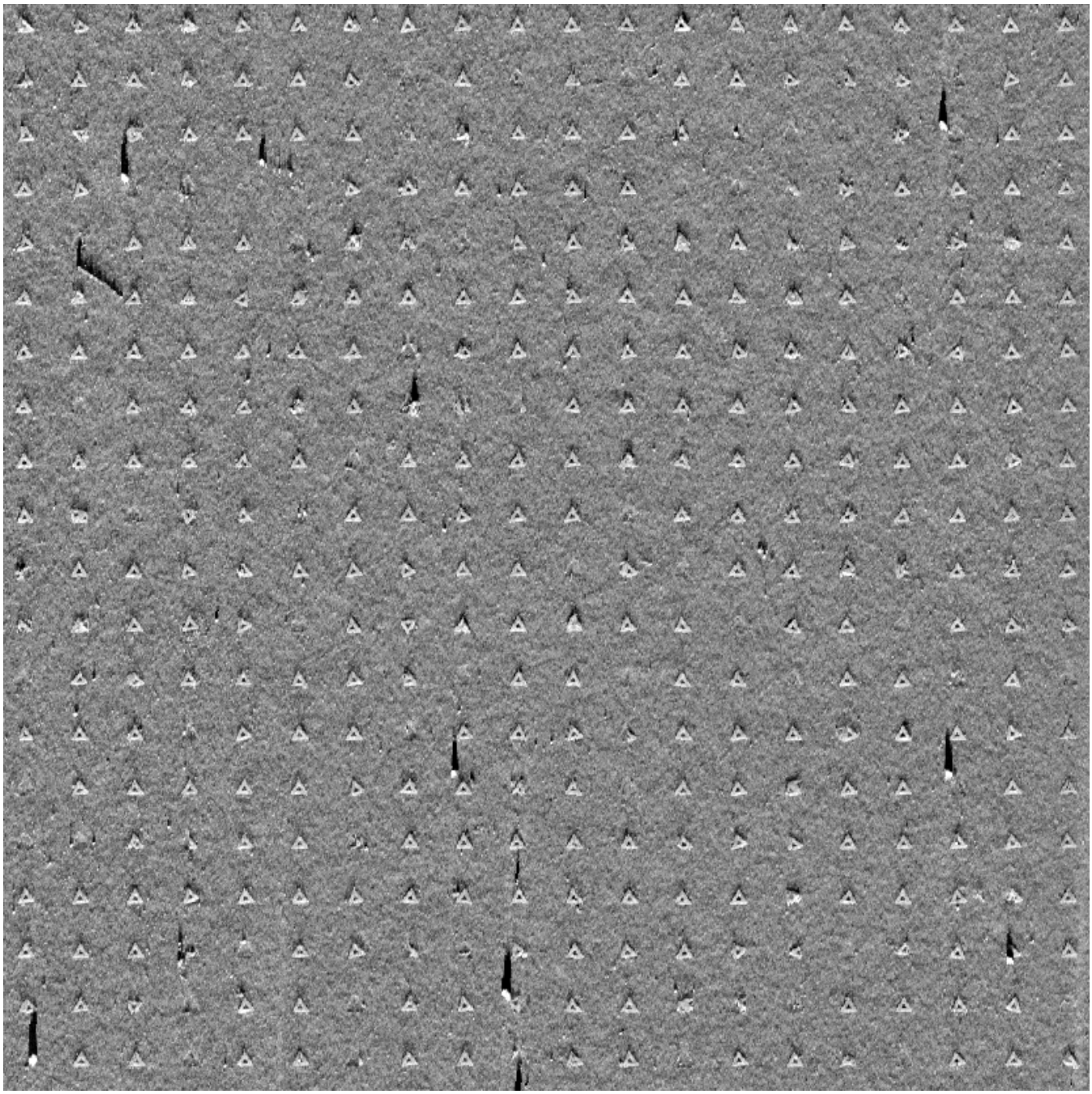

Figure S 68. Covalent immobilization of origami using CDAP. After standard placement using Mg^{2+}, amine-functionalized origami were covalently-coupled to the surface *via* the formation of isourea bonds. Here, AFM shows that the array is stable in the complete absence of Mg^{2+} in 1$\times$ PBS buffer, pH 8.3.

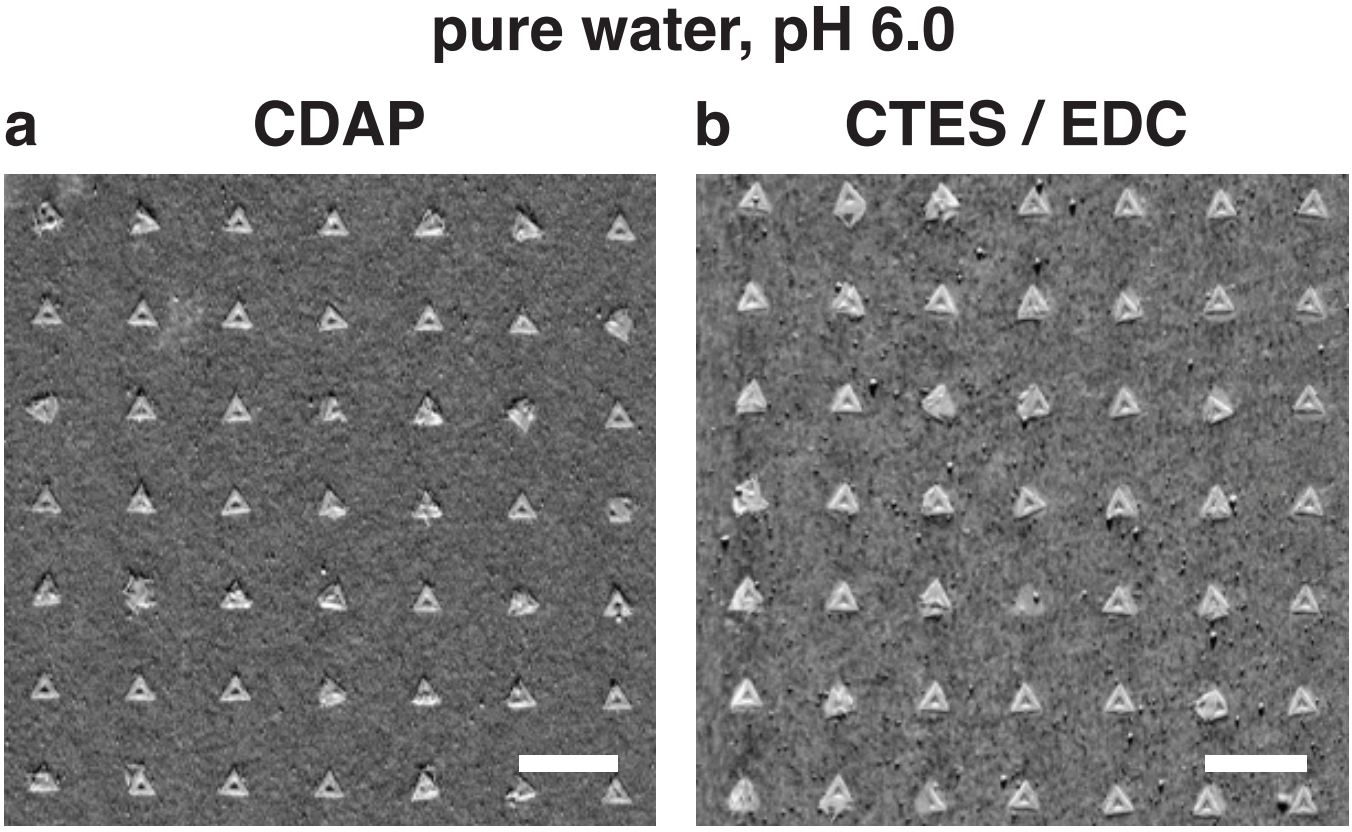

Figure S69. Covalently immobilized origami nanoarrays under water, pH 6.0. **a**, Immobilized with CDAP. **b**, Immobilized with CTES/EDC. Scale bars, 400 nm.

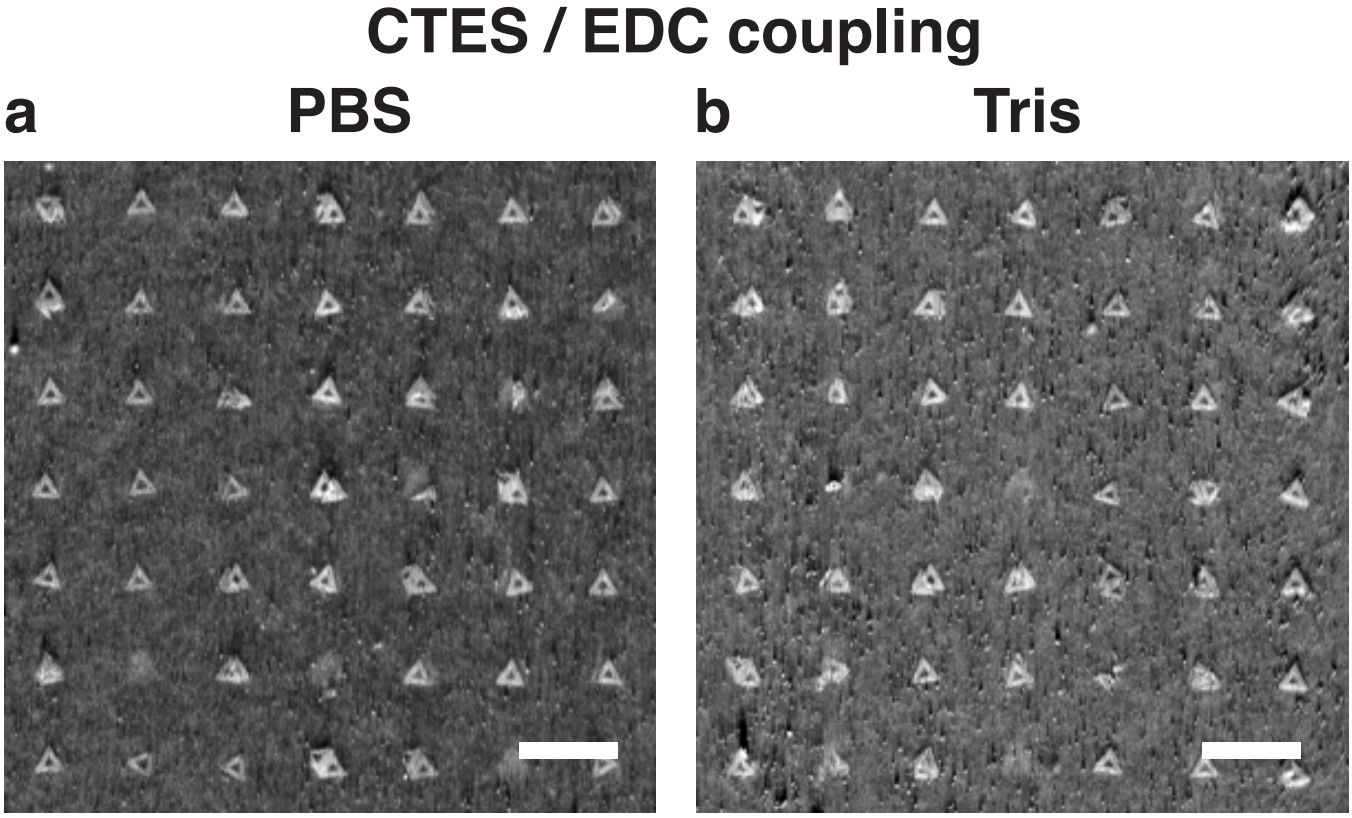

Figure S70. CTES/EDC immobilized origami nanoarrays. a, Under 1× PBS buffer, pH 8.3. **b**, Under 10 mM Tris buffer, ph 8.3. CTES/EDC immobilized arrays feature amide bonds that do not undergo aminolysis in Tris buffers like the isourea bonds generated by CDAP. Scale bars, 400 nm.

References

1. Rothemund, P. W. K. Folding DNA to Create Nanoscale Shapes and Patterns. *Nature* **2006**, *440*, 297–302.

2. Stahl, E.; Martin, T. G.; Praetorius, F.; Dietz, H. Facile and Scalable Preparation of Pure and Dense DNA Origami Solutions. *Angew. Chem. Int. Edit.* **2014**, *53*, 12735–12740.

3. Becker, J.; Pysch, D.; Leimenstoll, A.; Hermle, M.; Glunz, S. Wet-Chemical Pre-Treatment of c-Si Substrates Enhancing the Performance of a-Si: H/c-Si Hetero-Junction Solar Cells. 24th European PV Solar Energy Conference and Exhibition, Hamburg, Germany. 2009.

4. Hung, A. M.; Micheel, C. M.; Bozano, L. D.; Osterbur, L. W.; Wallraff, G. M.; Cha, J. N. Large-Area Spatially Ordered Arrays of Gold Nanoparticles Directed by Lithographically Confined DNA Origami. *Nat. Nanotechnol.* **2010**, *5*, 121–126.

5. Argaman, M.; Golan, R.; Thomson, N. H.; Hansma, H. G. Phase Imaging of Moving DNA Molecules and DNA Molecules Replicated in the Atomic Force Microscope. *Nucleic Acids Res.* **1997**, *25*, 4379–4384.

6. James, P.; Antognozzi, M.; Tamayo, J.; McMaster, T.; Newton, J.; Miles, M. Interpretation of Contrast in Tapping Mode AFM and Shear Force Microscopy. A Study of Nafion. *Langmuir* **2001**, *17*, 349–360.

7. Shlyakhtenko, L. S.; Gall, A. A.; Filonov, A.; Cerovac, Z.; Lushnikov, A.; Lyubchenko, Y. L. Silatrane-Based Surface Chemistry for Immobilization of DNA, Protein-DNA Complexes and Other Biological Materials. *Ultramicroscopy* **2003**, *97*, 279–287.

8. Ageno, M.; Dore, E.; Frontali, C. The Alkaline Denaturation of DNA. *Biophys. J.* **1969**, *9*, 1281–1311.